
Distributed Hybrid Parallelism for Large Language Models: Comparative Study and System Design Guide

Hossam Amer*

Toronto Ascend Team, Huawei Canada

hossam.amer1@huawei.com

Rezaul Karim*

Toronto Ascend Team, Huawei Canada

rezaul.karim3@huawei.com

Ali Pourranjbar

Toronto Ascend Team, Huawei Canada

ali.pourranjbar@h-partners.com

Weiwei Zhang

Toronto Ascend Team, Huawei Canada

weiwei.zhang2@huawei.com

Walid Ahmed

Toronto Ascend Team, Huawei Canada

walid.ahmed1@huawei.com

Boxing Chen

Toronto Ascend Team, Huawei Canada

boxing.chen@huawei.com

Abstract

With the rapid growth of large language models (LLMs), a wide range of methods have been developed to distribute computation and memory across hardware devices for efficient training and inference. While existing surveys provide descriptive overviews of these techniques, systematic analysis of their benefits and trade-offs—and how such insights can inform principled methodology for designing optimal distributed systems—remain limited. This paper offers a comprehensive review of collective operations and distributed parallel strategies, complemented by mathematical formulations to deepen theoretical understanding. We further examine hybrid parallelization designs, emphasizing communication–computation overlap across different stages of model deployment, including both training and inference. Recent advances in automated search for optimal hybrid parallelization strategies using cost models are also discussed. Moreover, we present case studies with mainstream architecture categories to reveal empirical insights to guide researchers and practitioners in parallelism strategy selection. Finally, we highlight open challenges and limitations of current LLM training paradigms and outline promising directions for the next generation of large-scale model development.

*Equal contribution.

Contents

1	Introduction	3
2	Distributed Strategies Background	5
2.1	Collective Operations	5
2.2	Data Parallelism	6
2.3	Model Parallelism	7
2.4	Activation Parallelization	9
2.5	Memory Optimization Techniques	10
2.6	Communication Overlap Techniques	10
3	Hybrid Systems	13
3.1	Multi-Parallelism	13
3.2	Frameworks	15
4	Workload Parallelization Design	17
4.1	System Design Implications	17
4.2	System Design Considerations	20
4.3	Toward Auto Parallelization	23
5	Parallel Strategies Theoretical Analysis	24
5.1	GQA Theoretical Analysis	25
5.2	MLP Theoretical Analysis	27
5.3	Mamba Theoretical Analysis	28
5.4	Summary of the Theoretical Analysis	36
6	Parallelization Strategy Selection for Transformer and Mamba: A Case Study	36
6.1	Experimental Setup	36
6.2	Attention Experiments	37
6.3	Mamba Experiments	43
6.4	Summary of Empirical Insights	47
7	Open Challenges and Future Directions	47
8	Conclusion	50

1 Introduction

The empirical findings of neural scaling laws demonstrate continued performance gains when scaling model size, training data, and computation budget, underscoring the importance of efficient distributed training strategies [51]. In recent years, models with hundreds of billions to trillions of parameters have achieved unprecedented results across diverse benchmarks, marking a significant step toward artificial general intelligence [33, 1, 3, 38, 41, 106]. These successes, coupled with the scaling law evidence, have fueled growing demand for efficient training and inference on large distributed systems comprising GPUs, TPUs, or NPUs.

To meet these demands, modern systems combine parallelization techniques such as Data, Pipeline, Tensor, and Context Parallelism, often augmented with memory optimization techniques like activation recomputation [17] and distributed optimizers [88]. Communication overlap methods further reduce bottlenecks in distributed environment. Notably, the best mix of strategies varies between training and inference due to differing workload requirements [89, 38]. Since each parallelization method introduces distinct communication and efficiency trade-offs, there is a pressing need for a unified understanding of how to integrate them effectively.

Despite progress, distributed strategies for large-scale model training have often been developed independently, leaving a fragmented understanding of the overall landscape. Existing surveys provide valuable overviews [27, 137], but a deeper analysis of their trade offs in balancing scalability, memory efficiency, and communication cost is needed to guide system design. Even a modest efficiency gains in a distributed strategy design for a large scale model can yield significant benefits as training of foundation models consumes vast energy resources [100]. Hardware-aware optimization and datacenter efficiency can further mitigate the carbon impact [83], aligning distributed AI with the principles of “Green AI,” where sustainability is prioritized alongside accuracy [91]. Therefore, a holistic perspective on distributed strategies is crucial for both advancing large-scale AI and ensuring ecological sustainability.

In this paper, we address the above needs and fill the gap in literature with a comprehensive review, design guidelines, systematic analysis and insights. We omit discussion on model compression techniques [138, 35] including pruning [18], quantization [124], low-rank adaptation [125] in favor of broader discussion on system level optimization. The key concepts covered in this study are highlighted in Figure 1. We begin with a comprehensive background on parallel distributed strategies and collective operations. Then, we turn to hybrid parallelization and their associated deep learning frameworks. We also add a section to discuss the parallelization system design considerations including evaluation metrics with discussions on training and inference considerations. Based on this, we formulate the hybrid parallelization problem for system design, review existing frameworks, examine automatic parallelization methods. We support our analysis with theoretical and empirical validations.

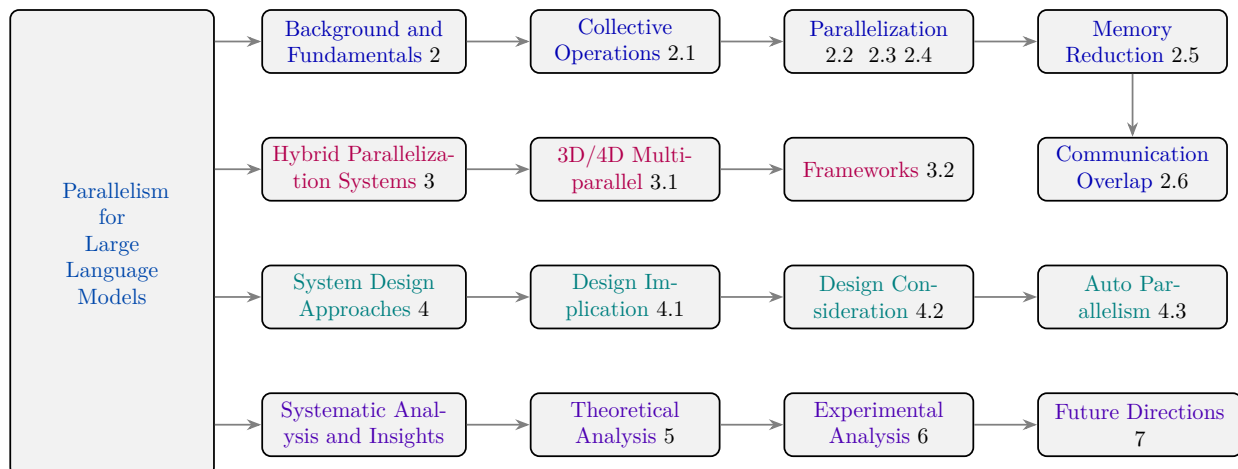


Figure 1: Overview of the key aspects of scalable efficient distributed systems for AI workloads that we cover in this study.

This study goes beyond a traditional survey by using a comparative study, system design guidelines, and practical use cases as highlighted in Table 1. We offer this paper to both researchers and practitioners as a guide for distributed parallel strategies to support model development. While this paper does not aim to be fully exhaustive, we hope it provides a useful foundation upon which the community can build and extend the analyses. A concise outline of our key contributions include:

- Present a cohesive and coherent literature review covering parallelization strategies, memory reduction, communication overlap, hybrid system design, and automatic parallelization aiming for a holistic understanding of efficient training and inference in distributed setting.
- Present a comparative study of tradeoffs and benefits of workload distribution strategies accompanied by examples to provide practical insight and use cases of these strategies.
- Highlight our key findings from this study that would be insightful for researcher and practitioners in this field. Key findings highlight the need for distinct parallelization strategies tailored to the unique workload requirements of training and inference. These strategies are essential for hybrid approaches that combine complementary methods to achieve optimal performance in both stages. Additionally, efficient system design requires jointly considering memory, compute throughput, bandwidth, and collective communication patterns.
- Consolidate our insights on emerging trends, emphasizing automated discovery of optimal parallelization strategies across large-scale cluster topologies. This involves leveraging cost models and aligning with service-level requirements to guide efficient strategy selection.
- Provide both theoretical and empirical analysis to parallel strategies to support researchers and practitioners in parallel strategy selection.
- Summarize important future key points that can be extended from this paper.

Table 1: Comparison of related surveys on distributed parallel strategies.

Category	Zeng et al. (2023) [131]	Li et al. (2024) [59]	Duan et al. (2024) [27]	Zeng et al. (2025) [132]	This survey
Covers distributed parallel strategies broadly	Limited	Limited	Yes	Yes	Yes
Covers memory reduction strategies broadly	Yes	Yes	Yes	Yes	Yes
Covers communication overlap strategies broadly	No	No	Yes	Yes	Yes
Discusses distributed parallel frameworks	Limited	Yes	Yes	No	Yes
Discusses auto parallelism	No	No	Yes	Limited	Yes
Discusses the parallel strategy selection success metrics	No	Yes	No	Limited	Yes
Covers both training and inference	Training	Yes	Training	Training	Yes
Provides mathematical and analytical understanding to parallel strategies	No	No	No	Yes	Yes
Provides empirical analysis of parallel strategy selection using case studies	No	No	No	No	Yes
Provides parallelization strategy selection guidelines	No	No	Limited	Yes	Yes
Proposes future research directions	Limited	Limited	Limited	Yes	Yes

2 Distributed Strategies Background

Efficient distributed deep learning strategies rely on utilizing complementary benefits from a broad set of parallelization, memory optimization, and communication–computation overlap techniques. These sets of parallelization techniques can be data parallel, model parallel, or activation parallel algorithms that have evolved over time. *Data parallelism* replicates the model across accelerators (e.g., GPU, TPU, NPU) and distributes input data across them, while *model parallelism* distributes the model parameters across accelerators. Another form of parallelism, *activation parallelism*, distributes the intermediate activations across accelerators, usually along the sequence dimension. Since a typical parallelization of a large model involves using a combination of these, an in-depth understanding of individual parallelization strategies as well as comparative benefits and trade-offs is critically important for both researchers and practitioners.

Complementary methods for efficient scaling of deep learning workloads address the memory and communication bottlenecks stemming from large sequences, large model parameters, and synchronization among distributed workers. Memory optimization techniques play an important role in fitting activations for large input sequences and parameters of large models within hardware memory constraints. Collective communication is required to synchronize computation on data subsets or computations from subsets of model parameters. Hence, computation–communication overlap plays an important role in reducing latency by minimizing wait time for communication to be completed.

To develop a comprehensive foundation for efficient distributed deep learning, this section first introduces the core concepts of collective communication operations. It then examines prominent strategies for parallelization, memory optimization, and communication–computation overlap, and concludes with a comparative analysis of these approaches.

2.1 Collective Operations

Collective communication primitives are fundamental to distributed training, enabling synchronization and data exchange across multiple devices or ranks. Below we summarize the most widely used operations.

Reduce. The *Reduce* operation aggregates data from multiple ranks and delivers the result to a designated root rank. Typical reduction functions include but not limited to summation, product, minimum and maximum.

Gather. The *Gather* operation collects data from all participating ranks and delivers it to a single root rank. Unlike Reduce, the data is simply gathered rather than aggregated.

AllGather. The *AllGather* operation extends Gather by collecting data from every rank. When a group of N devices (ranks) participate in this collective communication with each containing data of a `tensor_size`, after this operation each of the ranks in the group will have data of size $N \times \text{tensor_size}$. This differs from Gather, where only the root rank receives the result.

A visual depiction of the *AllGather* operation for four ranks is shown in Figure 2. In this example, each of the four ranks initially contains a distinct data element: rank 0 holds a , rank 1 holds b , rank 2 holds c , and rank 3 holds d . After the *All-Gather* operation, all ranks receive the complete set of data elements aggregated across all ranks. As a result, each rank contains the full sequence (a, b, c, d) .

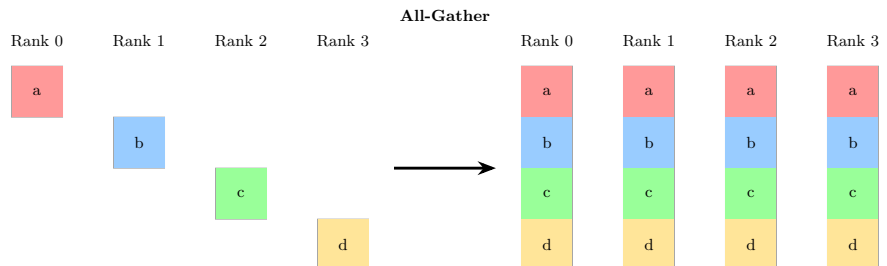


Figure 2: All-Gather operation: before (left) each rank holds only its reduced slice; after (right) each rank holds all slices.

ReduceScatter. The *ReduceScatter* operation first performs a reduction across ranks (as in Reduce) and then evenly scatters the reduced result across all ranks. Each rank thus receives only the portion of the output corresponding to its index, reducing communication overhead compared to AllReduce. An example of the reduce-scatter is visualized in Figure 3.

In this example, the four ranks initially contain the data sequences (a_0, a_1, a_2, a_3) , (b_0, b_1, b_2, b_3) , (c_0, c_1, c_2, c_3) , and (d_0, d_1, d_2, d_3) , respectively. After the *ReduceScatter* operation, the data is reduced via sum aggregation, and each rank receives a slice of the aggregated sequence corresponding to its index. As a result, rank 0 contains the first slice of the reduced (aggregated) result, which is $(a_0 + b_0 + c_0 + d_0)$. The other ranks receive similar slices.

AllReduce. The *AllReduce* operation performs a reduction (e.g., sum, min, max) across all ranks and distributes the final result back to every rank. Conceptually, AllReduce is equivalent to performing a Reduce followed by a Broadcast. However, this naive strategy creates a bottleneck at the root server. In practice, optimized implementations use the *Ring-AllReduce* algorithm, in which data is first partitioned and reduced in a distributed manner (ReduceScatter), followed by redistribution of the reduced blocks (AllGather). High-performance systems, such as IBM’s BlueConnect, adopt this approach [20]. We consider a similar example of *AllReduce* with four ranks containing initial data sequences (a_0, a_1, a_2, a_3) , (b_0, b_1, b_2, b_3) , (c_0, c_1, c_2, c_3) , and (d_0, d_1, d_2, d_3) , respectively. In such case, the data in the ranks 0, 1, 2, 3 after the *ReduceScatter* operation becomes $(a_0 + b_0 + c_0 + d_0)$, $(a_1 + b_1 + c_1 + d_1)$, $(a_2 + b_2 + c_2 + d_2)$, and $(a_3 + b_3 + c_3 + d_3)$. A following *All-Gather* operation on these reduced slices will result in all rank containing all the slices, which is the complete reduced sequence: $(a_0 + b_0 + c_0 + d_0, a_1 + b_1 + c_1 + d_1, a_2 + b_2 + c_2 + d_2, a_3 + b_3 + c_3 + d_3)$. This result corresponds to the output of *All-Reduce*. We omit including a visual example for *All-Reduce* for brevity, since its behavior is quite understandable from the visual examples of *ReduceScatter* and *All-Gather*.

All-to-All. The *All-to-All* operation (also known as total exchange or personalized communication) enables each rank to send a distinct message to every other rank, including itself. At the end of the operation, each rank holds one piece of data from every participant. A common use case is in Mixture-of-Experts (MoE) training, where tokens must be dynamically routed to experts across ranks via one All-to-All exchange, and then results are routed back with another [93].

A comparative summary of the volume of data communication per device for the aforementioned collective operations are presented in Table 2. For *Reduce* and *Gather*, each rank sends its tensor to a designated root, resulting in a communication cost of $(N - 1) \times \text{tensor_size}$. In contrast, ring-based collectives such as *AllGather* and *ReduceScatter* evenly distribute communication across all devices, thus reducing the per-device cost to $\frac{(N-1) \times \text{tensor_size}}{N}$ for a group of N devices. This balanced communication pattern improves scalability by mitigating bottlenecks and making more efficient use of available bandwidth. More complex collectives are often constructed from these primitives; for example, *AllReduce* is commonly implemented as a *ReduceScatter* followed by an *AllGather*, resulting in a total cost of $2 \times \frac{(N-1) \times \text{tensor_size}}{N}$.

2.2 Data Parallelism

Data parallelism (DP) is the most common parallel training strategy for deep neural networks [36, 60]. This approach splits the entire mini-batch across multiple devices, where each device executes a single replica of the model and communicates with each for synchronization at the end of each training step. This synchronization requires an all-reduce communication among the gradients of all ranks within the DP group. Enabling more devices to train large minibatches with this strategy is easier. Several recommendations from the literature

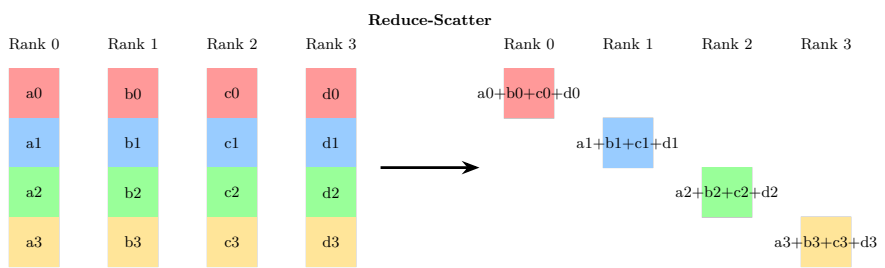


Figure 3: Reduce-Scatter operation: before (left) each rank holds all slices; after (right) each rank holds the reduced slice.

Table 2: Data movement per device for common collective operations. N is the number of ranks and `tensor_size` is the size of the tensor in each rank before the collective operation.

Collective Operation	Data Moved Per Device
Reduce	$(N - 1) \times \text{tensor_size}$
Gather	$(N - 1) \times \text{tensor_size}$
Ring AllGather	$\frac{(N-1) \times \text{tensor_size}}{N}$
Ring ReduceScatter	$\frac{(N-1) \times \text{tensor_size}}{N}$
All-to-All	$\frac{(N-1) \times \text{tensor_size}}{N}$
AllReduce (ReduceScatter + Ring AllGather)	$2 \times \frac{(N-1) \times \text{tensor_size}}{N}$

suggest that training speed varies almost linearly with the number of devices [99, 128, 36, 129]. However, arbitrarily increasing data parallelism beyond a critical batch size may yield diminishing returns or even negatively impact the convergence [96]. Furthermore, data parallelism improves throughput by distributing different inputs across devices, but it does not reduce latency since each device must still process the full forward and backward pass of a single input independently and sequentially. Thus, more efforts are needed to ensure the convergence performance [53, 11]. In addition, replicating the weights of large transformers is limited by the memory available per device.

2.3 Model Parallelism

As transformer models scale towards trillions of parameters, model parallelism is required to distribute model parameters, activations, and optimizer state across devices for them to fit into device memory and be trainable in a realistic amount of time. In general, model parallelism reduces the number of parameters stored on each device approximately linearly with the parallelism size. For example, the number of parameters per device is halved when the model parallel size is doubled. Different forms of model parallelism require distinct communication patterns, and the efficiency of these patterns depends heavily on connectivity bandwidth and cluster topology. These factors play a critical role in determining the trade-off considerations for various model parallel techniques and their combinations [140]. In the following, we discuss different model parallelism techniques commonly used for LLM training and inference.

Pipeline Parallelism (PP)

Pipeline Parallelism (PP) distributes consecutive layers as pipeline stages across multiple GPUs and each GPU processes a different stage of the network sequentially [76]. The pipelining of stages can increase the throughput by pipelining multiple micro batches although it does not help in improving latency of a single batch. However, the sequential dependency of the pipeline stages introduces idle time in the pipeline which is referred as *bubbles*. These *bubbles* causes efficiency issues, and various pipeline scheduling algorithms have emerged to address the bubble issue. Popular instances of pipeline scheduling algorithms are *GPipe* [43], *PipeDream* [76], *TeraPipe* [64], *Zero Bubble 1F1B* [87], and *DualPipe* [113].

In *GPipe*, a mini-training batch is split into smaller microbatches for which a group of deep neural network layers is executed [43]. This approach caused some pipeline bubbles between stages. *PipeDream* improves upon *GPipe* by eliminating pipeline bubbles through an interleaved scheduling strategy, known as 1 Forward 1 Backward (1F1B) [76]. In this 1F1B pipeline scheduling, each pipeline stage alternates between executing a forward pass for a new micro-batch and a backward pass for an earlier one. This ensures that all devices remain fully utilized once the pipeline is warm, unlike *GPipe*'s schedule which incurs idle periods at the start and end of a batch. To maintain correctness, *PipeDream* introduces *weight versioning*, storing multiple copies of the parameters so that the backward pass of each micro-batch uses the same weight version as its forward pass. While this design significantly increases training throughput, it does so at the cost of additional memory overhead from maintaining multiple weight copies, as well as scheduling complexity. To address this memory increase, works in [15] and [77] address this issue through weight prediction, and a novel weight update scheme, respectively. Another following pipeline scheduling algorithm, *TeraPipe*, introduced a novel form of pipelining tailored to single-transformer architectures by performing pipelining across tokens rather

than micro-batches [64]. Despite these advances, there still remains the pipeline bubble issue. Conversely, Zero Bubble 1F1B proposed an idea to independently schedule the backward computation of two parts, backward for input and backward for gradient, which allow for a pipeline schedule with minimal bubbles. Further replacing the before-hand global state synchronization with a post validation, this algorithm allows to bypass synchronizations during the optimizer step and can result in zero bubbles in the pipeline [87]. Most recently, DeepSeek extended the Zero Bubble 1F1B schedule with bidirectional pipeline scheduling to introduce the DualPipe algorithm, which achieves greater computation–communication overlap and further reduces pipeline *bubbles* [69].

Tensor Parallelism (TP)

Tensor Parallelism (TP) enables the training of large models by distributing model parameters across multiple GPUs, thereby reducing the computational workload per device [95]. In contrast to PP, which partitions the model vertically into sequential stages distributed across devices, TP partitions the parameters of projection layers and distributes them across devices. Specifically, matrices involved in matrix multiplications are divided either column-wise or row-wise depending on the operation, followed by a communication step to synchronize partial results. More concretely, TP requires collective operations, such as `all-reduce`, to synchronize activations during the forward pass and gradients during the backward pass. While TP is effective to accommodate extremely large models by sharding the weight matrices, the associated communication overhead can become a significant bottleneck in bandwidth limited scenarios. Because of bandwidth constraints, a common practice is to use TP among GPUs within a single host node. Furthermore, increasing the degree of TP too high leads to too small matrix multiplications, which can be less efficient and may reduce overall resource utilization. Research efforts have addressed in these limitation leading to various communication overhead reduction techniques [112, 11, 94, 17], further discussed in Section 2.6.

Beyond this standard one-dimensional tensor parallelism (1D TP), several extensions have been proposed to improve scalability and communication efficiency. Two-dimensional tensor parallelism (2D TP) partitions tensors along both row and column dimensions to reduce communication overhead [119]. Building on this, two-and-a-half-dimensional tensor parallelism (2.5D TP) strikes a balance between memory usage and communication cost by combining aspects of 1-D and 2-D schemes [112]. It is termed as 2.5D as the algorithm contains special cases of both 2D and 3D matrix multiplication. Conversely, three-dimensional tensor parallelism (3D TP) generalizes these approaches by adopting a 3D parallel matrix multiplication approach, enabling efficient training of extremely large models on massive GPU clusters [11]. While these higher-dimensional schemes provide improved trade-offs between communication cost, memory efficiency, and scalability, one-dimensional tensor parallelism remains the most widely adopted form of TP in practice due to its simplicity and broad framework support. Therefore, we primarily focus on 1-D TP throughout this paper, and unless otherwise specified, TP would refer to the generic 1-D TP approach.

Expert Parallelism in Mixture of Experts (MoE)

Expert Parallelism (EP) is a parallelization strategy designed specifically for Mixture-of-Experts (MoE) architectures. The evolution of MoE from early works such as GShard [57] and Switch Transformer [29] to modern implementations including Mixtral [49] and DeepSeek [23] reflects the ongoing trend of leveraging sparse gating and distributed computation to scale large language models efficiently. In MoE architectures, a set of smaller multilayer perceptron (MLP) networks, referred to as experts, replaces a single large MLP. Tokens are dynamically routed to a sparse subset of experts [93], which reduces computation per token while enabling massive overall model capacity and scalable training.

In expert parallelism, these small experts are distributed across multiple GPUs and tokens are dynamically routed to the appropriate experts across GPUs [72]. For example, in DeepSeek-MoE-16B, the model includes 64 routed experts and 2 shared experts [23]. When EP=16, each GPU holds 4 routed experts and the 2 shared experts, totaling 6 experts per device. DeepSeek uses device-limited routing to reduce communication overhead—ensuring that the top-k experts selected for a token are located on a limited number of devices. This reduces cross-device traffic without significantly hurting model performance. For balanced utilization, the MoE router must distribute tokens evenly across experts to prevent scenarios where some experts are overused and others are starved. This is often achieved using load balancing losses or bias-based methods. An all-to-all collective communication is performed before the MoE layer to route tokens to the designated GPUs

where their corresponding activated experts reside. A second all-to-all communication is then performed at the end of the MoE layer to reorganize the tokens into their appropriate sequential order and redistribute them across GPUs according to the parallelization strategy of the succeeding layer.

2.4 Activation Parallelization

In LLM training, a large memory space is needed to store the input and output activations of the network layers. NeMo Framework provides effective activation distribution methods, which is critical in training LLM with a large sequence length or large per-GPU micro-batch size. [54] [12]

Sequence Parallelism (SP)

Sequence Parallelism (SP) is a parallelism technique introduced to efficiently train large language models on long input sequences. First formally presented in ACL 2023 by [54], SP addresses the memory bottlenecks encountered in traditional parallelism methods when handling long contexts. Unlike data parallelism, which replicates input batches across devices, sequence parallelism partitions the input along the sequence dimension, allowing activations to be distributed across devices while keeping the full model replicated. This enables more efficient memory utilization without altering the model’s architecture.

In practice, SP divides each input sequence into chunks that are processed in parallel across devices. Although SP still replicates model parameters and optimizer states across devices, similar to data parallelism, its unique ability to scale with sequence length makes it particularly useful for long-context training [61]. To maximize efficiency and scalability, SP is typically used in conjunction with tensor parallelism (TP), pipeline parallelism (PP), and data parallelism (DP).

Modern implementations include Megatron’s Tensor-Parallel Sequence Parallelism (TPSP), DeepSpeed-Ulysses’ Sequence Parallelism (UP, a.k.a. TPUP) [45], and Ring-Attention Context Parallelism (CP)—all designed to extend SP for training increasingly large models with longer context windows.

Context Parallelism (CP)

Context parallelism (CP) is a system optimization technique that improves the latency and scalability of LLM inference, particularly for long contexts. Without modifying the underlying dense attention algorithms, CP offers several advantages for long-context LLM inference [121]. For example, it is reported to take around 60 seconds to serve 128K context length or around 1200 seconds to serve 1M context length for Llama3 405B model with a single H100 GPU host of 8 GPUs making a suitable application scenario for CP [121].

CP uses sequence parallelization within attention layer. The input sequence is split into multiple chunks along the sequence dimension, with each chunk handled by a different GPU or processor. A ring communication is used to transfer Q or KV chunks between GPUs through point-to-point (P2P) communication. The communication happens in a ring network where each rank communicates with its predecessor and successor [71].

To tackle the scalability and efficiency issue of sequence parallelism, LoongTrain proposed a 2D-Attention mechanism termed as Double-Ring-Attention [39]. In particular, it combines head-parallel of DeepSpeed UP [45] and context-parallel techniques of Ring Attention [71] in a 2D parallelism fashion to improve scalability, p2p communication efficiency, and better compute-communication overlap.

Linear Attention Sequence Parallelism (LASP)

Modern generative AI architectures often combine traditional softmax attention with linear attention to handle longer context lengths efficiently. To accelerate both training and inference of such models, two versions of Linear Attention Sequence Parallelism (LASP) have been proposed [103, 104]. LASP-1 introduces a P2P ring-style communication scheme for both forward and backward passes across devices, either within a node or across multiple nodes. This approach optimizes the use of right-product kernel tricks in linear attention by exchanging only a single intermediate state, rather than both key and value states as in alternative methods. LASP-2 further improves communication and computation parallelism for training linear attention transformers on very long sequences. Unlike the first version, LASP-2 requires only a single AllGather operation on intermediate memory states, whose size is independent of sequence length, reduc-

ing communication overhead and enabling better overlap between computation and communication. This version has also been extended to support hybrid model architectures that encompass both attention and Mamba blocks.

2.5 Memory Optimization Techniques

Training and inference of large language models (LLMs) are limited not only by compute throughput but also by GPU memory capacity. As models scale to hundreds of billions of parameters, memory reduction strategies become essential. Three widely used approaches are activation checkpointing, redundancy elimination, and memory offloading, often integrated into modern training frameworks.

Activation Checkpointing. Checkpointing reduces activation memory by storing only a subset of intermediates during the forward pass and recomputing the rest during backpropagation [17]. Optimized scheduling methods such as Checkmate [46] and Tempo [5] balance recomputation cost with memory savings, enabling significantly larger models within fixed budgets.

Gradient Release. Gradient release is a layer-wise execution strategy to achieve constant memory usage [86, 116] by fusing backward computation and optimizer step. This approach compute gradient and take optimizer step layer by layer enabling early release of gradient memory of each layer and hence gradient of full model is not realized at once. This allows for efficient gradient handling and memory savings during large-scale neural network training.

Redundancy Elimination (ZeRO). Data-parallel training typically replicates optimizer states, gradients, and parameters across devices. ZeRO [88] partitions these components, with ZeRO-1 sharding optimizer states, ZeRO-2 extending to gradients, and ZeRO-3 extending to parameters. Though later stages increase communication overhead, ZeRO underpins large-scale frameworks such as DeepSpeed and has enabled trillion-parameter training.

Memory Offloading. Offloading transfers activations or model states from GPU to CPU or NVMe storage, effectively extending memory at the cost of latency. Early work (vDNN [90], SuperNeurons [114]) explored static/dynamic policies, while later systems (Capuchin [84], Mobius [31]) improved efficiency via adaptive scheduling and compression. ProTrain addresses this by autonomously optimizing memory, computation, and IO for efficient, expert-free training. Recently, ProTrain introduces an automated training system that coordinates memory, computation, and IO, achieving faster performance than existing frameworks without manual tuning [123].

System-Level Integration. Frameworks such as DeepSpeed, Colossal-AI, and Megatron-LM combine checkpointing, ZeRO, and offloading in unified systems. Recent work like FPDT [126] addresses fragmentation and inefficient allocation to further improve effective utilization.

Performance Implications. Beyond memory savings, these techniques can reduce communication overhead by lowering tensor or pipeline parallelism requirements, and increase batch size for higher kernel efficiency, thereby directly improving training throughput.

2.6 Communication Overlap Techniques

Co-optimization and overlap of computation and communication have become critical techniques for improving scalability and system efficiency of distributed deep learning. A major challenge in achieving such overlap is data dependency, which can be categorized into *weak* and *strong* forms. Weak data dependency occurs when the computation of one component can proceed concurrently with the communication associated with a different component. A common example is the all-reduce of gradients in data parallelism, where gradient synchronization for one mini-batch can be overlapped with the forward computation of another mini-batch. In contrast, strong data dependency arises when the next computation step requires strict completion of a communication phase. For instance, in Mixture-of-Experts (MoE) architectures, the

all-to-all routing of token embeddings must fully complete before expert computation. The feasibility of overlapping communication with computation depends directly on the type of dependency involved as strong dependencies introduce strict synchronization barriers and substantially limit overlap, often necessitating more sophisticated algorithms. To address these challenges, recent research proposes combined computation–communication algorithms that explicitly account for dependency patterns and employ fused kernels to reduce synchronization overhead. This section will begin with the communication volume comparison for different parallelization and then summarize communication optimization techniques.

Communication Volume Comparison. Different parallelization techniques require distinct collective communication patterns aligned with the chosen parallelization strategies. Table 3 reports the communication volume and collective operations per device for the forward pass and the attention layer:

- **DP:** No communication in the forward pass; gradient synchronization requires an all-reduce in the backward pass.
- **TP:** Communication volume scales as $\frac{TP-1}{TP}$, implemented with ring all-reduce collectives. For attention in Table 3, the communication cost is $bs\frac{d}{TP}$ over $(TP - 1)$ links, multiplied by four. The factor of four accounts for two contributions from reduce-scatter and two from all-gather, since each collective operation involves both sending and receiving the tensor.
- **CP:** Less communication volume than TP and typically realized with point-to-point or ring structures. Due to the limited bandwidth of inter-node communication, CP helps TP in inter-node communication. The factor of four in Table 3 arises from two contributions for the key tensor and two for the value tensor, with each tensor involving both a send and a receive operation.
- **TPSP:** Requires both reduce-scatter and all-gather collectives, with volume growing alongside the sequence partitioning factor. The attention’s communication volume for TPSP is the same as TP.
- **TPUP:** Requires four all-to-all exchanges attention layer, for query, key, value and output. The communication scales as $\frac{TPUP-1}{TPUP^2}$, which implies less communication volume per device for increasing number of GPUs. Here, we show the breakdown of communication volume for query, key, value, and output.

$$\text{Comm}_{\text{query}} = 2 \cdot \frac{s}{TPUP} \cdot \frac{ad_h}{TPUP} \cdot (TPUP - 1)$$

$$\text{Comm}_{\text{key}} = 2 \cdot \frac{s}{TPUP} \cdot \frac{kd_h}{TPUP} \cdot (TPUP - 1)$$

$$\text{Comm}_{\text{value}} = 2 \cdot \frac{s}{TPUP} \cdot \frac{kd_h}{TPUP} \cdot (TPUP - 1)$$

$$\text{Comm}_{\text{output}} = 2 \cdot \frac{s}{TPUP} \cdot \frac{ad_h}{TPUP} \cdot (TPUP - 1)$$

Hence, the total communication volume for each attention layer is the sum of these four components as shown in Table 3. By adding the components, we get the following:

$$\text{Comm}_{\text{attention}} = 4 \frac{(TPUP - 1)}{TPUP^2} \cdot bsd_h(a + k)$$

Overall, these results highlight distinct trade-offs: DP minimizes communication but maximizes weight redundancy, TP and TPSP provide better memory efficiency at the cost of collective communication overhead, and TPUP achieves compute and activation savings but incurs the highest communication complexity. CP distributed activation memory and computation which is beneficial for ultra-long context.

Table 3: Communication volume and collective operations per attention layer per device for different parallelism strategies during forward pass. Here, b is the batch size, s is the sequence length, d is the transformer hidden dimension, k is number of key-value heads, d_h is head dim.

Parallelism	Communication volume	Vol-	Collective Operation
DP	0		None in forward pass
TP	$\frac{4(TP-1)}{TP} \cdot bsd$		Ring AllReduce (ReduceScatter + Ring AllGather)
CP	$\frac{4(CP-1)}{CP} \cdot bskd_h$		Point-to-Point / Ring ($kd_h < d$ for GQA and 2 for each of send & recv)
TPSP	$\frac{4(TPSP-1)}{TPSP} \cdot bsd$		Ring AllGather / Ring ReduceScatter
TPUP	$\frac{4(TPUP-1)}{TPUP^2} \cdot bsd_h(a + k)$		All-to-All (4 per layer)

Data Decomposition. To alleviate the overhead stemming from inter-device communication, most commonly used computation-communication overlap strategy employ data decomposition techniques. This type of methods partition the data into smaller slices and then interleave the computation of one slice of the data to the computation communication of another slice using asynchronous communication. In this manner, computation and communication can proceed concurrently to reduce idle time of computing unit and improve overall resource utilization. This type of approaches are widely supported in large-scale AI infrastructure frameworks, including *Nvidia Megatron* and *Huawei MindSpeed*. In Megatron-LM, this approach is used for all-reduce in tensor parallelism(TP) [95] which is subsequently extended for all-gather and reduce-scatter in Tensor Parallelism with Sequence Parallelism (TPSP) [54]. Similarly, this type of merged computation-communication approach have been applied in the training of *Pangu Ultra* on Ascend NPUs [127]. Nevertheless, despite the advantages of such decomposition techniques, residual communication overhead persists. Specifically, while intermediate chunks benefit from overlapping communication with computation, the final chunk incurs unavoidable latency, often referred to as *tail overhead*. This limitation underscores the need for further optimization in balancing communication and computation in large-scale distributed training.

Communication Algorithm Decomposition. Collective communication decompose based algorithms decompose the collective operation into steps of different communication pattern, such as P2P, while decoupling the interdependency of the steps. This decomposition of algorithm into different communication pattern allows to loosen the strong data dependency in a manner to allow better overlap possibility than data decomposition based approaches. Notable that the decomposed algorithm also use data decompose (e.g., slicing) and schedule the computation and communication jointly for a better overlap than the approaches that decompose only the data. Example approach is the Decompose algorithm used in TPU platform [115]. A graph transformation is used for transforming the fine grained computation to semantically equivalent graph with decoupled asynchronous instruction scheduling that allow higher overlapping. This approach breaks down blocking collective communication into a sequence of single-step, non-blocking collectives. It also decomposes computation operations into finer-grained tasks that can be overlapped, then combines them in a simple sequence to accumulate partial results.

Kernel Fusion. Central to the computation-communication overlap is efficient kernel fusion where both the computation and communication of a layer is implemented in a single kernel utilizing some overlap strategy. The fused kernel may implement data decomposition or communication decompose based overlap approach in a single kernel. Early work on kernel fusion include CoCoNet [47] which provided a domain specific language(DSL). They developed a compiler-based system that facilitates generating co-optimized custom computation and communication kernels with hardware specific optimized implementations for target specific topology, and data sizes. Followingly, various kernel frameworks and libraries has evolved over time [63, 13]. A recent framework, Concerto, presented a compiler framework that can automatically optimize and schedule communication along with auto-decomposition to create overlap opportunity for critical

communication [19]. Another recent framework is TileLink, which addresses the challenges of operator decomposition and kernel fusion in terms of performance and complexity by decoupling communication and computation and linking them through tile-centric primitives [136]. Multi-gpu kernels are also emerging as a promising direction. A recent framework in this direction is Parallel Kittens that allows to easily write fast computation-communication overlapped multi-GPU kernels supporting data, tensor, sequence, and expert parallelism [102].

Communication Optimization. Another direction uses communication optimization integrated with parallelization strategy rank assignments and work scheduling and automated tuning of communication parameters. One example of such approach is implemented in *MiCS* that introduces a data-parallel training system to minimizes communication overhead by reducing communication scale through scale-aware partitioning and hierarchical communication [134]. Another similar example is AlpaComm [140] which proposed a pipelining schedule named *eager-1F1B* extending the *1F1B* [76] and developed communication library, AlpaComm, that supports integration to the parallelization library Alpa [135].

Automated tuning. Automated tuning based approaches rely on automated search of optimal low-level performance sensitive parameters for communication. An example of such approach is AutoCCL, which implemented automated tuning method on top of NCCL to search for optimal low-level performance sensitive parameters using a divide-and-conquer algorithm [118].

3 Hybrid Systems

Training and inference of large scale language models at trillion-parameter scale requires more than a single form of parallelism, as strategy brings unique advantages and limits when used in isolation. To overcome these bottlenecks, hybrid approaches has become common practice in industry, often referred to as multi-parallelism. This section discusses most common multi-parallelism strategies, focusing on 3D and 4D parallelization, and popular frameworks that enable their practical deployment.

3.1 Multi-Parallelism

Different parallelization strategies offer distinct advantages by distributing weight memory, activation memory, and computation across groups of devices. Efficient training and inference of large-scale models must address challenges in memory capacity, bandwidth, and compute requirements, while meeting task-specific goals such as high throughput or low latency. These challenges are best addressed through tailored combinations of strategies that balance trade-offs. Comparative analyses show that hybrid parallelism achieves greater speedups than single-device training [9], and recent large-scale models further validate the effectiveness of hybrid approaches [38, 121].

3D Multi-Parallelism. 3D multi-parallelism combines data parallelism (DP), pipeline parallelism (PP), and tensor parallelism (TP) by assigning GPUs to these respective parallel groups [89]. For a total of N GPUs, with N_{DP} , N_{PP} , and N_{TP} GPUs allocated to DP, PP, and TP groups respectively, the relationship is given by $N_{DP} \times N_{PP} \times N_{TP} = N$. The combination of multi-parallelism is designed to optimize resource allocation, e.g., allocating accelerators, to achieve an optimal trade-off that integrates the complementary benefits of different parallelization strategies. Integrating these three orthogonal strategies with an optimal rank group assignment enables efficient training of models with hundreds of billions to trillions of parameters that would otherwise exceed the capacity of single parallelization techniques. We present an example of 3D multi-parallelism in Figure 4. This example of 3D multi-parallelism considers $N = 8$ GPUs with GPU ranks $0, 1, \dots, 7$ and the parallelization strategy considers $(N_{DP}, N_{PP}, N_{TP}) = (2, 2, 2)$. This $(2, 2, 2)$ grouping of 8 GPUs is for example purpose only, any combination that meets $N_{DP} \times N_{PP} \times N_{TP} = N$ is valid where the grouping strategy is an important concern for parallelization design, detailed explanation is presented in Section 4. Hence, the most outer parallelization is DP with the DP group containing two replica of PP,TP groups with GPU ranks $0, \dots, 3$ and ranks $4, \dots, 7$. Within each DP group, there are two identical PP groups. Each PP group contains a TP group of two GPUs. Corresponding collective communication operation happens within the GPU ranks of each parallelization groups.

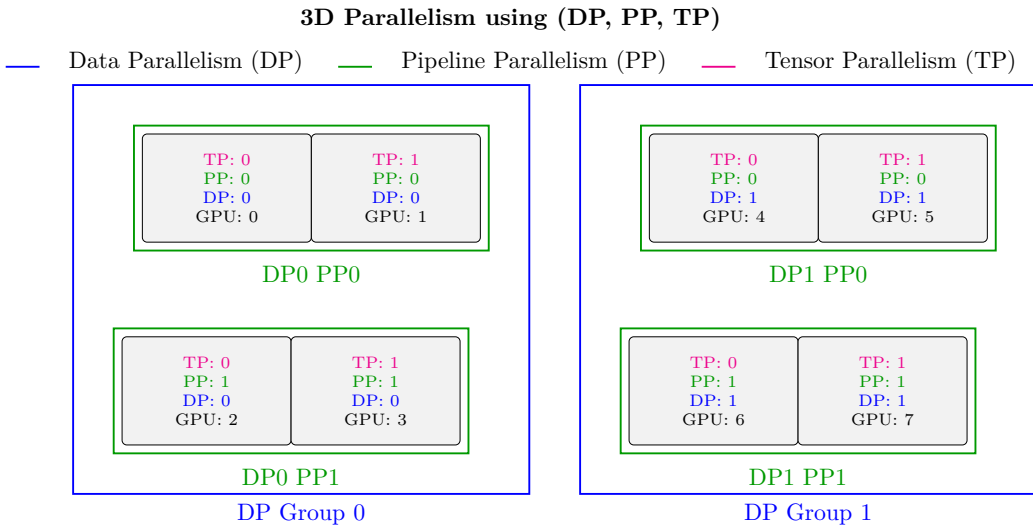


Figure 4: Illustration of 3D parallelism showing DP, PP, and TP groupings for 8 GPUs with (DP,PP,TP) as (2,2,2). The ranks assignments for parallelization groups here are DP: [[0,1,2,3], [4,5,6,7]]; PP: [[0,2], [1,3], [4,6], [5,7]]; TP: [[0,1], [2,3], [4,5], [6,7]].

4D Multi-parallelism 4D multi-parallelism extends 3D multi-parallelism by adding context parallelism (CP) as another orthogonal parallelization strategy [38]. For a total of N GPUs, with N_{DP} , N_{PP} , N_{TP} , and N_{CP} GPUs allocated to DP, PP, TP, and CP groups respectively, the relationship is given by $N_{DP} \times N_{PP} \times N_{TP} \times N_{CP} = N$. This extension to 4D parallelism includes CP to support for ultra-long sequences with extremely large models. Since the parallelization ranks assigned to different GPUs are more sophisticated compared to 3D parallelism, we also present an example of 4D multi-parallelism in Figure 5. This example of 4D multi-parallelism considers $N = 16$ GPUs with GPU ranks 0, 1, ..., 15. The parallelization strategy considers $(N_{DP}, N_{PP}, N_{TP}, N_{CP}) = (2, 2, 2, 2)$. Similar to the example of 3D parallelism, here also we present this $(2, 2, 2, 2)$ grouping of 16 GPUs in favor of simplicity and for example purpose only, any combination that meets $N_{DP} \times N_{PP} \times N_{TP} \times N_{CP} = N$ is valid as long as it meets other constraints, e.g., memory of individual GPUs. Hence, the most outer parallelization is DP with the DP group containing two replica of PP, TP, CP groups with GPU ranks 0, ..., 7 and ranks 8, ..., 15. Within each DP group, there are two identical PP groups, e.g., GPU ranks 0, ..., 3 and 4, ..., 7 within the first DP group. Each PP group contains a TP, CP group of four GPUs. For example the TP groups within the first PP group of the first DP group is 0, 1 and 2, 3 where CP group is 0, 2 and 1, 3. This rank assignment considers the outer to inner ordering of the parallelization strategies used. Corresponding communication operation happens within the GPU ranks of each parallelization groups.

Communication Optimization in Multi-parallelism. In a distributed setting, communication can become a bottleneck when compute devices need to wait for certain dependent communication to be complete. To address this challenge, recent hybrid algorithms also focus one overlapping collective communications, such as reduce-scatter, all-gather and all-reduce , discussed in detail in Section 2.6. When multiple parallelization strategies are combined in a hybrid parallelization for large scale models, it brings challenges of multiple collective communication patterns appearing at different part of forward and backward computation graph. Centauri [14] introduces a training system that enhances training efficiency and communication overlap in LLM training by partitioning collective communications into intra-node and inter-node group communications. It employs a hybrid parallelization scheduling approach that optimizes overlapping across operation, layer, and model levels. At the operation level, coordinating communication among partitioned groups facilitates fine-grained overlapping, while adaptive scheduling and model-level optimization maximize overlap across forward, backward, and model update phases in hybrid parallel configurations. For PP, traditional solution is to use a Virtual Pipeline (VP) which uses a virtual pipeline of generally 2 stages within each pipeline stages. This allows for the communication of pipeline stages of the half of the micro-batch to

4D Parallelism using (DP, PP, TP, CP)

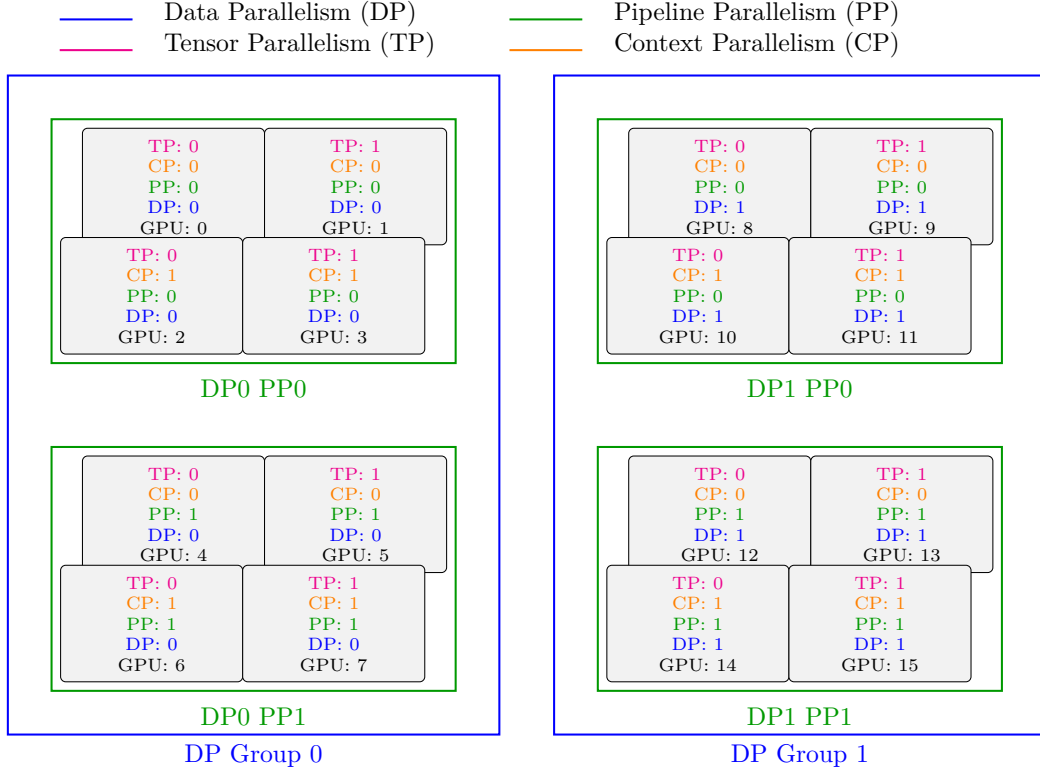


Figure 5: Illustration of 4D parallelism showing DP, PP, TP, and CP groupings for a cluster of 16 GPUs with (DP, PP, TP, CP) as $(2, 2, 2, 2)$. The ranks assignments for parallelization groups here are DP: $[[0, 1, 2, 3, 4, 5, 6, 7], [8, 9, 10, 11, 12, 13, 14, 15]]$; PP: $[[0, 1, 2, 3], [4, 5, 6, 7], [8, 9, 10, 11], [12, 13, 14, 15]]$; CP: $[[0, 2], [1, 3], \dots]$; TP: $[[0, 1], [2, 3], \dots]$.

happen while the other half is doing computation. Prominent libraries, such as Megatron-LM uses compute-communication overlap strategies for reduce-scatter and all-gather by chunking the data and overlap compute and communication of independent chunks [82].

3.2 Frameworks

The foundational work on distributed training of large models emphasized parallelism strategies to partition model computation across multiple devices. Table 4 presents a shortlist of most notable industry-grade frameworks.

Megatron-LM and NeMo. Megatron-LM pioneered tensor-model parallelism by splitting weight matrices across GPUs, later combining this with pipeline parallelism to achieve scalability for trillion-parameter models [95]. Megatron-LM and NeMo are two popular framework supporting multi-parallelism. Megatron-LM is widely recognized as the backbone of trillion-parameter LLMs such as GPT-3 and BLOOM, offering comprehensive support for data, tensor, pipeline, sequence, and expert parallelism. Its strength lies in enabling hybrid combinations of these strategies, allowing fine-grained profiling and tuning across GPU clusters to maximize throughput and memory efficiency. However, its complexity and reliance on NVIDIA hardware can limit accessibility for non-GPU ecosystems. NeMo complements Megatron-LM by focusing on multimodal and speech models, supporting tensor, pipeline, and sequence parallelism.

DeepSpeed. DeepSpeed focused on memory-footprint reduction with multi parallelism. It introduced the Zero Redundancy Optimizer (ZeRO) and gradient partitioning to minimize memory overhead, alongside mixed-precision training for efficiency at scale [89]. DeepSpeed supports data, tensor, and pipeline parallelism, with robust expert parallelism (MoE) capabilities, making it highly effective for hybrid parallelization strategies. Its profiling and tuning tools are tightly integrated with PyTorch, simplifying adoption across research and enterprise environments.

MindSpeed-LLM. MindSpeed-LLM presents a distributed training framework tailored for the Ascend AI platform [7, 66]. It supports large-scale language model development through multi-parallelism strategies such as tensor, pipeline, sequence, and expert parallelism. By integrating these dimensions, MindSpeed-LLM enables efficient 3D and 4D parallel training optimized for Ascend NPUs. This platform also include MindSpeed-RL [30] for LLM post-training and Mind-VL [16] for multi-modal LLMs.

SageMaker and Neuron. Amazon SageMaker Model Parallelism provided a cloud-native implementation of tensor, pipeline, and data parallelism, making large-scale model training accessible in industrial environments [52]. This framework presented an effective solution for distributed training and inference, even though it require to manually configure the combination of different parallelization groups. The Neuron SDK presents suitable system for custom hardware chips, supporting tensor, sequence, and data parallelism. Neuron excels in profiling and hardware-aware tuning, but expert parallelism remains constrained.

Miscellaneous. PaddlePaddle is a full-stack deep learning framework with support for data and model parallelism with distributed training and provides a rich ecosystem of domain-specific libraries for vision, language, and scientific applications [6]. It extended memory optimization direction by incorporating hybrid parallelism that allow sharding memory across diverse hardware environments. It is widely used as more of a general-purpose platform than a specialized LLM training engine. In another direction of adopting multiple parallelization strategies and dynamic transition among them based on workload includes dynamic hot switching [34] and resharding [101]. HotSPa introduced a dynamic hot switching approach for training which apply different parallelism strategies within a single mini-batch by using their graph compiler and hot switch planner [34]. The graph compiler generates distributed computation graph while the hot switch planner heuristically determines a plan to accelerate between a pair of parallelism strategies. Seesaw, on the other hand, introduced an LLM inference engine that allows for reconfiguration of parallelization strategies from prefill to decode [101]. The method is termed as dynamic model resharding which adopts different parallelization to address unique workload challenges of prefill and decode.

Together, these frameworks illustrate the diversity of approaches to hybrid parallelism beyond the industry leaders. They serve as important complements and experimental testbeds, advancing ideas in profiling, tuning, and workload balancing that may eventually influence the mainstream frameworks dominating large-scale LLM training. Despite the richer feature sets, current distributed frameworks still require manual configuration of parallelization and memory-optimization strategies, leaving model developers with a complex search space to achieve peak efficiency.

Table 4: Industry-grade frameworks supporting multi-parallelism (DP, TP, PP, SP, EP/MoE)

Framework	Developer Company	DP	TP	PP	SP	EP/MoE
Megatron-LM [95]	NVIDIA	✓	✓	✓	✓	✓
MindSpeed-LLM [7]	Huawei	✓	✓	✓	✓	✓
DeepSpeed [89]	Microsoft	✓	✓	✓	Limited	✓
Amazon SageMaker [52]	Amazon Web Services (AWS)	✓	✓	✓	Limited	Limited
AWS Neuron [2]	Amazon Web Services (AWS)	✓	✓	✓	✓	Limited
NVIDIA NeMo [81]	NVIDIA	✓	✓	✓	✓	Limited

4 Workload Parallelization Design

4.1 System Design Implications

An optimized parallelization system design for large scale models, e.g., LLMs, training and inference has profound implications for scalability and efficiency. System level optimization makes the scaling to large scale models and training them on a large cluster and deployment on inference system efficient. Designing such a parallelization system for large scale models requires addressing the distinct requirements for training and inference system optimization as discussed below.

Commonly Used Metrics. Before delving deeper into system design implications, it is due to introduce some commonly used metrics and terms in describing AI workload performance characteristics.

Time To First Token (TTFT). This metric measures how quickly the model's output generation starts after providing a query [80]. Low waiting times for a response are essential in real-time interactions, such as chat applications. This metric is driven by the time required to process the prompt and then generate the first output token. Hence, TTFT is primarily determined by prefill time (i.e., prompt processing and attention state initialization), while system overhead (including tokenization, detokenization, networking, scheduling, and framework delays) constitutes secondary factors.

$$TTFT \approx T_{\text{prefill}} + T_{\text{system_overhead}}$$

Time Per Output Token (TPOT). This metric measures the time to generate each output token after the prefill time. This metric is also known as *Inter-Token Latency (ITL)* [80]. This metric corresponds with how each user will perceive the "speed" of the model. TPOT (a.k.a. ITL) is define below:

$$TPOT = \frac{e2e_latency - TTFT}{\text{Total_output_tokens} - 1}$$

Latency. The overall time it takes for the model to generate the full response for a query. Overall response latency can be calculated as below:

$$\text{Latency} = TTFT + TPOT \cdot (\text{Total_output_tokens} - 1)$$

Throughput. Throughput in large language models (LLMs) is the rate of tokens or samples processed per unit time. This is also known as Token Per Second (TPS) [80]. During training it measures hardware efficiency as the number of training samples or tokens per second, while during inference it measures responsiveness as the number of output tokens per second across users. In both cases, it counts the number of tokens per second. Formally,

$$\text{Training Throughput} = \frac{\text{Total training tokens}}{\text{Training time}}$$

$$\text{Inference Throughput} = \frac{\text{Total output tokens}}{\text{inference time}}$$

Arithmetic Intensity. The *Arithmetic Intensity* is defined as the ratio of total flops of an operation to total memory access. It is a characteristics of an operator.

$$\text{Arithmetic Intensity (A.I.)} = \frac{\text{Total FLOPs}}{\text{Total Bytes Transferred}} \quad (1)$$

Hardware Ridge Point. The *Hardware Ridge Point* is defined as as hardware characteristics with the ratio of peak flops to peak memory bandwidth.

$$\text{Ridge Point (I)} = \frac{\text{Peak FLOPs}}{\text{Peak Bandwidth}} \quad (2)$$

$$\text{Operation is } \begin{cases} \text{Compute-bound,} & \text{if A.I.} > I, \\ \text{Memory-bound,} & \text{if A.I.} < I. \end{cases}$$

Compute Bound. These operations does not need to wait for memory access.

Memory Bound. These operations are bottle-necked by memory access and computing unit needs to wait for memory access to be completed. Hence computing capability of the hardware is idle during that time.

Bandwidth Bound. The *Bandwidth Bound* scenario also can happen in distributed scenario when the distributed operator needs to wait for communication to be completed for synchronization purposes. This also leads to idle time in computing unit.

Model Flops Utilization. The *Model Flops Utilization* (MFU) have been used in the literature as a measure of Flops utilization [21] and its unit is percentage.

$$\text{Model FLOPs Utilization (MFU)} = 100.0 \cdot \frac{\text{Achieved FLOPs}}{\text{Peak FLOPs}} \quad (3)$$

Most of the operators or computations of transformer based models have higher arithmetic intensity during training and prefil phase. As a result, they are mostly compute bound and hence can utilize hardware peak flop capacity leading to high MFU. On the other hand, most of the operations of transformer models in the decode phase of LLMs have low arithmetic intensity and often memory bound resulting to low MFU. In general, high MFU results in high throughput. So, system optimization needs to consider individual stage workload characteristics to achieve optimal result in target metrics.

Problem Formulation. The problem of hybrid parallelization system design can be formally defined as allocating computing accelerators of a given cluster across a set of parallelization strategies in order to optimize overall system performance while satisfying memory constraints and meeting service level objectives, such as maximizing throughput, minimizing latency and ensuring the highest accuracy. So, given a Model M , cluster W , and a set of parallelization strategies S_l for layer l , the high level formulation of the problem is,

$$\begin{aligned} & \text{optimize} \quad \text{ServiceLevelObjective}(M, W, S_l) \\ & \text{subject to} \quad \prod_{i=1}^n w_i = W \quad \forall i \in S_l \end{aligned} \quad (4)$$

where $S_l = \{DP, PP, TP, \dots\}$. We omit the detailed attributes of M and W , e.g., model parameters and cluster configurations here in favor of simplicity. The model attributes to consider may include model parameter, depth, hidden size, layer type etc. The cluster configuration may include the memory capacity of each node, peak flops, memory access bandwidth, cluster topology, intra-node and inter-node bandwidth. For example, we may consider a system using a cluster W with N_w accelerators and employing $S_l = \{DP, PP, TP, CP\}$ as a 4D parallelization strategy for training a transformer model. Let w_i denote the number of accelerators allocated to parallelization strategy i . Then, the total number of accelerators satisfies the relation $w_{DP} \times w_{PP} \times w_{TP} \times w_{CP} = W$ while meeting the memory constraints and maximizing the throughput and maintaining operators accuracy.

The service level objective is generally different for training and inference with managing memory and communication overhead being a shared criteria. For training, the primary concern is how fast the training can be completed while inference requires rapid model execution with reduced computational overhead to

deliver fast responses. In other words, training necessitates high throughput as a service level objective. This demands strategies that optimize computational load distribution and minimize synchronization delays. In contrast, time for individual queries matter during inference, as users expect quick replies. This necessitates prioritizing low latency and minimal memory footprint, often requiring a trade-off with throughput. Although achieving both high throughput and low latency is ideal, trade-offs are common. For instance, lower latency can imply higher throughput, but the reverse is not always true. An inference system may need to use a large batch size to increase throughput; however, this can result in higher latency. Therefore, latency is often prioritized when making an optimal trade-off with throughput, particularly in interactive chat based applications [107]. The optimal partitioning strategy also changes when trading off between latency and throughput in addition to the model size, sequence length and cluster size considerations [85].

For example, the $ServiceLevelObjective(M, W, S_l)$ may be to minimize latency for inference and maximize throughput for training. A *Service Level Objective (SLO)* also defines the target performance level for a particular metric, setting the standard for what is considered acceptable service quality [10]. For instance, an SLO for *Time To First Token (TTFT)* might specify TTFT below T_{thres} milliseconds. SLOs are typically part of a broader *Service-Level Agreement (SLA)* between a provider and its users. Mathematically, the SLO for training can be,

$$P(\text{TPS}) \geq \tau$$

which implies that the throughput for training should be at least τ .

Similarly, the SLO for the inference is often expressed as percentile constraints on performance metrics [26, 79]:

$$P_q(M) \leq T$$

where $P_q(M)$ is the q -th percentile of metric M (e.g., latency), and T is the threshold. A particular instance can be,

$$P_{95}(\text{TTFT}) < 200 \text{ ms}$$

meaning that 95% of requests must have a Time To First Token under 200 milliseconds.

Parallelization Assignment. The assignment of accelerator to optimize service level objective conventionally considers grid search based approach. This type of approaches begin with considering search space of various combination of parallelization strategies spanning the accelerators on the given cluster. Then they employ the roofline model as a manual analytical framework to assess and compare parallelization strategies. By mapping arithmetic intensity against hardware ceilings such as memory bandwidth and peak floating-point throughput, the roofline model enables researchers to determine whether workloads are compute-bound or bandwidth-bound, guiding choices among data, model, pipeline, and hybrid parallelization approaches [117, 122]. Extensions such as multi-dimensional and distributed roofline models have further supported performance analysis of deep learning workloads, offering insights into tensor operations, communication costs, and scaling inefficiencies across heterogeneous clusters [74]. More recently, roofline-based analysis has been applied to large language models (LLMs), highlighting its role in forecasting inference latency, training efficiency, and communication overheads in distributed GPU clusters [55, 44, 130].

Pruning of the search tree is a traditional way of optimizing the grid search. The criteria used to prune the search space includes memory constraints and cluster topology for communication bottleneck consideration for parallelization strategies. Despite the emergence of automated ML-driven predictors, the roofline model remains a foundational manual approach for workload characterization and parallelization design in LLM training and inference. While this conventional manual approach has been foundational, the future of workload design is increasingly optimistic, with emerging auto-parallelization strategies promising to automate bottleneck detection and parallelization decisions at scale. We include a comprehensive discussion on emerging auto-parallelism strategies in Section 4.3.

Major challenges in hybrid parallelization for large-scale AI models requires careful optimization of communication overhead, computation overlap, memory efficiency, and bandwidth constraints to balance training throughput and inference latency. The inter-node bandwidth of the cluster topology often limits the TPSP group size. DP requires optimized gradient synchronization necessitating homogeneous bandwidth among the participating ranks. CP can be efficient when there is a good overlap of the ring communication with computation. The choice of TPSP, DP, and PP ranks directly impacts performance, requiring careful placement to align with intra-node and inter-node bandwidth constraints. Again the choice of number of accelerators in each parallelization is another important factor to performance. A well-designed hybrid system strategically integrates these parallelization methods to maximize scalability, throughput, and low-latency inference performance for AI workloads.

4.2 System Design Considerations

Parallelization Trade-Off Considerations. The primary consideration of multi-parallelism strategies depends on the complementary benefits and trade-offs across different forms of parallelization. Different parallelization strategies offer unique advantages making their integration into a hybrid system to consider for complementary benefits while optimizing for specific service level demand, e.g., training or inference performance. The effectiveness of multi-parallelism lies in balancing these trade-offs. Toward this end, we summarize them to establish the foundation for a systematic comparative analysis of parallelization strategies. A curated summary of complementary benefits and trade-offs of prominent parallelization strategies are presented in Table 5. The analysis includes summary on scalability by splitting data across devices (DP), reducing memory and compute per device by distributing model parameters (TP), and pipeline micro-batches to improve throughput (PP). Corresponding to the current discussion of the benefits, DP and PP directly impacts throughput, TP/TPSP impacts latency, PP, TP, CP impacts memory.

By strategically combining these parallelization methods with an optimal resource allocation to each group, a hybrid approach can achieve an optimal balance between compute distribution, memory efficiency and communication overhead reduction. As a result, systems can be optimized for a scalable and high-performance AI systems for specific service level demands. To complement the summary of DP, TP, and CP, we also provide a theoretical validation by deriving the FLOPs, memory consumption (including both weight and activation memory), and communication overhead for the GQA, MLP, and Mamba blocks in Section 5.

Memory Constraint. The parallelization group allocation search space generally begins with considering the memory constraints of the accelerators on the cluster. So, the first step filters the potential set of parallelization group combinations that allow to fit the model parameters, activation memory, and additional memory requirements on the given cluster. The additional memory requirements considered include gradient and optimizer state for training and transformer k/v-cache for inference. An important consideration here is the impact of different parallelization strategies on total memory footprint. The DP groups can reduce memory by using Zero optimizer which shards optimizer states, gradient and parameters among the accelerators in a DP group. However, there might still problem to fit a large model with DP only. PP groups can further reduce memory by vertically sharding the model layers among the PP groups in a pipeline. TP groups allow to reduce both weight and activation memory by distributing the parameter and compute of a layer. However conventionally it is used withing same node with high bandwidth connection due to the need for collective communication. In scenarios for very long sequence, where activation memory is the critical challenge compared to parameter memory, CP is a useful technique. In particular, the size of the model plays an important role in this choice as small model with long sequence length benefits from CP more than a large model with long context length.

Flops Utilization. Flops Utilization is a critical metric of efficient resource allocation across distributed clusters. Model Flops Utilization (MFU) captures the alignment between the model’s computational graph and the hardware execution pattern. Both are essential for maximizing training throughput and minimizing cost per token. Arithmetic intensity based roof-line model has been widely used and is a dominant approach til date to analyze a parallelization group assignment under service level requirements, e.g., sequence length and maximum workload meeting memory constraints, e.g., batch size. The roof-line model works by catego-

Table 5: Pros and cons of different distributed parallelism strategies.

Strategy	Pros	Cons
Data Parallel (DP)	<ul style="list-style-type: none"> Simple to implement Boosts throughput by distributing training data across devices Minimal communication during forward/backward pass 	<ul style="list-style-type: none"> Requires full model replica on each device High gradient synchronization overhead Inefficient memory usage for very large models
Tensor Parallel (TP)	<ul style="list-style-type: none"> Splits weight and activation memory across devices Enables training of very large models High compute efficiency when scaling within a node 	<ul style="list-style-type: none"> Heavy communication overhead across layers Best efficiency requires high bandwidth connectivity (e.g., NVLink, Infiniband) Harder to implement compared to DP
Context Parallelism (CP)	<ul style="list-style-type: none"> Reduces activation memory by partitioning sequence length dimension Can complement TP/DP Helps scale attention-heavy models to support ultra-long sequences especially in multinode settings 	<ul style="list-style-type: none"> Load balancing is a critical challenge requiring sophisticated algorithms Requires sequence reassembly for some operations Requires replica of weights similar to DP
Expert Parallel (EP)	<ul style="list-style-type: none"> Efficient scaling for Mixture-of-Experts High parameter count without proportional compute Flexible load balancing with routing 	<ul style="list-style-type: none"> Complex routing and load balancing Communication overhead from token routing Training instability if experts are imbalanced
Pipeline Parallel (PP)	<ul style="list-style-type: none"> Splits model layers across devices Reduces memory footprint per device Good for scaling long/deep networks 	<ul style="list-style-type: none"> Pipeline bubbles reduce efficiency Imbalanced stage partitioning causes idle time More complex scheduling

rizing operations under given workload as memory bound or compute bound where compute bound implies better flops utilization.

To improve flops utilization, both the model design and parallelization strategy design should consider for operations to be compute bound. Different parallelization strategies affect Flops Utilization in distinct ways. Data Parallelism (DP) scales batch processing across devices which typically increase Flops utilization by allowing larger batch size. Pipeline bubbles in Pipeline Parallelism (PP) may reduce flops utilization requiring large batch sizes to saturate the pipeline and sophisticated algorithms with less bubbles. Tensor

Parallelism (TP) splits tensor operations such as matrix multiplications across devices which can reduce latency. However, larger TP group can lead to too thin compute load resulting in lower arithmetic intensity and also demand high-bandwidth interconnects to avoid communication bottlenecks. Context Parallelism (CP) which is considered for accommodating ultra long sequences may increases orchestration complexity for synchronizing peer-to-peer communications for improved flops utilization. Careful considerations for these aspects are critically important for a good parallelization strategy allocation.

Furthermore, hyper-parameters such as batch size, sequence length, and micro-batch size directly influence Flops Utilization. Larger batch sizes improve flops utilization increasing arithmetic intensity. Longer sequences increase FLOPs per token which can enhance flops utilization. In pipeline parallelism, larger micro-batches reduce idle time. In grid search-based parallelization planning, Flops Utilization serves as a primary scoring criterion. Candidate configurations are first filtered for feasibility (e.g., memory fit), then ranked by estimated MFU for maximum possible workload. Yet there are some specific consideration regarding system design for training vs. inference.

Consideration in Training. In the training phase of large language models (LLMs), the selection of optimal parallelization strategy groups is guided by success metrics and service-level objectives that balance performance, scalability, and resource efficiency. In addition to general considerations of Flops Utilization, key metrics specific to training include training throughput (tokens/sec) and time-to-target-loss. These success metrics collectively reflect the system’s ability to meet convergence goals within hardware and budget constraints. These metrics are evaluated during parallelization plan search. Allocation of groups of accelerators in the cluster to parallelization strategies such as data, tensor, and pipeline parallelism are assessed for their impact on latency, memory footprint, and inter-device communication. DP enhances throughput by distributing training data across multiple accelerators while PP improves throughput by processing micro-batches in a staggered manner. TP efficiently distributes computation across GPUs while TPSP further optimizes LayerNorm with efficient sequence-level computations. A hybrid system leveraging DP for scale, TP for computational efficiency, and PP for pipelining can significantly enhance model training throughput while reducing synchronization delays. Grid search frameworks incorporate these objectives into scoring functions to ensure that selected configurations satisfy feasibility constraints as well as optimize for training efficiency and reliability under real-world deployment conditions [78, 68].

Considerations in Inference. Considerations of success metrics and service-level objectives (SLOs) for the allocation of parallelization strategies to accelerators within a compute cluster during large language model (LLM) inference deployment generally include latency, throughput, and cost-efficiency. Unlike training, where the primary objective is to maximize throughput (tokens/second), inference emphasizes low latency to ensure real-time responsiveness to individual queries. Inference systems generally prioritize low latency, potentially trading off some throughput to meet interactive performance requirements. For instance, larger batch size leads to high throughput with high latency while small batch size leads to low throughput and low latency scenario. As a result an optimal balance with a trade-off is often considered.

During inference, TP is particularly effective for compute-intensive layers, as it enables parallel execution of operations within a single layer across multiple devices. This approach enhances computational throughput by distributing workloads at a fine-grained level. In contrast, PP reduces memory footprint by staging execution across sequential model partitions. Data parallelism (DP) does not directly reduce the latency of individual queries. However, DP can still be beneficial in high-throughput environments serving highly frequent queries, where batching and distributing queries across replicas to improve overall throughput is also important. Competitive trade-offs arise when selecting between TP and PP: TP offers superior compute saturation but demands high-bandwidth interconnects, while PP alleviates memory pressure but may underutilize devices during sequential execution. State-of-the-art hybrid strategies balance memory constraints with latency requirements combining these strategies [4, 85]. Optimal allocation strategies are typically determined through heuristic or grid search methods that evaluate candidate configurations against service-level objectives (SLOs), ensuring that the deployed plan satisfies latency constraints and maximizes accelerator utilization.

By carefully designing a hybrid parallelization system that combines different parallel strategies, AI models can achieve high efficiency, scalability, and performance for both training and inference. The right balance of parallelism ensures that training workloads maximize throughput, while inference remains low-latency and memory-efficient, making modern LLM systems robust and adaptable to growing computational demands.

4.3 Toward Auto Parallelization

Auto-parallelism is an automated method that selects and applies efficient parallel execution strategies for a neural network model on a specific hardware cluster [65]. It can be formulated as an optimization problem: choosing the best combination of available techniques—including parallelism strategies and memory footprint reduction methods—while ensuring that the memory usage stays within the hardware capacity. The inputs to this problem are an LLM model, a target GPU hardware, and a global batch size. The search space of possible configurations is extremely large; for example, an 80-layer transformer can already yield up to the order of 10^{125} possible configurations due to the large number of parallel and memory optimizations (Figure 5 in [139]). Auto-parallelism systems typically address this by building and optimizing a cost model tailored to the model–hardware setup, then deploying the strategy using a runtime system that maps tasks to devices. These techniques automatically divide computation and memory across devices, optimizing for training throughput, prefill latency, and low-latency decoding. This section discusses the motivation for auto-parallelization, reviews the successes and limitations of state-of-the-art approaches, and highlights remaining challenges and future directions. Our focus is on the most recent advances, while a more comprehensive overview of earlier works is available elsewhere [65]. We primarily aim to provide a comparative discussion of modern auto parallelization approaches and to identify key opportunities for future research.

Neural scaling law contributed to significant increase in model size and training data which has outgrown the capability of single compute device [51, 42]. In response, parallelization strategies has been appeared which brings diverse advantages and solve some particular aspects of the whole problem [95, 76]. Training and inference efficiency of the frontier models require to combine multiple parallelism method in a hybrid approach where scaling performance relies on properly tuning the combination of the parallelism strategies in a multi dimensional parallelism [120, 97, 98, 38]. This type of hybrid combination also requires to use large clusters of heterogeneous hardware, such as GPUs, TPUs, NPUs [50]. The hardware’s are connected with different bandwidths and different topology requiring careful assignment of parallelization ranks to hardware. This scenario makes the manual engineering of finding optimal parallelization strategy tedious and time consuming or even impractical for industry grade models.

Efficiency also requires to consider training and inference separately as well as the prefill and decode phase of the inference. The search space of possible combinations also grow exponentially with parallelization techniques and cluster size. Moreover, the complexity of the problem as becoming more sophisticated as recent proposal also include in-device parallelization in addition to inter device parallelization [24]. Furthermore, this is not just a once a time work, change in hardware require repetition of the work tuning on different hardware types. This makes the manual analysis, estimate or cost model estimate for different configuration quite impractical.

The need for automating parallelization is crucial for both model developers and infrastructure providers. From the model developer’s perspective, large-scale models demand efficient utilization of computation and memory across distributed devices to reduce training time and cost. Meanwhile, hardware vendors and infrastructure providers must ensure that their systems support flexible parallelization strategies to meet varied workloads and client demands. Ignoring hardware-specific factors such as communication topology, memory bandwidth, and interconnect speed can lead to significant inefficiencies in multi-node environments [78].

The growing scale of deep learning models and the increasing complexity of hardware clusters have motivated a large body of work on automatic parallelization. Early frameworks primarily combined existing forms of parallelism—such as data, pipeline, and tensor parallelism—into unified search spaces, and then developed cost models and optimization strategies to explore them (see Table 6).

An early system is Piper [105], which introduced dynamic programming for automatic partitioning, but did not fully consider device heterogeneity. Building on this foundation, several 2022 works refined the search process. Alpa [135] organizes parallelism strategies into a hierarchical space aligned with the compute cluster

topology, distinguishing between inter-operator partitioning and intra-operator partitioning. By solving these levels independently through integer linear programming and dynamic programming, Alpa achieves practical solutions, but remains sub-optimal and does not explicitly address load imbalance across microbatches. In the same year, Galvatron [75] introduced a decision-tree decomposition of the search space, pruning suboptimal combinations and applying dynamic programming to optimize each pipeline stage under memory constraints, but without fully modeling optimizer states or device heterogeneity. Complementarily, AMP [58] targeted heterogeneous clusters using symbolic cost models and dynamic programming to select pipeline and tensor strategies efficiently, though its reliance on lookup tables limited accuracy across hardware types.

Subsequent works in 2023 extended automation and usability. Colossal-AI [62] expanded automation to 4D parallelism (data, pipeline, tensor, and sequence), incorporating advanced tensor sharding schemes such as 2D, 2.5D, and 3D tensor parallelism [119, 111, 11]. These reduce communication costs but impose topological constraints. Colossal-AI further improves over Alpa with greedy sharding conversion and integrated activation checkpointing. Merak [56] also embraces 3D parallelism but emphasizes usability with a PyTorch framework that automatically partitions and allocates models, requiring fewer code modifications than Alpa or Colossal-AI. In parallel, SuperScaler [67] introduced a unified scheduling framework with three stages: model transformation, space-time scheduling, and data-dependency preserving execution, enabling flexible but not fully automatic parallelism planning.

In 2024, the focus shifted toward heterogeneity and overlap. nnScaler [68] extended scheduling approaches but demonstrated results only on transformer architectures. Metis [110] explicitly addressed heterogeneous GPU capabilities through profiling, cost estimation, and pruned search algorithms to balance loads across diverse devices. Aceso [70] tackled pipeline inefficiency by co-optimizing communication and computation at the microbatch level, reducing pipeline bubbles with overlap-aware scheduling.

Most recently, Mist [139] pushed the frontier by co-optimizing memory footprint reduction with parallelism strategy selection. Its imbalance-aware hierarchical tuning method decouples inter-stage pipeline partitioning from intra-stage microbatch balancing, linked via Pareto frontier sampling. This design mitigates search space explosion and pipeline imbalance while achieving fine-grained overlap between computation and communication.

Overall, these systems demonstrate a clear evolution: from early dynamic-programming partitioners, to hierarchical and greedy search frameworks, to heterogeneity-aware and overlap-optimized approaches. While significant progress has been made, challenges remain in controlling the combinatorial explosion of strategies, supporting diverse hardware environments, and ensuring usability in practice.

Table 6: Comparison of recent automatic parallelism frameworks (ordered by year).

System	Year	Parallelism Types	Search / Optimization
Piper [105]	2021	PP, TP	Dynamic programming
Alpa [135]	2022	DP, PP, TP	Integer linear programming, dynamic programming
Galvatron [75]	2022	DP, PP, TP	Decision tree + Dynamic programming
AMP [58]	2022	PP, TP	Dynamic programming + symbolic cost model
Colossal-AI [62]	2023	DP, PP, TP, SP	Greedy search
Merak [56]	2023	DP, PP, TP	Graph-sharding heuristic
Metis [110]	2024	DP, PP, TP	Pruned search algorithm
Mist [139]	2025	DP, PP, TP	Mixed integer linear programming

5 Parallel Strategies Theoretical Analysis

In this section, we present a unified theoretical analysis of FLOPs, memory consumption, and communication overhead for GQA, MLP, and Mamba across different parallelization scenarios. Our work is inspired by prior analyses in [54, 32], which quantified per-GPU memory usage (weights and activations) for GQA and MLP layers. Building on these foundations, we extend the analysis by providing a detailed breakdown of FLOPs, memory, and communication for these blocks (Sections 5.1 and 5.2). Moreover, we incorporate the Mamba

block [25], which has not been covered in previous studies (Section 5.3). The parallel strategies in this section are TP, DP, and CP, while we experiment with PP in Section 6.

For clarity, we ignore layer normalization and focus on the dominant multiply-add operations (vector FLOPs are omitted). Our analysis considers the forward pass over a full sequence, which corresponds to the *forward* step during training and the *prefill* stage of inference; we use these terms interchangeably. Extending the results to training is feasible: the backward pass roughly doubles the FLOPs due to gradient computations with respect to both inputs and weights. Memory analysis for the backward pass is left for future work. We also neglect the optimizer states and focus on key blocks’ weights as well as activations.

We conclude with a summary of the main insights in Section 5.4. Parameter definitions and notation are provided in Table 7.

Symbol	Meaning
b	Batch size
s	Sequence length
l	Chunk size
n	State dimension (latent recurrent size) maintained by each SSM head
d	Transformer hidden dimension
d_h	Transformer head dimension
I	Intermediate dimension of the FFN (expansion size)
a	Number of attention heads
k	Number of KV heads
v	Vocabulary size (unique tokens)
$\text{expand}_{\text{mamba}}$	Mamba expansion factor for transformer hidden dimension
d_{inner}	Total SSM channel width after expansion
$ngroups_{\text{ssm}}$	Number of groups used to partition SSM parameters
h	Number of mamba heads
p	Mamba head dimension
a_{byte}	Bytes per activation element
w_{byte}	Bytes per weight element

Table 7: Parameter definitions used in the transformer and Mamba theoretical derivations.

Let TP be the tensor-parallel degree, DP be the data-parallel degree, and CP be the context-parallel degree. Suppose that the total number of devices (world size) fixed such that

$$\text{TP} \times \text{CP} \times \text{DP} = \text{worldsize}.$$

We decompose the transformer hidden dimension as $d = a \cdot d_h$, where a is the number of attention heads.

The SSM hidden width is then given by $d_{\text{inner}} = \text{expand}_{\text{mamba}} \cdot d$.

5.1 GQA Theoretical Analysis

Attention GQA FLOPs Breakdown

- **Self-Attention (Q, K, V Linear Projection):** $2bsad_h \cdot ad_h + 4bskd_h \cdot ad_h$ or $2bsd \cdot d + 4bskd_h d$
- **Attention (QK^\top):** $2bs^2ad_h$ or $2bs^2d$
- **Softmax softmax(QK^\top):** $5bs^2a$ or $5bs^2a$ [max, subtraction, exponent, sums, division]
- **Attention Output (SV):** $2bs^2ad_h$ or $2bs^2d$
- **Final Linear Projection ($(SV) \cdot W_O$):** $2bsad_h \cdot ad_h$ or $2bsd \cdot d$

Total FLOPs for GQA:

$$4bsd^2 + 4bskd_h d + 4bs^2d + 5bs^2a$$

FLOPs with TP Per Device:

$$4bs \frac{d^2}{TP} + 4bs \frac{kd_h}{TP} + 4bs^2 \frac{d}{TP} + 5bs^2 \frac{a}{TP}$$

FLOPs with CP Per Device:

$$4bd^2 \frac{s}{CP} + 4bkd_h \frac{s}{CP} + 4bds \frac{s}{CP} + 5bsa \frac{s}{CP}$$

FLOPs with DP Per Device:

$$4sd^2 \frac{b}{DP} + 4skd_h \frac{b}{DP} + 4ds^2 \frac{b}{DP} + 5s^2a \frac{b}{DP}$$

Conclusion:

FLOPs(TP, CP, DP) is invariant w.r.t. the TP-CP-DP split.

GQA Activation Memory Breakdown

- **Linear Projections** (W_Q, W_K, W_V): $bsd + 2bsd \cdot \frac{k}{a}$
- **Attention** (QK^\top): 0 (due to FlashAttention)
- **Softmax**: 0 (due to FlashAttention)
- **Attention Output** (SV): bsd
- **Final Linear Projection** ($SV \cdot W_O$): bsd

Total Activation Memory for GQA:

$$(3bsd + 2bsd \cdot \frac{k}{a}) \cdot a_{\text{byte}}$$

Total Activation TP for GQA Per Device:

$$(bsd + 2bs \frac{d}{TP} + 2bs \frac{d}{TP} \cdot \frac{k}{a}) \cdot a_{\text{byte}}$$

Total Activation CP for GQA Per Device:

$$(bd \frac{s}{CP} + 2bd \frac{s}{CP} + 2bd \frac{s}{CP} \cdot \frac{k}{a}) \cdot a_{\text{byte}}$$

Total Activation DP for GQA Per Device:

$$(sd \frac{b}{DP} + 2sd \frac{b}{DP} + 2sd \frac{b}{DP} \cdot \frac{k}{a}) \cdot a_{\text{byte}}$$

Conclusion: $\text{memory}_{\text{act}}^{(\text{gqa})}(\text{TP}) > \text{memory}_{\text{act}}^{(\text{gqa})}(\text{CP})$ AND $\text{memory}_{\text{act}}^{(\text{gqa})}(\text{TP}) > \text{memory}_{\text{act}}^{(\text{gqa})}(\text{DP})$ AND $\text{memory}_{\text{act}}^{(\text{gqa})}(\text{CP}) \approx \text{memory}_{\text{act}}^{(\text{gqa})}(\text{DP})$

The activation memory per device is lower with a larger CP or DP value. At the same CP and DP values, the activation memory per device is the same for CP and DP.

GQA Weight Memory Breakdown

Total Weight Memory for GQA: (W_Q, W_K, W_V, W_O): $2d^2 \left(1 + \frac{k}{a}\right) \cdot w_{\text{byte}}$

Total Weight TP for GQA per device:

$$2 \frac{d^2}{TP} \left(1 + \frac{k}{a}\right) \cdot w_{\text{byte}}$$

Total Weight CP for GQA per device:

$$2d^2 \left(1 + \frac{k}{a}\right) \cdot w_{\text{byte}}$$

Total Weight DP for GQA per device:

$$2d^2 \left(1 + \frac{k}{a}\right) \cdot w_{\text{byte}}$$

Conclusion: $\text{memory}_{\text{wt}}^{(\text{gqa})}(\text{TP}) < \text{memory}_{\text{wt}}^{(\text{gqa})}(\text{CP})$ AND $\text{memory}_{\text{wt}}^{(\text{gqa})}(\text{TP}) < \text{memory}_{\text{wt}}^{(\text{gqa})}(\text{DP})$ AND $\text{memory}_{\text{wt}}^{(\text{gqa})}(\text{CP}) \approx \text{memory}_{\text{wt}}^{(\text{gqa})}(\text{DP})$

The weight memory per device is lower with a larger TP value.

5.2 MLP Theoretical Analysis

We assume that the SwiGLU is applied in this MLP as normally done in Llama architectures [92, 32].

MLP FLOPs Breakdown

- **MLP Up Projection:** $2bsd \cdot I$
- **MLP Gated Dot Product and SiLU operations:** $5bsI$ (4 for the sigmoid and 1 for the dot product)
- **MLP Gated Projection:** $2bsd \cdot I$
- **MLP Down Projection:** $2bsd \cdot I$

Total FLOPs for MLP:

$$6bsdI + 5bsI = bs(6dI + 5I)$$

FLOPs with TP Per Device:

$$6bsdI + 5bsI = \frac{bs}{TP}(6dI + 5I)$$

FLOPs with CP Per Device:

$$6bsdI + 5bsI = \frac{bs}{CP}(6dI + 5I)$$

FLOPs with DP Per Device:

$$6bsdI + 5bsI = \frac{bs}{DP}(6dI + 5I)$$

Conclusion:

FLOPs(TP, CP, DP) is invariant w.r.t. the TP-CP-DP split.

MLP Activation Memory Breakdown

- **Input:** bsd
- **Output of Up Projection:** bsI
- **Output of Gate Projection:** bsI
- **GELU Activation:** bsI
- **Input to Down Projection:** bsI

Total Activation Memory for FFN:

$$(2bsd + 4bsI) \cdot a_{\text{byte}}$$

Total Activation TP for MLP Per Device:

$$(2bsd + \frac{bs}{TP}4I) \cdot a_{\text{byte}}$$

Total Activation CP for MLP Per Device:

$$\frac{bs}{CP}(2d + 4I) \cdot a_{\text{byte}}$$

Total Activation DP for MLP Per Device:

$$\frac{bs}{DP}(2d + 4I) \cdot a_{\text{byte}}$$

Conclusion: $\text{memory}_{\text{act}}^{(\text{mlp})}(\text{TP}) > \text{memory}_{\text{act}}^{(\text{mlp})}(\text{CP})$ AND $\text{memory}_{\text{act}}^{(\text{mlp})}(\text{TP}) > \text{memory}_{\text{act}}^{(\text{mlp})}(\text{DP})$ AND $\text{memory}_{\text{act}}^{(\text{mlp})}(\text{CP}) \approx \text{memory}_{\text{act}}^{(\text{mlp})}(\text{DP})$

The activation memory per device is lower with a larger CP or DP value. At the same CP and DP values, the activation memory per device is the same for CP and DP

MLP Weight Memory Breakdown

Feed-Forward Network (FFN) Parameters: $3dI$

Feed-Forward Network (FFN) Parameters with TP (TPSP): $\frac{3dI}{TP}$

Feed-Forward Network (FFN) Parameters with CP: $3dI$

Feed-Forward Network (FFN) Parameters with DP: $3dI$

Conclusion: $\text{memory}_{\text{wt}}^{(\text{mlp})}(\text{TP}) < \text{memory}_{\text{wt}}^{(\text{mlp})}(\text{CP})$ AND $\text{memory}_{\text{wt}}^{(\text{mlp})}(\text{TP}) < \text{memory}_{\text{wt}}^{(\text{mlp})}(\text{DP})$ AND $\text{memory}_{\text{wt}}^{(\text{mlp})}(\text{CP}) \approx \text{memory}_{\text{wt}}^{(\text{mlp})}(\text{DP})$

The weight memory per device is lower with a larger TP value.

GQA and MLP Communication Overhead Analysis The total communication volume for both GQA and MLP for TP is:

$$= 2 * s * a * d_h$$

When CP with passKV is enabled, the total volume will be:

$$= 2 * s * k * d_h$$

Since the number of KV heads (k) is typically less than the number of attention heads a , the communication volume for CP is less than the communication volume for TP. For the DP and prefill scenario, there is no communication needed.

5.3 Mamba Theoretical Analysis

This section studies the Mamba-2 architecture [25] and presents analysis for the corresponding FLOPs, memory, and communication. In this analysis, we do not consider the convolution operation and focus on major GEMM operations.

Mamba Theoretical Fundamentals Before deriving the characteristics (FLOPs, memory, and communication) of Mamba, we *review* the theoretical fundamentals of Mamba-2 (originally developed in [25]) in a simple way to align with our following derivations:

SSM recurrence (scalar, time-varying): $h_{t+1} = a_{t+1} h_t + b_{t+1} x_{t+1}.$

$$\begin{aligned} h_{t+1} &= a_{t+1} h_t + b_{t+1} x_{t+1} \\ \text{Unroll one step:} \quad &= a_{t+1} (a_t h_{t-1} + b_t x_t) + b_{t+1} x_{t+1} \\ &= a_{t+1} a_t h_{t-1} + a_{t+1} b_t x_t + b_{t+1} x_{t+1}. \end{aligned}$$

Unroll further: $h_{t+1} = a_{t+1} a_t a_{t-1} h_{t-2} + a_{t+1} a_t b_{t-1} x_{t-1} + a_{t+1} b_t x_{t+1} + b_{t+1} x_{t+1}.$

General closed form (scalar, time-varying) for $t+1$ steps: $h_{t+1} = \left(\prod_{m=0}^t a_{m+1} \right) h_0 + \sum_{i=0}^t \left(\prod_{m=i+1}^t a_{m+1} \right) b_{i+1} x_{i+1}.$

Chunking notation: $\begin{cases} \text{chunk size } Q, \\ \text{chunk index } c \in \{0, \dots, K-1\}, \\ \text{in-chunk position } j \in \{0, \dots, Q-1\}, \\ \text{global time } t = cQ + j. \end{cases}$

Write $h_{c,j}$ for the state at chunk c position j .

Intra-chunk expansion (within chunk c): $h_{c,j} = \left(\prod_{m=0}^j a_{c,m} \right) h_{c,0} + \sum_{i=0}^j \left(\prod_{m=i+1}^j a_{c,m+1} \right) b_{c,i+1} x_{c,i+1}.$

In particular, the final state at the end of chunk c ($j = Q$): $h_{c,Q} = \left(\prod_{m=0}^Q a_{c,m} \right) h_{c,0} + \sum_{i=0}^Q \left(\prod_{m=i+1}^Q a_{c,m+1} \right) b_{c,i+1} x_{c,i+1}.$

Inter-chunk recurrence (carry between chunks): $h_{c+1,0} = A_c^{(Q)} h_{c,0} + U_{c+1},$

where we define the chunk-level decay and intra-chunk contribution

$$A_c^{(Q)} := \prod_{m=0}^Q a_{c,m}, \quad U_{c+1} := \sum_{i=0}^Q \left(\prod_{m=i+1}^Q a_{c,m+1} \right) b_{c,i+1} x_{c,i+1}.$$

By recursion across chunks: $h_{c,0} = \left(\prod_{i=0}^c A_i^{(Q)} \right) h_{0,0} + \sum_{i=0}^c \left(\left[\prod_{m=i+1}^c A_m^{(Q)} \right] U_{i+1} \right).$

$$\begin{aligned}
h_{c,j} = & \underbrace{\left(\prod_{m=0}^j a_{c,m} \right) h_{c,0}}_{\text{evolution of chunk-start state (inter)}} \\
\text{Combine intra + inter: final expression for } h_{c,j} : & \\
& + \underbrace{\sum_{i=0}^j \left(\prod_{m=i+1}^j a_{c,m+1} \right) b_{c,i+1} x_{c,i+1}}_{\text{intra-chunk inputs}}.
\end{aligned}$$

And $h_{c,0}$ is given by the inter-chunk prefix above, so $h_{c,j}$ equals

$$h_{c,j} = \left(\prod_{m=0}^j a_{c,m} \right) \left[\left(\prod_{i=0}^c A_i^{(Q)} \right) h_{0,0} + \sum_{i=0}^c \left(\prod_{m=i+1}^c A_m^{(Q)} \right) U_{i+1} \right] + \sum_{i=0}^j \left(\prod_{m=i+1}^j a_{c,m+1} \right) b_{c,i+1} x_{c,i+1}.$$

This equation clearly illustrates that in the Mamba2 architecture, the intra- and inter-chunk computations are structured such that each chunk depends only on its starting state.

Mamba FLOPs Breakdown Consider the following variable,

$$d_{inproj} = 2 * d_{inner} + 2 * ngroups * n + h$$

The first term $2d_{inner}$ arises because the input X is split into two branches: one feeding the state-space duality (SSD) path and the other producing the residual update Z , each of size d_{inner} . The second term $2(n\text{groups} \cdot n)$ corresponds to the B and C parameters of the selective SSD, where each SSD group contributes an n -dimensional vector for both B and C . The final term h comes from the projection generating the A -parameter of the SSD, which has dimensionality h .

In-Proj and Out-Proj FLOPs

- **In Projection:** $2bsd \cdot d_{inproj}$
- **Out Projection:** $2bs d_{inner} d$

SSD FLOPs To derive SSD FLOPs, we consider the following variables:

$$l = \text{chunk size}, \quad c = s/l.$$

We analyze the operations outlined in the Mamba-2 algorithm in [25].

Step 1 & Step 2: Computing Y_{diag} In Mamba-2 paper, they define the diagonal contribution as:

$$Y_{\text{diag}} = \text{einsum}("bclhn, bcsn, bhcls, bcsph \rightarrow bclhp", C, B, L, X).$$

Because we defined s to be the sequence length and the s variable in the equation is different, we replace s in the equation by v in the diagonal contribution for clarity:

$$Y_{\text{diag}} = \text{einsum}("bclhn, bcvhn, bhclv, bcvhp \rightarrow bclhp", C, B, L, X).$$

In `einsum`, any index that appears in *both* input tensors but *not in the output* is summed over (contracted). Based on this contraction rule, the computation of Y_{diag} can be understood step by step as follows:

I.

$$C_{bclhn} \cdot B_{bcvhn} \longrightarrow \text{intermediate}_{bcvhl}.$$

The index that appears in both input tensors but not in the output is n . All other indices (b, c, s, h, l) are kept in the output.

For the diagonal kernels in Mamba, the effective sequence length inside each kernel is equal to the chunk size $v = l$. This is because the diagonal SSM component operates only within each chunk, performing purely intra-chunk interactions. As a result, each chunk behaves as an independent sequence of length l , and the diagonal computation forms an $l \times l$ interaction pattern. This is precisely why the FLOPs expressions contain an l^2 term.

Over the full sequence of length s , we process s/l such chunks. Therefore, the FLOPs for the diagonal GEMMs are:

$$\text{FLOPs}_1 = 2b \left(\frac{s}{l} \right) h l^2 n \quad (\text{first GEMM, } Y_{\text{diag}})$$

The key idea is that the diagonal structure forces an $l \times l$ computation inside each chunk, while the factor s/l accounts for the number of chunks required to cover the full sequence.

II.

$$\text{intermediate}_{bcvhl} \cdot L_{bhclv} \longrightarrow \text{intermediate}_{bcvhl}.$$

This is an elementwise operation with no contraction. The shapes are $bhclv \times bhclv \rightarrow bhcls$. Therefore, the vector FLOPs are $bhclv$. Since we focus on cube FLOPs, we ignore this one in the total sum.

III.

$$\text{intermediate}_{bcvhl} \cdot X_{bcvhp} \longrightarrow Y_{\text{diag}, bclhp}.$$

The contraction is over the v dimension, and the final output has the desired shape (b, c, l, h, p) . The FLOPs for this is:

$$\text{FLOPs}_2 = 2b \left(\frac{s}{l} \right) h l^2 p \quad (\text{second GEMM, } Y_{\text{diag}}).$$

Step 3: Computing the intra-chunk states The updated states are computed using the einsum

$$\text{states} = \text{einsum}("bclhn, bhcl, bclhp \rightarrow bchpn", B, \text{decay_states}, X).$$

Here, the contraction proceeds as follows:

- $\text{decay_states} \in \mathbb{R}^{b \times h \times c \times l}$ is applied as an element-wise multiplication with a broadcast across n , introducing the state decay. We ignore vector operations in total FLOPs.
- $B \in \mathbb{R}^{b \times c \times l \times h \times n}$ and $X \in \mathbb{R}^{b \times c \times l \times h \times p}$ are contracted over the chunk dimension l , producing the resulting output tensor has shape $b \times c \times h \times p \times n$, corresponding to all heads, channels, and features aggregated across the chunks.

The corresponding cost is

$$\text{FLOPs}_3 = 2b \left(\frac{s}{l} \right) h l p n.$$

Step 4: Computing the inter-chunk recurrent states

$$\text{new_states} = \text{einsum}("bhzc, bchpn \rightarrow bzhpn", \text{decay_chunk}, \text{states}).$$

Note:

$$z = \left(\frac{s}{l} + 1 \right)$$

This corresponds to

$$\text{FLOPs}_{4, \text{naive}} = 2b h \left(\frac{s}{l} \right) \left(\frac{s}{l} + 1 \right) p n.$$

Note about inter-Chunk recurrent states calculation: Based on the previous theoretical development, the inter-chunk recurrence is defined as:

$$H_c = A_{c-1}^{(Q)} H_{c-1} + U_c,$$

where H_c is the state for chunk c , $A_{c-1}^{(Q)}$ is the decay factor between chunks, and U_c is the intra-chunk contribution.

$$U_c := \sum_{i=0}^{Q-1} \left(\prod_{m=i+1}^{Q-1} a_{c,m} \right) b_{c,i+1} x_{c,i+1}.$$

Naive computation: To compute all inter-chunk contributions explicitly, we would write:

$$H_1 = U_1, \quad H_2 = A_1 U_1 + U_2, \quad H_3 = A_2 (A_1 U_1 + U_2) + U_3, \dots$$

For $Z = s/l$ chunks, computing H_Z requires summing over all previous chunks, resulting in $\sim Z^2/2$ operations, i.e., quadratic in sequence length.

Concrete example: Suppose $s = 16$, $l = 4$, so $Z = s/l = 4$ chunks:

$$\begin{aligned} H_1 &= U_1 \\ H_2 &= A_1 H_1 + U_2 = A_1 U_1 + U_2 \\ H_3 &= A_2 H_2 + U_3 = A_2 (A_1 U_1 + U_2) + U_3 \\ H_4 &= A_3 H_3 + U_4 = A_3 (A_2 (A_1 U_1 + U_2) + U_3) + U_4 \end{aligned}$$

- Naively, we compute each H_c by multiplying all previous U 's by the decay factors \rightarrow quadratic in Z .

Parallel scan trick in [25]:

- The recurrence is **associative**:

$$H_c = \sum_{i=1}^c \left(\prod_{j=i}^{c-1} A_j \right) U_i$$

- This is exactly a **prefix-sum (scan)** over the chunks with multiplication by decay factors.

- Using a segmented parallel scan, we can compute all H_c in $\mathcal{O}(Z)$ **total operations**:

steps:

1. Compute cumulative products of A_j per chunk
2. Multiply with U_i using vectorized einsum
3. Sum contributions across chunks

Step-by-step for the example with $Z = 4$:

Step 1 (cumulative products): $P = [1, A_1, A_1 A_2, A_1 A_2 A_3]$

Step 2 (multiply with U_i): $H_i = P_i \cdot U_i$

Step 3 (sum contributions for each chunk): $H_c = \sum_{i=1}^c H_i$

- Each chunk only **needs one multiplication per U_i and one addition**, not a full nested loop over previous chunks.

- Total complexity reduces from $\mathcal{O}(Z^2)$ to $\mathcal{O}(Z)$, i.e., linear in the number of chunks.

Resulting FLOPs:

$$\text{FLOPs}_{4,\text{scan}} = 2 \cdot b \cdot h \cdot (s/l) \cdot p \cdot n \sim O(s)$$

- This is why Mamba achieves *linear complexity* in sequence length for inter-chunk recurrence.

Step 5: Computing Y_{off} (state-to-output contribution)

$$Y_{\text{off}} = \text{einsum}("bclhn, bchpn, bhcl \rightarrow bclhp", C, \text{states}, \text{state_decay_out}).$$

This operation has two steps: (i) a contraction operation between C and states over n ; (ii) an element-wise operation with broadcast over p between the intermediate tensor and state_decay_out .

Since we only focus on cube FLOPs, the cost of this final projection is the following:

$$\text{FLOPs}_5 = 2b \left(\frac{s}{l} \right) h p n l.$$

Total naive FLOPs for SSD section

$$\text{FLOPs}_{\text{SSD,naive}} = 2b \left[((s/l))hl^2n + (s/l)hl^2p + (s/l)hlpn + h(s/l)((s/l) + 1)pn + (s/l)hpn \right]$$

Total Parallel Scan FLOPs for SSD section

$$\text{FLOPs}_{\text{SSD,parallel}} = 2b \left[((s/l))hl^2n + (s/l)hl^2p + (s/l)hlpn + h(s/l)pn + (s/l)hpn \right]$$

Total Mamba FLOPs with Parallel Scan We sum the contributions from SSD section, in-projection, and out-projection:

$$\begin{aligned} \text{FLOPs}_{\text{total}} = & \underbrace{2b \left[((s/l))hl^2n + (s/l)hl^2p + (s/l)hlpn + h(s/l)pn + (s/l)hpn \right]}_{\text{SSD (parallel scan)}} \\ & + \underbrace{2bsd \cdot d_{\text{inproj}}}_{\text{In Projection}} \\ & + \underbrace{2bs d_{\text{inner}} d}_{\text{Out Projection}} \end{aligned}$$

All terms are in **multiply-add FLOPs**.

Total Mamba FLOPs with Parallel Scan and TP Applied

$$\begin{aligned} \text{FLOPs}_{\text{total}} = & \underbrace{\frac{2b}{TP} \left[((s/l))hl^2n + (s/l)hl^2p + (s/l)hlpn + h(s/l)pn + (s/l)hpn \right]}_{\text{SSD (parallel scan)}} \\ & + \underbrace{2bsd \cdot \frac{d_{\text{inproj}}}{TP}}_{\text{In Projection}} \\ & + \underbrace{2bs d_{\text{inner}} \frac{d}{TP}}_{\text{Out Projection}} \end{aligned}$$

Total Mamba FLOPs with Parallel Scan and CP Applied

$$\begin{aligned}
\text{FLOPs}_{\text{total}} = & \underbrace{\frac{2b}{CP} \left[((s/l))hl^2n + (s/l)hl^2p + (s/l)hlpn + h(s/l)pn + (s/l)hpn \right]}_{\text{SSD (parallel scan)}} \\
& + \underbrace{2bd \frac{s}{CP} \cdot d_{inproj}}_{\text{In Projection}} \\
& + \underbrace{2bd d_{inner} \frac{s}{CP}}_{\text{Out Projection}}
\end{aligned}$$

Total Mamba FLOPs with Parallel Scan and DP Applied

$$\begin{aligned}
\text{FLOPs}_{\text{total}} = & \underbrace{\frac{2b}{DP} \left[((s/l))hl^2n + (s/l)hl^2p + (s/l)hlpn + h(s/l)pn + (s/l)hpn \right]}_{\text{SSD (parallel scan)}} \\
& + \underbrace{2sd \frac{b}{DP} \cdot d_{inproj}}_{\text{In Projection}} \\
& + \underbrace{2sd d_{inner} \frac{b}{DP}}_{\text{Out Projection}}
\end{aligned}$$

Conclusion:

FLOPs(TP, CP, DP) is invariant w.r.t. the TP–CP–DP split.

Mamba Memory Breakdown

In-Projection Memory The symmetric in-projection dimension is

$$d_{in_proj_sym} = 2d_{ssm,local} + 2n_{groups,local}s_{ssm,state} + n_{heads,local}.$$

Then the memory cost for the in-projection is

$$\text{memory}_{in_proj} = b \cdot s \cdot d_{model} \cdot a_{byte} + d_{model} \cdot d_{in_proj_sym} \cdot w_{byte} + b \cdot s \cdot d_{in_proj_sym} \cdot a_{byte}$$

Out-Projection Memory

$$\text{memory}_{out_proj} = b \cdot s \cdot d_{inner} \cdot a_{byte} + d_{model} \cdot d_{inner} \cdot w_{byte} + b \cdot s \cdot d_{model} \cdot a_{byte}$$

SSD Section Memory per GEMM

1. First GEMM (Y_{diag}) : $\text{bcshn}, \text{bclhn} \rightarrow \text{bchls}$

$$\begin{aligned} \text{memory}_1 &= \left(b \cdot l \cdot (s/l) \cdot n \cdot h + b \cdot h \cdot (s/l) \cdot n + h \right) \cdot a_{\text{byte}} \\ &\quad + \left(b \cdot (s/l) \cdot h \cdot l^2 \right) \cdot a_{\text{byte}} \end{aligned}$$

2. Second GEMM (Y_{diag}) : $\text{bchls}, \text{bcschp} \rightarrow \text{bclhp}$

$$\begin{aligned} \text{memory}_2 &= \left(b \cdot (s/l) \cdot h \cdot l^2 + b \cdot (s/l) \cdot l \cdot h \cdot p \right) \cdot a_{\text{byte}} \\ &\quad + \left(b \cdot (s/l) \cdot l \cdot h \cdot p \right) \cdot a_{\text{byte}} \end{aligned}$$

3. Third GEMM (intra-chunk states) : $\text{cbhpl}, \text{bclhn} \rightarrow \text{bchpn}$

$$\begin{aligned} \text{memory}_3 &= \left(b \cdot (s/l) \cdot h \cdot p \cdot l + b \cdot (s/l) \cdot l \cdot h \cdot n \right) \cdot a_{\text{byte}} \\ &\quad + \left(b \cdot (s/l) \cdot h \cdot p \cdot n \right) \cdot a_{\text{byte}} \end{aligned}$$

4. Fourth GEMM (new_states, inter-chunk) : $\text{bhzc}, \text{bchpn} \rightarrow \text{bzhp}$

$$\begin{aligned} \text{memory}_4 &= \left(b \cdot h \cdot ((s/l) + 1) \cdot (s/l) \right) \cdot a_{\text{byte}} \\ &\quad + \left(b \cdot (s/l) \cdot h \cdot p \cdot n \right) \cdot a_{\text{byte}} \\ &\quad + \left(b \cdot ((s/l) + 1) \cdot h \cdot p \cdot n \right) \cdot a_{\text{byte}} \end{aligned}$$

5. Fifth GEMM (Y_{off}) : $\text{bchpn}, \text{bclhn} \rightarrow \text{cbhpl}$

$$\begin{aligned} \text{memory}_5 &= \left(b \cdot (s/l) \cdot h \cdot p \cdot n + b \cdot (s/l) \cdot l \cdot h \cdot n \right) \cdot a_{\text{byte}} \\ &\quad + \left(b \cdot (s/l) \cdot h \cdot p \cdot l \right) \cdot a_{\text{byte}} \end{aligned}$$

Total SSD Memory

$$\text{memory}_{\text{SSD, total}} = \sum_{i=1}^5 \text{memory}_i$$

Conclusion

- **In-/Out-Projection Weight Memory (per device).**

$\text{memory}_{\text{weight}}^{(\text{in/out})}(\text{TP}) < \text{memory}_{\text{weight}}^{(\text{in/out})}(\text{CP})$ AND $\text{memory}_{\text{weight}}^{(\text{in/out})}(\text{TP}) < \text{memory}_{\text{weight}}^{(\text{in/out})}(\text{DP})$ AND $\text{memory}_{\text{weight}}^{(\text{in/out})}(\text{CP}) \approx \text{memory}_{\text{weight}}^{(\text{in/out})}(\text{DP})$

Increasing tensor parallelism further partitions the projection weights, thus reducing the parameter memory per device.

- **In-/Out-Projection Activation Memory (per device).**

$\text{memory}_{\text{act}}^{(\text{in})}(\text{TP}, \text{CP}, \text{DP})$ is invariant w.r.t. the TP-CP-DP split.

- **SSD / GEMM Memory (per device).**

$\text{memory}_{\text{SSD}}(\text{TP}, \text{CP}, \text{DP})$ is approximately invariant w.r.t. the TP-CP-DP split.

The local chunk/state size per device does not roughly change as long as the total number of devices is fixed. All the terms in the activation memory except one term $b \cdot (\frac{s}{l}) \cdot l^3$ has either b or s or h where DP, CP, and TP divide, respectively.

Mamba Communication Breakdown The communication cost of tensor-parallel state propagation (TPSP) scales as

$$\text{Comm}_{\text{TPSP}} = \mathcal{O}(d \cdot d_{\text{state}} \cdot \text{seqlen}).$$

In contrast, the communication cost of context parallelism (CP) scales as

$$\text{Comm}_{\text{CP}} = \mathcal{O}(d \cdot d_{\text{state}} \cdot \text{CP}).$$

Since typically

$$\text{CP} \ll \text{seqlen},$$

we conclude that

$$\text{Comm}_{\text{CP}} < \text{Comm}_{\text{TPSP}},$$

that is, *CP with Mamba incurs less communication than TPSP. DP requires no communication in the prefill scenario.* We do not include the communication analysis for TP because Mamba typically uses TP for the Mamba layers and SP for the linear layers (TPSP).

Method	Communication Volume	Collective Operation
TPSP	$\mathcal{O}(d \cdot d_{\text{state}} \cdot \text{seqlen})$	AllReduce
CP	$\mathcal{O}(d \cdot d_{\text{state}} \cdot \text{CP})$	All-Gather
DP	0	-

Table 8: Comparison of TPSP, CP, DP communication in Mamba-2 Prefill.

5.4 Summary of the Theoretical Analysis

Bringing the analysis together, we emphasize the following key insights:

- **FLOPs remain unchanged across parallelization strategies.** The total computational workload is invariant to whether we select TP, CP, or DP.
- **Communication cost is an important factor in selecting a parallel strategy.** Both communication volume and the available bandwidth largely determine which configuration is most efficient.
- **TP configurations generally require the least weight memory.** In contrast, CP and DP often incur higher weight storage overhead.
- **Activation memory is comparable across TP, CP, and DP.** None of the strategies significantly reduces or increases the activation memory footprint.

6 Parallelization Strategy Selection for Transformer and Mamba: A Case Study

After establishing the background and theoretical foundations of parallelization strategies, we present a case study using Transformer-like and Mamba-like architectures to illustrate how to select an appropriate parallel strategy in a pretraining setting. We first describe the experimental setup, then report results for Transformer-like models, followed by results for Mamba models. We conclude the empirical analysis with a summary of key findings in Section 6.4.

6.1 Experimental Setup

Models: We used two Transformer and two Mamba models with parameter sizes of 1B and 7B in both categories for this case study. We employed LLaMA [133, 108] as the representative Transformer model and utilized Mamba-2 [25] to conduct experiments with the Mamba architecture. The detailed configuration of the models in each category are described in detailed in their corresponding sections, 6.2 and 6.3. None of these models includes a Mixture-of-Experts, so EP is ignored in this empirical analysis.

Evaluation Metrics: The evaluation metrics include throughput, step time, MFU, and average memory consumption. We consider best strategy with highest MFU which also corresponds to lowest step time and highest throughput. We report memory consumption as an additional metric.

Parallel Strategies: We examine various combinations of four parallelization schemes: data parallelism (DP), pipeline parallelism (PP), tensor parallelism (TP), and context parallelism (CP). For each model, we select the hybrid combination of parallelization strategies that delivers the highest throughput and analyze its operation in detail using our in-house analysis tool. Specifically, the tool feeds a random input tensor into the model and measures the elapsed time of each computation and communication operation. These timing measurements are then captured and used for detailed model performance analysis. We describe the parallelization strategy using either the explicit tuple representation, ($DP = m$, $PP = n$, $TP = o$, $CP = p$), or the abbreviated format, (m, n, o, p) implying $DP = m$, $PP = n$, $TP = o$, and $CP = p$. As the primary goal of this section is to highlight the impact of parallelization configurations on MFU, we limit our analysis to reporting the average memory consumption, and defer the study of memory optimization techniques to future work.

Hardware Configuration: All experiments are conducted on a single host equipped with eight Ascend 910B Neural Processing Unit (NPU) cards. This NPU is based on the Da Vinci architecture and each offers 60 GB of high bandwidth memory and delivers 378.88 teraflops (TF) of compute for matrix multiplication operations. Throughout our report, we use ‘Cube’ to imply the operations performed at this high speed cores dedicated for batched matrix multiplication operations also known as general matrix multiply (GEMM) operations. The element-wise operations are reported as ‘Vector’ operations.

Implementation Details Following many prior studies that use approximately 4 million (4M) tokens per training step for large-scale language models (e.g., [109]), we also adopt a step size of 4 million tokens in our experiments. To this end we set the micro-batch size to 1, a global batch size of 1024, and a sequence length of 4096 across all considered parallelization scenarios.

6.2 Attention Experiments

In this section, we present our observation and analysis of Transformer models using LLaMA 1B [73] and LLaMA 7B [108] as representative architecture. The configurations of the models under study are presented in Table 9.

Table 9: LLaMA models configuration

Model	Layers	Hidden size	Attention heads	Group query	FFN hidden size
LLaMA 1B	16	2048	32	4	8192
LLaMA 7B	32	4096	16	-	11008

6.2.1 Performance Analysis of Parallelization Strategies for LLaMA 7B

Observation. We present the detailed result of various parallelization configuration for LLaMA 7B model in Table 10. We observe that the configuration (**DP = 4, PP = 2, TP = 1, CP = 1**) achieves **the highest MFU** of 63.7%, with a step time of 101.8 s and throughput of 41.2 K tokens/s. This parallelization combination offers the best balance between meeting the memory constraints of each device and maximizing utilization of compute capability. The moderate pipeline depth of two stages allows addressing memory needs with effective parallel execution with minimal communication overhead as the memory footprint of 45.85 GB remains well within the Ascend 910B’s available capacity. Conversely, maintaining four data-parallel replicas ensures sufficient global batch size for maximizing compute utilization.

In contrast, the configuration (**DP=1, PP=1, TP=4, CP=2**) exhibits the **lowest MFU** of 14.8%, with a step time of 437.1 s and throughput of only 9.6 K tokens/s. The poor utilization stems from using high degree of tensor parallelism and additional context splitting at the cost of reduced data parallelism. Both of these strategy increase inter-NPU communication, and hence, may be beneficial when required

to meet other constraints, such as memory or latency for extremely large models or ultra long sequences. Tensor parallelism introduces large all-reduce operations at every layer, while context parallelism fragments the attention computation across sequence segments leading to lower cube utilization for small sequences. The combined overhead of these two, where not required by other constraints, leads to under-utilization of compute capability of the device.

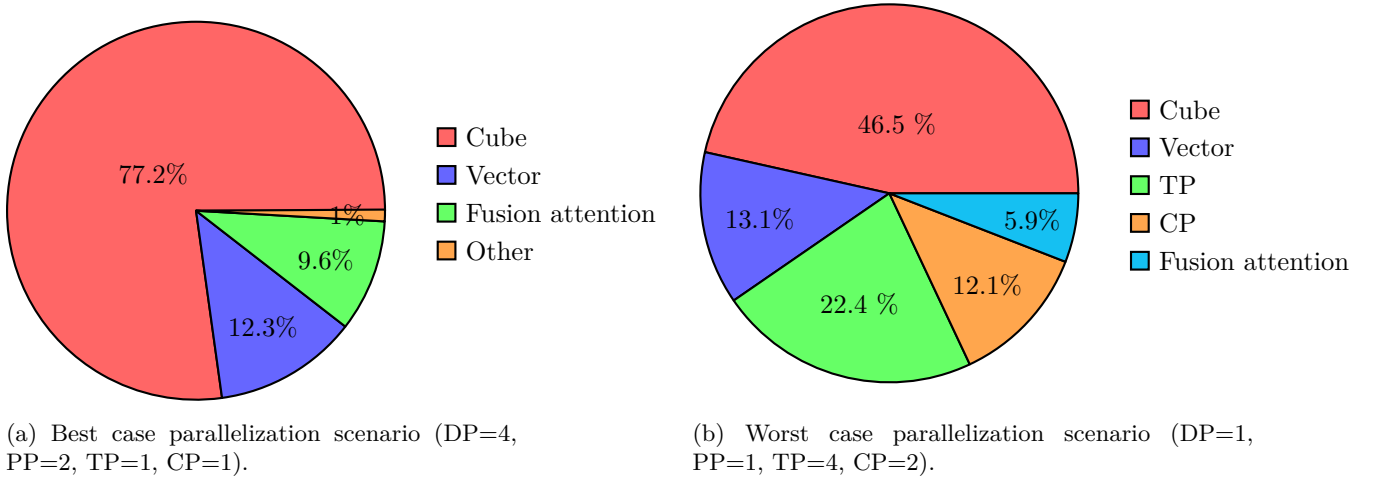
Other intermediate configurations, such as (DP=2, PP=4, TP=1, CP=1) and (DP=1, PP=8, TP=1, CP=1) yields second and third best results of MFU 59.7% and 51.7% indicating the benefits of PP as a strong candidate for preferred parallelization strategy to scale to satisfy memory constraints. Other combinations, such as (DP=2, PP=2, TP=1, CP=2) and (DP=2, PP=2, TP=2, CP=1) achieve MFU value of 43.5% and 40.0% indicating additional context or tensor splits produce diminishing returns. These findings confirm that for mid-scale transformer models, coarse-grained model partitioning scaling DP and PP yields the most favorable trade-off between efficiency, latency, and memory scalability.

Table 10: Performance Analysis of Parallelization Strategies for LLaMA 7B

DP	PP	TP	CP	Step Time (s)	Throughput (K tokens/s)	Mem (GB)	MFU (%)
4	1	2	1	157.3	26.7	41.2	41.2
4	2	1	1	101.8	41.2	45.9	63.7
4	1	1	2	145.7	28.8	60.0	44.5
2	1	4	1	172.4	24.3	26.6	37.6
2	4	1	1	108.5	38.6	33.7	59.7
2	1	1	4	180.6	23.2	55.3	35.9
2	2	2	1	162.2	25.9	29.2	40.0
2	2	1	2	149.2	28.1	38.9	43.5
2	1	2	2	213.9	19.6	36.3	30.3
1	1	8	1	353.6	11.9	18.6	18.3
1	8	1	1	125.5	33.4	27.2	51.7
1	1	1	8	363.8	11.5	53.3	17.8
1	4	2	1	190.8	22.0	22.6	34.0
1	1	2	4	434.6	9.7	33.8	14.9
1	2	4	1	214.9	19.5	20.1	30.2
1	1	4	2	437.1	9.6	24.0	14.8
1	4	1	2	172.5	24.3	21.5	37.6
1	2	1	4	214.9	19.5	35.3	30.2

Analysis of Operations. To better understand the utilization patterns reported in Table 10, we examine the operation-level execution characteristics of the best and worst performing configurations. Figure 6 shows the kernel-level time distribution for the best and worst configurations, (DP=4, PP=2, TP=1, CP=1) and (DP=1, PP=1, TP=4, CP=2). The differences in the ratios of the time spent in different type of operations for these two configuration shed light on the mechanisms responsible for the observed MFU gap.

In the best-performing setting (DP=4, PP=2, TP=1, CP=1), the execution is dominated by **Cube** kernels, which account for **77.2%** of the total runtime. These kernels correspond to the dense General Matrix Multiply (GEMM) operations arising in the attention projections and feed-forward pathways. TP = 1 presents large GEMM operations allowing the Ascend NPU cube units to operate close to their peak efficiency. The remaining operations of Vector kernels (12.3%) and Fused Attention kernels (9.6%) introduce minimal overhead, as the model is neither tensor- nor context-partitioned. Crucially, the choice of **PP=2, TP=1, CP=1** ensures that the attention kernels operate on the full sequence with full layer parameter in each pipeline stage requiring no communication overhead other than that between the two pipeline stages. This



(a) Best case parallelization scenario (DP=4, PP=2, TP=1, CP=1). (b) Worst case parallelization scenario (DP=1, PP=1, TP=4, CP=2).

Figure 6: Runtime composition of LLaMA 7B under best and worst parallelization strategies with (DP, PP, TP, CP) order. The best-case setup increases the cube operation from 46.5% in the worst case to 77.2% in the best case. Also, the worst case decreases the vector operation from 13.1% to 12.3%.

allows the attention computation to proceed with minimal synchronization and preserving a compute-heavy profile.

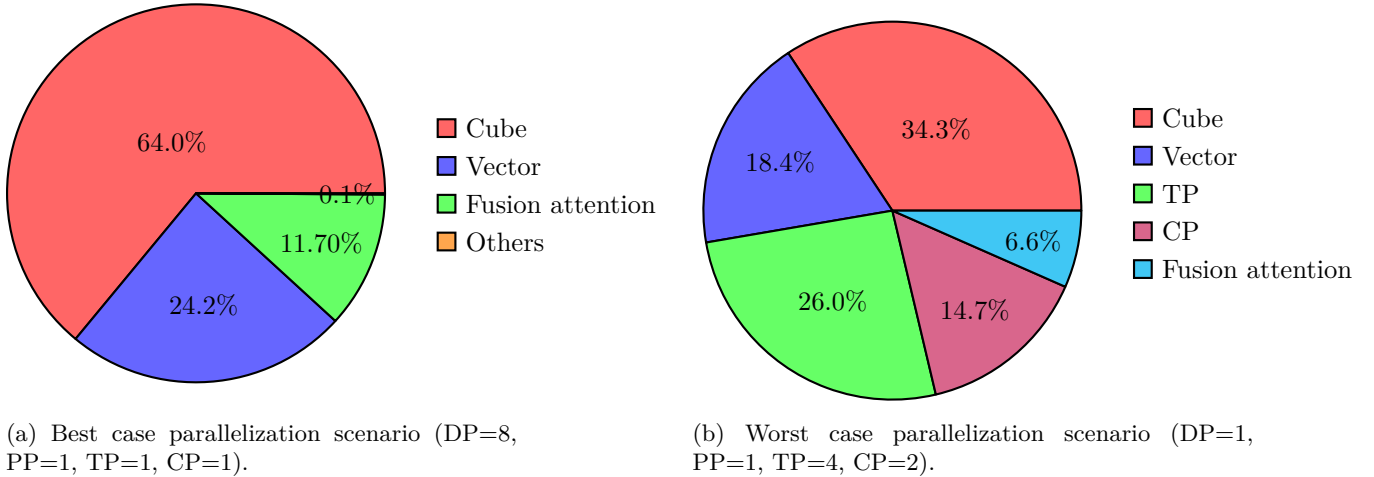
In contrast, the worst-performing parallelization combination (DP=1, PP=1, TP=4, CP=2) exhibit a higher ratio of time spent on communication compared to minimal communication overhead in best case. The share of time spent on GEMM operations drops sharply from 77.2% to **46.5%**, indicating lower utilization of Cube. The use of high degree of tensor parallelism (**TP=4**) splits GEMM operations into four shards reducing matrix dimensions and tile reuse as well as triggering frequent cross-device synchronization. This fragmentation manifests directly in the **22.4%** of runtime consumed by TP-related communication, a stark contrast with the negligible overheads in the best case. Context parallelism (**CP=2**) further amplifies this effect by partitioning the sequence into two segments. This further contributes to an additional **12.1%** CP communication overhead. Overall, the system spends a substantial portion of its runtime waiting for communication rather than performing numerical computation, which fully explains the sharp drop in MFU and throughput reported in Table 10.

6.2.2 Performance Analysis of Parallelization Strategies for LLaMA 1B

Observations. To study the impact of model size on different parallelization techniques, we also analyze the LLaMA 1B model. We present the detailed results of LLaMA 1B in table 11. The results demonstrate a strong dependence between MFU and the chosen parallelization scheme. Similar to the 7B model, increasing the degree of data parallelism generally leads to higher flops utilization, while extensive tensor or context partitioning reduces efficiency due to communication and frequent synchronization overheads. However, because the 1B model is significantly smaller, the computation-to-communication ratio is lower, making the system more sensitive to communication latency. Thus, for smaller models, simpler parallelization structures—favoring data parallelism—tend to yield superior efficiency.

The **best configuration** for this model is (**DP=8, PP=1, TP=1, CP=1**) showcasing MFU of 43.3%, with a step time of 28.3 s and a throughput of 148.4 K tokens/s. This setup corresponds to a purely data-parallel configuration, where each NPU holds a full copy of the model and processes a distinct batch of data. Since the model and activations fits into each device’s memory, not using any model or activation parallelization scheme allows for best utilization of computational capability. The absence of tensor or pipeline communication minimizes synchronization delays resulting in minimal overhead across all configurations.

In contrast, the **worst configuration** for LLaMA 1B is (**DP=1, PP=1, TP=4, CP=2**) which exhibits MFU of 6.2%, with a step time of 197.0 s and a throughput of only 21.3 K tokens/s. The substantial drop



(a) Best case parallelization scenario (DP=8, PP=1, TP=1, CP=1). (b) Worst case parallelization scenario (DP=1, PP=1, TP=4, CP=2).

Figure 7: Runtime composition of the LLaMA-1B model under the best and worst parallelization strategies, reported in (DP, PP, TP, CP) order. The best-case configuration (DP = 8, PP = 1, TP = 1, CP = 1) is characterized by the highest proportion of cube operations, whereas the worst-case configuration (DP = 1, PP = 1, TP = 4, CP = 2) exhibits a lower cube share with increased vector and parallelization overhead.

in efficiency arises from the combined use of high degree of tensor and context parallelism. Each transformer layer requires multiple all-reduce operations across four tensor partitions and synchronization of context parallelism communication. Because the model is relatively small, the communication-to-computation ratio becomes unfavorable, and NPUs spend a large portion of time waiting for synchronization rather than performing useful computation. As a result, hardware resources are severely underutilized.

Intermediate configurations, such as (DP=4, PP=2, TP=1, CP=1) and (DP=2, PP=4, TP=1, CP=1), yield MFU values in the 36–38% range, with throughputs around 124–131 K tokens/s. These settings demonstrate that shallow pipeline parallelism can complement data parallelism without imposing excessive communication overhead, but further increases in pipeline depth reduce efficiency due to synchronization bubbles. Configurations with $CP \geq 4$ or $TP \geq 4$ consistently report MFU below 20%, confirming that fine-grained model partitioning introduces significant communication costs that outweigh computational benefits for small models.

Analysis of Operations. Figure 7 presents the operation breakdown for the purely data-parallel configuration (DP=8, PP=1, TP=1, CP=1) which achieves the highest flops utilization, and for the most communication-heavy configuration of (DP=1, PP=1, TP=4, CP=2) resulting the lowest MFU. These distributions highlight how the interplay between model size and partitioning strategy shapes the balance between computation and communication.

In the best-performing setting, shown in Figure 7a, execution is dominated by **Cube** (GEMM) kernels, which constitute **64.0%** of the total runtime. These large GEMMs form the bulk of the attention and feed-forward computations, and because **TP=1**, they remain fully intact and run efficiently on the Ascend NPU cube units. The remaining operations—**Vector** kernels (24.2%) and **Fused Attention** kernels (11.70%) execute with minimal overhead, as the model is neither tensor- nor context-partitioned. Notably, **CP=1** ensures that attention operates on the complete sequence without requiring any communication needs. Since the 1B model and activations for sequence length of 4K fits well into a single device’s memory, no context splitting is needed to meet memory constraints. These together enable each device to sustain a high ratio of computation relative to communication. This compute-dominated execution pattern explains the comparatively high MFU observed for this configuration and underscores why pure data parallelism is particularly effective at the 1B model scale with 4K input sequence.

In contrast, the poorest-performing configuration (DP=1, PP=1, TP=4, CP=2), shown in Figure 7b, displays an execution profile that is far more communication-bound. Here, the proportion of time spent in GEMM

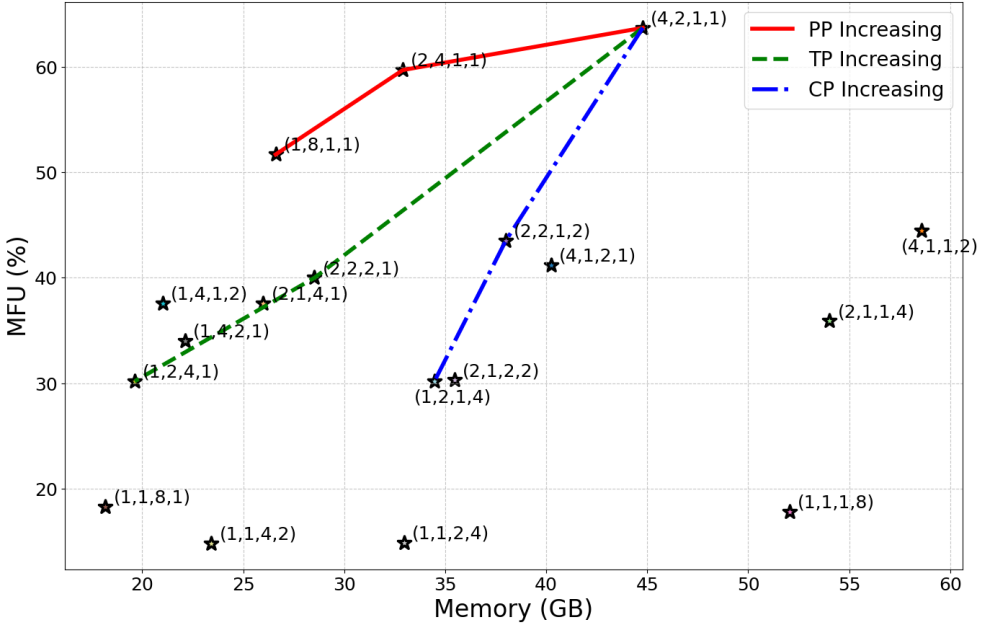
Table 11: Performance Analysis of Parallelization Strategies for LLaMA 1B

DP	PP	TP	CP	Step Time (s)	Throughput (K tokens/s)	Mem (GB)	MFU (%)
8	1	1	1	28.3	148.4	17.3	43.3
4	1	2	1	61.7	68.0	11.0	19.8
4	2	1	1	32.1	130.6	12.1	38.3
4	1	1	2	43.7	95.9	14.1	28.0
2	1	4	1	75.2	55.8	7.3	16.3
2	4	1	1	33.9	123.9	9.4	36.1
2	1	1	4	83.2	50.4	12.6	14.7
2	2	2	1	46.8	89.5	8.3	26.1
2	2	1	2	47.0	89.2	10.0	26.0
2	1	2	2	96.7	43.4	9.4	12.6
1	1	8	1	150.9	27.8	4.8	8.1
1	8	1	1	43.6	96.2	7.6	28.1
1	1	1	8	174.4	24.1	11.4	7.0
1	4	2	1	59.2	70.9	6.6	20.5
1	2	4	1	75.7	55.4	5.9	16.1
1	1	4	2	197.0	21.3	6.5	6.2
1	4	1	2	53.4	78.6	7.7	23.0
1	2	1	4	87.1	48.1	8.9	14.1

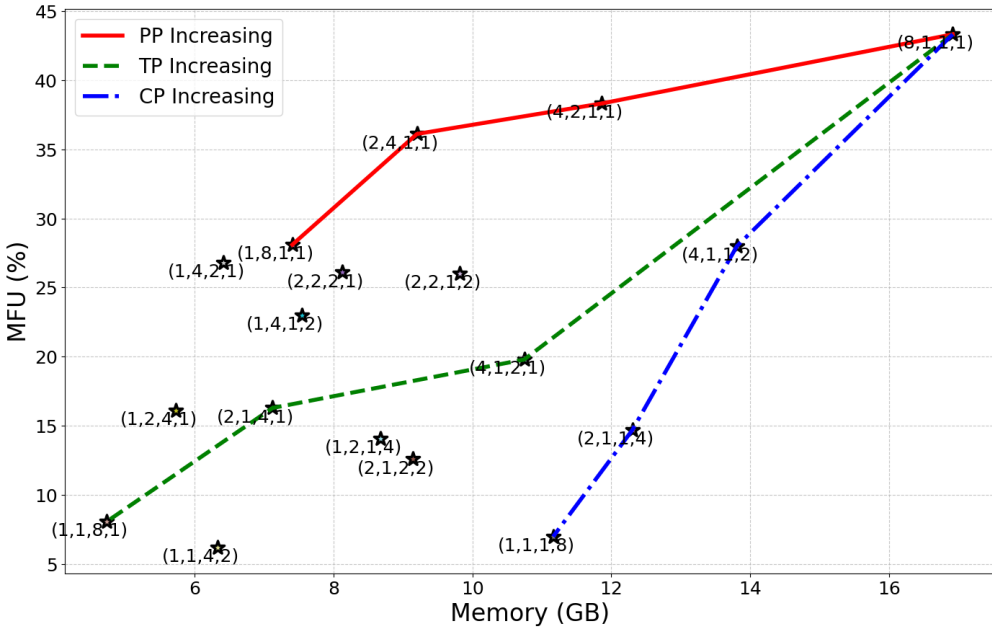
computation drops to **34.3%**, while communication-intensive categories expand significantly. Deep tensor parallelism (**TP=4**) forces every GEMM to be partitioned into four smaller fragments, reducing matrix sizes and dramatically lowering arithmetic intensity. This fragmentation is directly reflected in the **26.0%** of total runtime attributed to TP-related synchronization. At the same time, **CP=2** divides the sequence dimension into two segments, requiring intermediate communication, which results in **14.7%** of runtime spent on CP-related communication. The fused-attention pathway increases to **6.6%**, not because attention becomes more computationally demanding, but because sequence partitioning disrupts its natural computation pattern and increases the number of communication steps required per attention head. In short, For a small model such as LLaMA 1B, whose computation-to-communication ratio is inherently lower, the communication overhead and synchronization costs of this setting dominate the iteration time, leading to the lowest MFU among all configurations.

6.2.3 Impact of Parallelism on MFU and Memory Consumption for LLaMA models

To contextualize the behavior observed in Table 10, Figure 8 illustrates the relationship between *Model FLOPs Utilization (MFU)* and memory consumption across the all parallelization configurations evaluated for both LLaMA 7B and LLaMA 1B. To better illustrate how MFU varies as data parallelism decreases, which corresponds to the highest MFU, and as other forms of parallelism increase, we connect the corresponding configurations with colored lines in our plots: the DP→PP trend is shown in red, DP→TP in green, and DP→CP in blue. Results highlight that, for both considered models, the highest and lowest memory consumption are associated with the DP and TP partition groups, respectively. For instance, the average memory consumption of (DP=4, PP=2, TP=1, CP=1) is 45 GB, while the average memory consumption of (DP=1, PP=1, TP=8, CP=1) is 27 GB for LLaMA-7B. A similar trend holds for LLaMA-1B, where the highest memory consumption is 17.3 GB for (DP=8, PP=1, TP=1, CP=1), and the lowest is 4.8 GB for (DP=1, PP=1, TP=8, CP=1). The former has the highest memory usage, since no partitioning occurs and both weights and activations are fully replicated across devices and the later has low memory footprint since most of the memory consumption related to weights. The PP memory footprint can be considered the second-best scenario in terms of memory consumption after TP, because both activations and weights

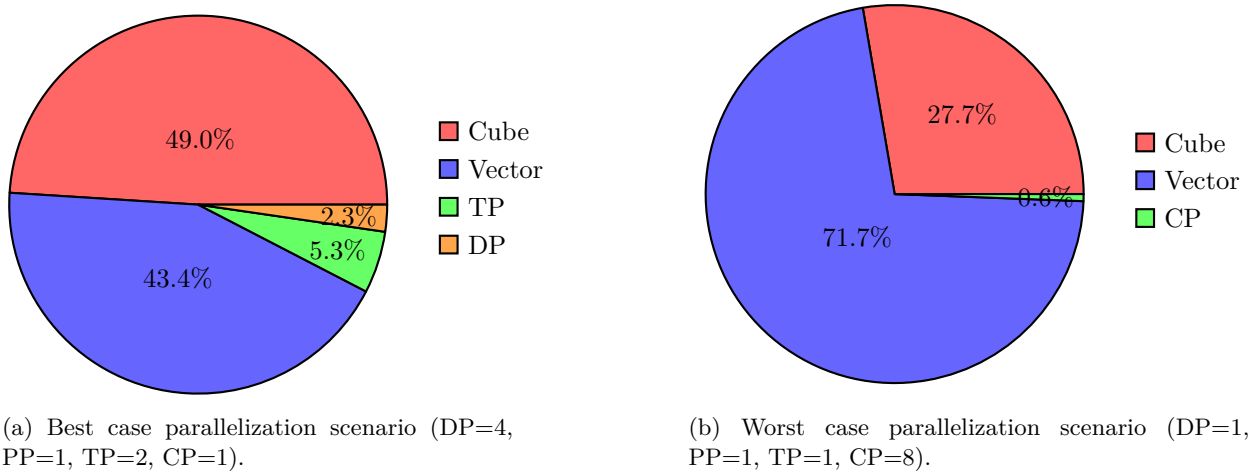


(a) LLaMA 7B



(b) LLaMA 1B

Figure 8: MFU versus memory consumption for LLaMA models under different parallelism types. Starting from the highest MFU datapoint at the rightmost end of the curve, we vary PP, TP, or CP while keeping the total number of devices fixed. DP yields the highest efficiency, whereas TP minimizes memory usage; PP provides the strongest middle-ground trade-off. The figure's tuple format (a,b,c,d) reflects the same (DP=a, PP=b, TP=c, CP=d) values used in the text.



(a) Best case parallelization scenario (DP=4, PP=1, TP=2, CP=1).

(b) Worst case parallelization scenario (DP=1, PP=1, TP=1, CP=8).

Figure 9: Runtime operation breakdown of the Mamba-7B model for the best and worst parallelization configurations, reported in (DP, PP, TP, CP) order. In the best-case setup (DP = 4, PP = 1, TP = 2, CP = 1), Cube and vector operations contribute comparably to the overall runtime. In contrast, the worst-case setup (DP = 1, PP = 1, TP = 1, CP = 8) is overwhelmingly dominated by vector operations, with only a minor contribution from Cube operations.

are partitioned across different pipeline stages. CP ranks third, since it partitions only the activations, and due to the low sequence length, activation memory remains relatively small. Considering MFU as the main evaluation metric, DP and PP has the first and second ranks respectively. The reason behind this order is that DP has no communication overhead, making it the most efficient. PP ranks second because it requires only limited communication, mainly for transferring activations between stages.

For both LLaMA based models, graphs indicate that configurations with higher DP are preferable to achieve higher MFU. However, when memory becomes the limiting factor, PP should be considered first, as it offers a low memory footprint while maintaining high computational efficiency. The trade-off between memory and computational efficiency for PP is better than TP as shown in the curve.

6.3 Mamba Experiments

We further extend our analysis of parallelization strategy selection to the Mamba models and analyze the Mamba-7B and Mamba-1B models in detail. The configurations of the models under study are presented in Table 12.

Table 12: Mamba models configuration

Model	Layers	Hidden size	State dim	Num groups	FFN hidden size	Expand	chunk siz
Mamba-1B	16	2048	64	8	4096	2	64
Mamba-7B	40	4096	128	8	10880	2	64

6.3.1 Performance Analysis of Parallelization Strategies for Mamba 7B

Observation. Table 13 summarizes the performance of the Mamba-7B model under the considered parallelization scenarios. Across all tested configurations, MFU ranges from approximately 8% to 20%, which is lower than that of LLaMA-based models and reflects the distinct computational pattern of the Mamba architecture—one that emphasizes sequential state updates rather than dense matrix multiplications—resulting in lower effective. The configuration with DP=8 could not satisfy the memory requirements on a single device. Even splitting the activations with CP=2 did not allow the model to fit on a single card as CP only distributed activation memory. Using PP=2 could be helpful to distribute layers across multiple devices; however, unlike the LLaMA model—where the best MFU is achieved with PP=2—the Mamba architec-

ture cannot be placed across two cards due to its very large linear layers that generate state space duality (SSD) components. As a result, the best MFU is obtained with $TP=2$, which is the only configuration with minimal model partitioning that fits the model by distributing its large linear and convolutional components efficiently across two tensor partitions while preserving strong data-parallel scaling. This configuration (**DP=4, PP=1, TP=2, CP=1**) achieves the **highest MFU** of 20.2%, with a step time of 191.6 s and a throughput of 21.9 K tokens/s.

The configuration (**DP=1, PP=1, TP=1, CP=8**) exhibits the **lowest MFU** of 8.4%, with a step time of 461.1 s and a throughput of 9.1 K tokens/s. The steep performance degradation is primarily attributed to the extensive context partitioning ($CP=8$), which significantly reduces the amount of cube operations proportion and consequently lowers overall compute utilization. Moreover, in Mamba, the vector operations contain large fixed costs that do not shrink much when the sequence becomes shorter. These include chunk-boundary prefix work, memory-bound state updates, and fixed NPU overheads such as launching many small kernels, repeated synchronizations, and shared-memory setup. Because these costs remain nearly constant while the matmul-based cube operations shrink substantially, vector time decreases much less than cube time, increasing its share in the overall runtime.

Intermediate setups such as ($DP=2, PP=2, TP=2, CP=1$) and ($DP=1, PP=2, TP=4, CP=1$) yield MFU values around 16–18% with throughput between 18–20 K tokens/s. Overall, moderate tensor parallelism provides slight gains by enabling limited intra-layer concurrency, whereas excessive pipeline or context partitioning consistently degrades performance. Heavy context partitioning shifts computation away from cube-intensive operations toward lightweight vector work, leaving the cube units underutilized and the hardware effectively “compute-starved.” Since the model already fits under TP, additional pipelining is unnecessary and would only introduce bubbles, further reducing arithmetic intensity, throughput, and utilization.

Table 13: Performance Analysis of Parallelization Strategies for Mamba 7B

DP	PP	TP	CP	Step Time (s)	Throughput (K tokens/s)	Mem (GB)	MFU (%)
4	1	2	1	191.6	21.9	56.0	20.2
2	1	4	1	210.9	19.9	33.2	18.4
2	2	2	1	215.0	19.5	40.7	18.0
2	2	1	2	217.3	19.3	53.8	17.8
2	1	2	2	247.5	16.9	45.0	15.6
1	1	8	1	299.9	14.0	20.5	12.9
1	1	1	8	461.1	9.1	59.2	8.4
1	4	2	1	254.2	16.5	31.1	15.2
1	1	2	4	435.1	9.6	38.2	8.9
1	2	4	1	232.3	18.1	25.0	16.7
1	1	4	2	359.3	11.7	27.3	10.8
1	4	1	2	264.0	15.9	38.8	14.7
1	2	1	4	295.2	14.2	42.7	13.1

Analysis of Operations Figure 9a presents the operation breakdown for the configuration ($DP=4, PP=1, TP=2, CP=1$), which achieves the highest overall performance, and, in contrast, the configuration ($DP=1, PP=1, TP=1, CP=8$), which yields the lowest MFU. A comparison between these two settings shows that the primary reason for MFU degradation is the substantial reduction in Cube FLOPs from 49.0 to 27.7 percent. This drop results from overly partitioning the sequence length, which reduces the amount of GEMM computation per device and leaves the Ascend hardware under-utilized. Since the computational throughput of Ascend devices is significantly higher for GEMM operations than for vector operators, the reduction in GEMM workload is especially detrimental, further reducing the MFU.

Compared to attention-based models, the Mamba architecture exhibits a lower ratio of Cube FLOPs in both its best and worst configurations. This indicates that Mamba is inherently less efficient in terms of hardware

utilization, as it provides fewer high-intensity GEMM operations relative to attention. This confirms that Mamba has lower A.I. than LLaMA, showing that Mamba operates in a memory-bound regime, while attention-based models are compute-bound. Another important observation is that the communication overhead of CP in Mamba is substantially lower than in attention. This is because Mamba only exchanges its recurrent state, whose dimension does not depend on the sequence length, whereas attention-based models must exchange the full key–value tensors, leading to significantly higher communication costs.

6.3.2 Performance Analysis of Parallelization Strategies for Mamba 1B

Observation. The MFU values for Mamba 1B range from 3.1% to 20.4% across all parallelization configurations under consideration. This behavior reflects Mamba’s state-space architecture: sequential state propagation limits fully parallelizable work, reducing arithmetic intensity relative to attention-based models. Results show that the configuration (**DP=8, PP=1, TP=1, CP=1**) achieves the **highest MFU** of 20.4%, with a step time of 29.1 s and a throughput of 144.3 K tokens/s. This setting benefits from distributing the batch across eight devices, thereby maximizing locally available computation per card while keeping both pipeline and context partitioning disabled. The absence of deep model partitioning minimizes synchronization, and each device operates on sufficiently large micro-batches allowing the hardware to operate at its highest possible effective capacity.

In contrast, the configuration (**DP=1, PP=1, TP=1, CP=8**) yields the **lowest MFU** of 3.1%, with a step time of 191.1 s and a throughput of only 22.0 K tokens/s. The same trend holds for TP=8 and PP=8, with slightly better computational use. This degradation arises from excessive decrease of the workload on each device. In addition to that, communication overhead and bubble time are two reasons for the performance degradation of TP and PP.

Intermediate configurations such as (DP=4, PP=1, TP=2, CP=1), (DP=2, PP=1, TP=4, CP=1) and (DP=1, PP=2, TP=4, CP=1) yield MFU values in the 6–12% range. These results indicate that tensor parallelism provides moderate improvements by enabling limited intra-layer concurrency, yet its effectiveness diminishes rapidly once additional parallel dimensions are introduced. Configurations with $PP \geq 4$ or $CP \geq 2$ consistently exhibit reduced MFU. Increasing pipeline depth introduces unnecessary bubble time, diminishing compute overlap. In addition to that, communication overhead and bubble time are two reasons for the performance degradation of TP and PP.

Analysis of Operations Here, we examine the best and worst configurations for Mamba-1B, namely (DP=8, PP=1, TP=1, CP=1) and (DP=1, PP=1, TP=1, CP=8). As discussed extensively earlier, the highest MFU is achieved with (DP=8, PP=1, TP=1, CP=1), since this configuration maximizes data distribution while avoiding the additional communication overhead introduced by TP and CP as well as the pipeline bubble time caused by PP. In this setting, the highest possible amount of GEMM computation is executed. Similarly, context parallelism partitions the recurrent computation across devices, this shift increases the relative contribution of vector communication overhead compared to compute time, causing communication to dominate and ultimately degrading MFU.

Regarding the Mamba model, comparing the Cube FLOP ratio of Mamba-1B with LLaMA 1B shows a significant drop from 64.0 to 42.8 percent, alongside an increase in the vector-operation ratio from 24.2 to 57.1 percent. This reduction in cube-intensive computation, and the corresponding rise in vector-dominated workloads, is the main factor behind the MFU degradation when moving from LLaMA to Mamba (from 43.3% to 20.4%), reflecting the inherent structure of the Mamba architecture.

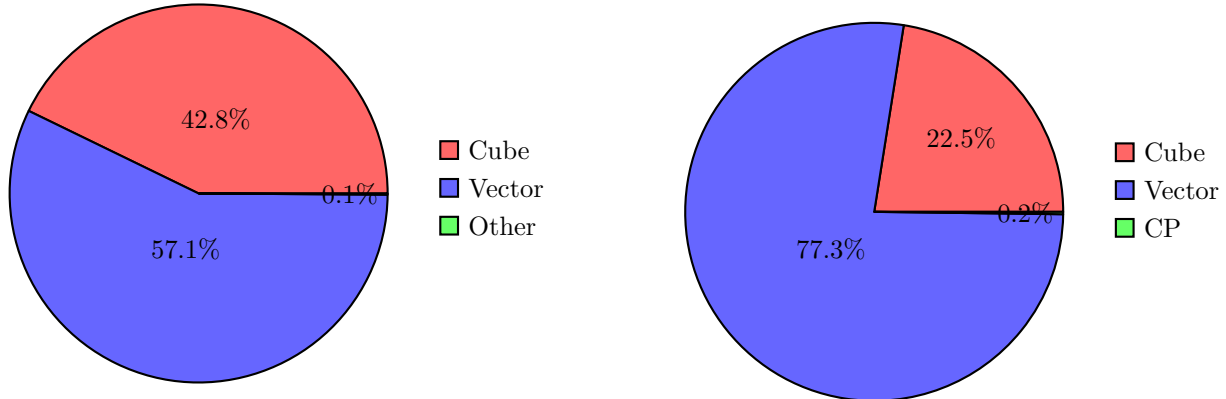
The operation-time breakdown of the lowest MFU configuration of (DP=1, PP=1, TP=1, CP=8) shows similar pattern to the Mamba-7B worst case scenario results. Excessively partitioning the sequence length reduces the proportion of Cube operations and forces the model to operate primarily on lightweight vector computations. This behavior indicates that, for relatively short sequence lengths such as 4K, the Mamba architecture does not benefit from high CP values.

6.3.3 Impact of Parallelism on MFU and Memory Consumption for Mamba models

In Figure 11, we examine MFU as a function of consumed memory across different parallelization configurations. In both figures, the dashed green curve corresponding to TP consistently appears above the others,

Table 14: Performance Analysis of Parallelization Strategies for Mamba 1B (MFU recalculated)

DP	PP	TP	CP	Step Time (s)	Throughput (K tokens/s)	Mem (GB)	MFU (%)
8	1	1	1	29.1	144.3	24.8	20.4
4	1	2	1	47.7	88.0	14.7	12.4
4	2	1	1	48.2	87.0	16.8	12.3
4	1	1	2	48.2	86.9	18.1	12.3
2	1	4	1	68.2	61.5	9.3	8.7
2	4	1	1	81.3	51.6	11.6	7.3
2	1	1	4	97.7	42.9	15.4	6.1
2	2	2	1	64.5	65.0	11.6	9.2
2	1	2	2	84.6	49.6	11.6	7.0
2	2	1	2	66.9	62.7	13.5	8.9
1	1	8	1	128.9	32.5	5.8	4.6
1	8	1	1	148.1	28.3	8.7	4.0
1	1	1	8	191.1	22.0	14.2	3.1
1	4	2	1	98.8	42.4	7.6	6.0
1	1	2	4	187.4	22.4	9.8	3.2
1	2	4	1	84.1	49.9	6.9	7.1
1	1	4	2	166.6	25.2	7.6	3.6
1	4	1	2	104.5	40.1	9.3	5.7
1	2	1	4	118.0	35.6	11.4	5.0



(a) Best case parallelization scenario (DP=8, PP=1, TP=1, CP=1).

(b) Worst case parallelization scenario (DP=1, PP=1, TP=1, CP=8).

Figure 10: Runtime operation breakdown of the Mamba-1B model under the best and worst parallelization configurations, reported in (DP, PP, TP, CP) order. In the best-case configuration (DP = 8, PP = 1, TP = 1, CP = 1), vector operations slightly outweigh Cube operations, with both contributing substantially to overall runtime. In the worst-case configuration (DP = 1, PP = 1, TP = 1, CP = 8), execution time is dominated by vector operations, while Cube operations account for a much smaller fraction.

indicating that TP achieves the highest MFU for the Mamba model. In addition, TP exhibits a smaller memory footprint compared to the other parallelization strategies. For example, Mamba-7B exhibits an average memory usage of 56 GB under the configuration (DP=4, PP=1, TP=2, CP=1), compared to 20.5 GB for (DP=1, PP=1, TP=8, CP=1). A similar pattern is observed for Mamba-1B, where memory usage

peaks at 24.8 GB with (DP=8, PP=1, TP=1, CP=1) and reaches a minimum of 5.8 GB under (DP=1, PP=1, TP=8, CP=1). In contrast, the dashed blue CP curve is positioned at the bottom, reflecting the lowest performance in terms of both memory usage and MFU. Therefore, when the model does not fit on a single device, TP is the most effective choice to apply first. For both LLaMA and Mamba, TP and CP deliver the highest and lowest memory efficiency, respectively. The underlying reason is the short sequence length, where model weights dominate the memory footprint compared to activations, making TP more beneficial than CP under these conditions. PP ranks second in memory efficiency because it partitions layers across devices but still requires each stage to store full activations for its portion of the sequence, leading to higher memory consumption than TP.

6.4 Summary of Empirical Insights

To obtain a broader perspective on the impact of parallelization strategy combinations across different model types and sizes, we summarize the best and worst strategies for all four models in our case study (Table 15). Notably, for small models of both Attention and Mamba, the optimal parallelization strategy involves using data parallelism (DP) only. As model size grows beyond the memory capacity of a single device, incorporating additional forms of model parallelism becomes beneficial, though only up to a moderate scale. For instance, scaling the Attention model from 1B to 7B parameters benefits from pipeline parallelism (PP = 2) while reducing DP to 4. Similarly, scaling Mamba from 1B to 7B parameters benefits from tensor parallelism (TP = 2) while also reducing DP to 4.

Table 15: Best and worst parallelization for Attention and Mamba models in case study

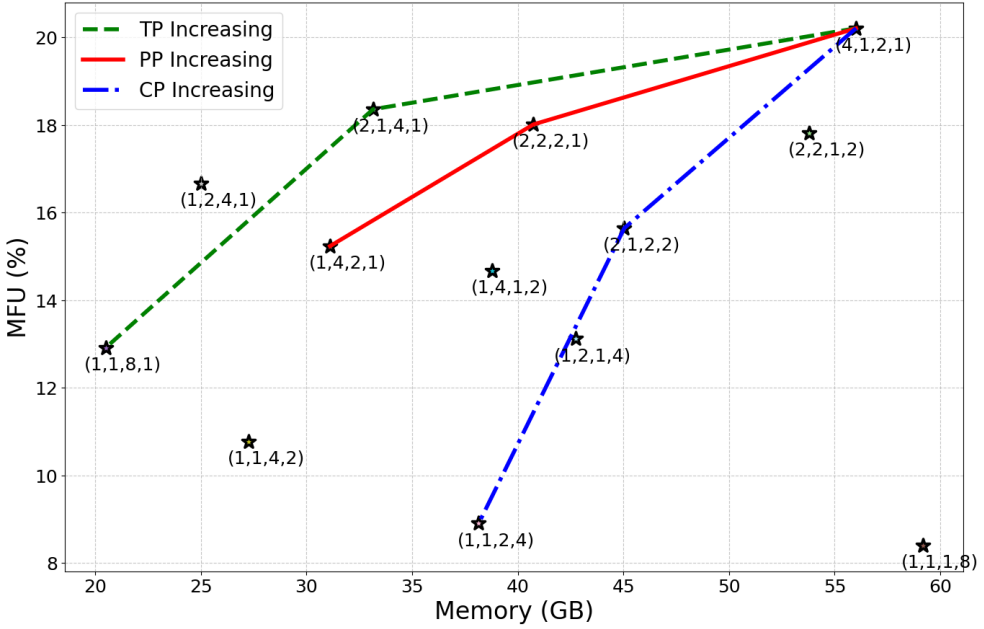
Model	Best Case		Worst Case	
	(DP,PP,TP,CP)	MFU(%)	(DP,PP,TP,CP)	MFU(%)
LLaMA 1B	(8,1,1,1)	43.3	(1,1,4,2)	6.2
LLaMA 7B	(4,2,1,1)	63.7	(1,1,4,2)	14.8
Mamba-1B	(8,1,1,1)	20.4	(1,1,1,8)	3.1
Mamba-7B	(4,1,2,1)	20.2	(1,1,1,8)	8.4

Insights on parallelization design practices evident from our experiments are summarized below:

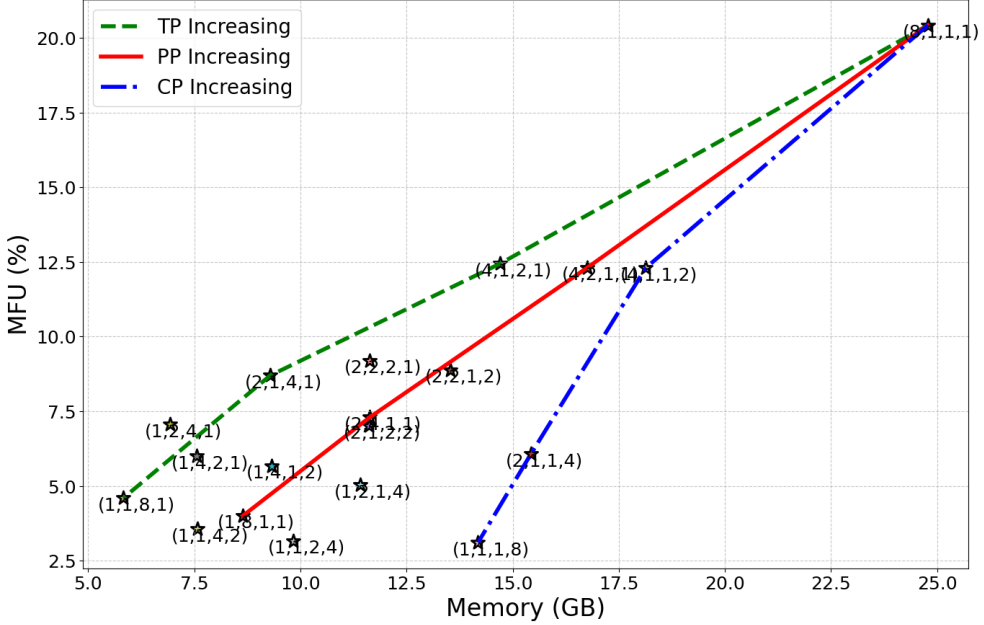
- For small models (e.g., 1B), data parallelism (DP) is generally preferred, as both the model and activations fit within memory constraints.
- As model size increases to moderate scales (e.g., 7B), introducing limited model parallelism (such as PP or TP) while maximizing DP within memory limits provides a balanced trade-off and yields the highest MFU. More specifically, PP is the most favorable choice for LLaMA models, whereas TP is more effective for Mamba models.
- Further increases in the degree of model parallelism (PP/TP) are expected to benefit extremely large models. Increasing context parallelism (CP) is expected to be advantageous for very long sequences; however, due to resource limitations, experimental validation of these scenarios is left for future work.

7 Open Challenges and Future Directions

This survey has examined acceleration strategies for efficient training and inference. Although the design of distributed AI infrastructure has advanced to support large-scale models and ultra-long contexts, significant challenges remain. In this section, we identify key unresolved issues and highlight research gaps that point to promising directions for future exploration. Some major open challenges include:



(a) Mamba 7B



(b) Mamba 1B

Figure 11: MFU as a function of memory consumption for Mamba under different parallelism settings. Starting from the highest MFU datapoint at the rightmost end of the curve, we vary PP, TP, or CP while keeping the total number of devices fixed. TP provides the most memory-efficient scaling, whereas CP results in the lowest MFU and highest memory usage. The tuple format (a, b, c, d) denotes $(DP = a, PP = b, TP = c, CP = d)$.

Resource Utilization Despite recent advancements in distributed training and inference systems, optimal hardware utilization remains a significant challenge. Overhead exists from various sources, such as memory access delays in memory-bound operations and communication wait times in bandwidth-bound operations. Additional auxiliary overhead also exists; some examples include kernel launches for small operations and cases where tensor shape dimensions do not favor optimal tiling to the parallel cores of the accelerators. Recent progress in Model FLOPS Utilization (MFU) has shown improved efficiency in attention-based architectures, yet a substantial gap remains compared to the hardware’s peak performance. Moreover, emerging models such as Mamba exhibit significantly lower MFU compared to conventional architectures like Transformers. This gap highlights the need for further research into both model architecture design and system-level optimization strategies that can better exploit hardware capabilities.

Energy Considerations As frontier models approach the trillion-parameter scale, energy constraints are becoming as critical as hardware availability. OpenAI has recently committed to gigawatt-scale compute, and Meta is investing billions to acquire roughly 350,000 GPUs—but such expansions are only feasible when sufficient power capacity exists to operate them. Energy availability increasingly shapes both research capability and service deployment [22, 28]. A fundamental yet underexplored trade-off exists between inference latency or training throughput and energy consumption, forming a Pareto frontier that is not fully addressed in this work or in the broader literature. Future research should systematically examine the theoretical and empirical relationships between energy usage, power efficiency, and distributed parallelization strategies. Advancing this line of inquiry will be essential for enabling both sustainable model development and truly *Green AI*.

Communication Overhead Recent research on reducing communication overhead in distributed training and inference has increasingly focused on communication overlap strategies. Emerging approaches in this direction have explored fine-grained slicing techniques, wherein the communication of one slice is overlapped with the computation of another. While these methods offer promising improvements in efficiency, they continue to suffer from tail-end overhead. Additionally, they also impose strict synchronization requirements at intermediate stages of the algorithm. These constraints present open challenges and underscore the need for further investigation into more flexible and scalable collective communication strategies.

Auto-parallelism Trending approaches for automatically finding optimal parallelization strategies typically rely on hierarchical search-based approaches. These methods often depend on profiling or executing the model under various configurations, which is costly, time-consuming, and often infeasible for extremely large models. Cost model based approaches are on the other hand are known to produce suboptimal solutions and often exhibit hardware dependencies. These limitations highlight the need for further research into efficient auto-parallelism methods.

In light of the current limitations, further advancements in model acceleration may be achievable through the following avenues:

Model-System Codesign Recent research in *Efficient AI* has observed a shift toward models and infrastructure evolving through a co-design paradigm rather than advancing independently. Despite this shift, joint optimization of hardware-aware model architectures and efficient distributed systems remains underexplored. Key challenges in this direction include designing efficient architectures that generalize across multiple device types and accounting for compute-bound, memory-bound, bandwidth-bound, and energy consumption considerations in model layer design. Further research can focus on developing concrete mathematical models of design objectives and solid theoretical foundations, in addition to relying solely on empirical or cost-model simulation-based optimization.

Parallel Strategies for Model Blocks Future work should place greater emphasis on developing principled guidelines for selecting parallelization strategies tailored to specific model blocks, such as attention mechanisms, Mamba blocks, or other emerging architectures across different modalities, such as text, vision, or speech. These architectures are certainly different and should be carefully studied. Current research often provides insights with limited theoretical examples into how different parallel strategies should be chosen

under varying architectural or workload settings. Constructing analytical models with formal mathematical underpinnings could help bridge this gap, enabling systematic evaluation of parallelization strategies. Such models would create a closed loop between workload analysis and architecture design, guiding the development of next-generation architectures that are both computation and communication-efficient.

Neural Autoparallelism Another promising direction is the advancement of autoparallelism—automatically selecting optimal parallelization strategies within the vast design space. In parallel, the rise of AI-driven techniques for solving low-level system challenges, such as automated GPU kernel generation (AI for Kernels), provides strong precedent for leveraging neural approaches in distributed training [37]. Similarly, methods inspired by neural architecture search, equipped with tailored cost functions, have shown success in discovering efficient mixtures-of-experts (MoE) and transformer architectures [48, 40, 8]. Extending these ideas to the problem of parallel strategy selection could yield significant breakthroughs. We therefore recommend further exploration of neural and learning-based methods for auto-parallelism as a key avenue for future research.

8 Conclusion

In this survey, we conduct a comprehensive review of distributed strategies for efficient LLM training and inference. Based on our findings, we present system design guidelines with a concrete formulation of design objectives. Most existing works show improvements in distributed systems to support trillion-parameter models with context lengths of up to millions of tokens, enabling efficient execution through a hybrid combination of multiple parallelism strategies and other acceleration techniques. Auto-parallelism is also gaining traction, where the optimal strategy can be searched in a simulation environment using a cost model for deploying large models. We presented theoretical and empirical analyses to guide researchers and practitioners to select parallel strategies for model development. In light of current trends, we also discussed prevailing concerns and potential directions for further improvements in accelerating large models. Finally, we hope this study serves as a hands-on reference for better understanding the current research progress on distributed strategies for efficient AI infrastructure and helps readers with system design recommendations and guidance for future research. Grounded in prior work, this survey reflects the current state of the field and is intended to guide and inspire subsequent research efforts.

Broader Impact Statement

This work focuses on the analysis and design of distributed parallelization strategies for training and deploying large language models. While our contribution is primarily methodological and systems-oriented, the techniques discussed here may indirectly influence the scale, accessibility, and efficiency of future AI systems.

On the positive side, improved parallel strategies can reduce computational overhead, lower energy consumption, and make large-scale training more cost-effective. These advances may enable a broader community of researchers and practitioners to experiment with state-of-the-art models, fostering openness, reproducibility, and innovation in the field.

However, the increased efficiency and scalability that arise from better parallelism may also accelerate the development and deployment of increasingly large models, which can raise ethical considerations. These include heightened energy usage, environmental impact, concentration of computational resources among a few institutions, and the downstream risks associated with more capable AI systems, such as misuse, bias propagation, or harmful applications. Although our work does not introduce new model capabilities, improved distributed training frameworks could indirectly contribute to enabling such systems.

We encourage users of this research to consider these broader implications when applying parallelization strategies in practice, particularly with respect to responsible resource allocation, transparency in system design, and the societal implications of large-scale AI development. Our analysis is intended to inform and support principled decision-making rather than promote unconstrained scaling, and we hope it motivates further research into environmentally conscious and ethically aligned AI infrastructure.

Acknowledgments

The authors gratefully acknowledge the support of the Toronto Ascend team. The authors also extend their special thanks to Austin Wen for generously sharing his knowledge and insights throughout this work.

References

- [1] Bo Adler, Niket Agarwal, Ashwath Aithal, Dong H Anh, Pallab Bhattacharya, Annika Brundyn, Jared Casper, Bryan Catanzaro, Sharon Clay, Jonathan Cohen, et al. Nemotron-4 340b technical report. *arXiv preprint arXiv:2406.11704*, 2024.
- [2] Amazon. Aws neuron. URL <https://github.com/aws-neuron/aws-neuron-sdk>.
- [3] Hossam Amer, Joe Osborne, Michael Zaki, and Mohamed Afify. On-device emoji classifier trained with gpt-based data augmentation for a mobile keyboard. *arXiv preprint arXiv:2411.05031*, 2024.
- [4] Reza Yazdani Aminabadi, Samyam Rajbhandari, Ammar Ahmad Awan, Cheng Li, Du Li, Elton Zheng, Olatunji Ruwase, Shaden Smith, Minjia Zhang, Jeff Rasley, et al. Deepspeed-inference: enabling efficient inference of transformer models at unprecedented scale. In *SC22: International Conference for High Performance Computing, Networking, Storage and Analysis*, pp. 1–15. IEEE, 2022.
- [5] Muralidhar Andoorveedu, Zhanda Zhu, Bojian Zheng, and Gennady Pekhimenko. Tempo: Accelerating transformer-based model training through memory footprint reduction. *Advances in Neural Information Processing Systems*, 35:12267–12282, 2022.
- [6] Yulong Ao, Zhihua Wu, Dianhai Yu, Weibao Gong, Zhiqing Kui, Minxu Zhang, Zilingfeng Ye, Liang Shen, Yanjun Ma, Tian Wu, et al. End-to-end adaptive distributed training on paddlepaddle. *arXiv preprint arXiv:2112.02752*, 2021.
- [7] Ascend. Mindspeed llm. URL <https://gitee.com/ascend/MindSpeed-LLM>.
- [8] Steve Bakos and Heidar Davoudi. Searching for the best student architecture in a knowledge distillation framework. *Knowledge-Based Systems*, pp. 114210, 2025.
- [9] Vishnu Vardhan Baligodugula and Fathi Amsaad. Optimizing distributed training approaches for scaling neural networks. *arXiv preprint arXiv:2503.23186*, 2025.
- [10] BentoML. Llm inference metrics. <https://bentoml.com/llm/inference-optimization/llm-inference-metrics>, 2025.
- [11] Zhengda Bian, Qifan Xu, Boxiang Wang, and Yang You. Maximizing parallelism in distributed training for huge neural networks. *arXiv preprint arXiv:2105.14450*, 2021.
- [12] Felix Brakel, Uraz Odyurt, and Ana-Lucia Varbanescu. Model parallelism on distributed infrastructure: A literature review from theory to llm case-studies. *arXiv preprint arXiv:2403.03699*, 2024.
- [13] Li-Wen Chang, Wenlei Bao, Qi Hou, Chengquan Jiang, Ningxin Zheng, Yinmin Zhong, Xuanrun Zhang, Zuquan Song, Chengji Yao, Ziheng Jiang, et al. Flux: fast software-based communication overlap on gpus through kernel fusion. *arXiv preprint arXiv:2406.06858*, 2024.
- [14] Chang Chen, Xiuhong Li, Qianchao Zhu, Jiangfei Duan, Peng Sun, Xingcheng Zhang, and Chao Yang. Centauri: Enabling efficient scheduling for communication-computation overlap in large model training via communication partitioning. In *Proceedings of the 29th ACM International Conference on Architectural Support for Programming Languages and Operating Systems, Volume 3*, pp. 178–191, 2024.
- [15] Chi-Chung Chen, Chia-Lin Yang, and Hsiang-Yun Cheng. Efficient and robust parallel dnn training through model parallelism on multi-gpu platform. *arXiv preprint arXiv:1809.02839*, 2018.

- [16] Feilong Chen, Yijiang Liu, Yi Huang, Hao Wang, Miren Tian, Ya-Qi Yu, Minghui Liao, and Jihao Wu. Mindvl: Towards efficient and effective training of multimodal large language models on ascend npus. *arXiv preprint arXiv:2509.11662*, 2025.
- [17] Tianqi Chen, Bing Xu, Chiyuan Zhang, and Carlos Guestrin. Training deep nets with sublinear memory cost. *arXiv preprint arXiv:1604.06174*, 2016.
- [18] Hongrong Cheng, Miao Zhang, and Javen Qinfeng Shi. A survey on deep neural network pruning: Taxonomy, comparison, analysis, and recommendations. *IEEE Transactions on Pattern Analysis and Machine Intelligence*, 2024.
- [19] Shenggan Cheng, Shengjie Lin, Lansong Diao, Hao Wu, Siyu Wang, Chang Si, Ziming Liu, Xuanlei Zhao, Jiangsu Du, Wei Lin, et al. Concerto: Automatic communication optimization and scheduling for large-scale deep learning. In *Proceedings of the 30th ACM International Conference on Architectural Support for Programming Languages and Operating Systems, Volume 1*, pp. 198–213, 2025.
- [20] Minsik Cho, Ulrich Finkler, David Kung, and Hillery Hunter. Blueconnect: Decomposing all-reduce for deep learning on heterogeneous network hierarchy. *Proceedings of Machine Learning and Systems*, 1:241–251, 2019.
- [21] Aakanksha Chowdhery, Sharan Narang, Jacob Devlin, Maarten Bosma, Gaurav Mishra, Adam Roberts, Paul Barham, Hyung Won Chung, Charles Sutton, Sebastian Gehrmann, et al. Palm: Scaling language modeling with pathways. *Journal of Machine Learning Research*, 24(240):1–113, 2023.
- [22] Jae-Won Chung, Jeff J Ma, Ruofan Wu, Jiachen Liu, Oh Jun Kweon, Yuxuan Xia, Zhiyu Wu, and Mosharaf Chowdhury. The ml. energy benchmark: Toward automated inference energy measurement and optimization. *arXiv preprint arXiv:2505.06371*, 2025.
- [23] Damai Dai, Chengqi Deng, Chenggang Zhao, RX Xu, Huazuo Gao, Deli Chen, Jiashi Li, Wangding Zeng, Xingkai Yu, Yu Wu, et al. Deepseekmoe: Towards ultimate expert specialization in mixture-of-experts language models. *arXiv preprint arXiv:2401.06066*, 2024.
- [24] Karan Dalal, Daniel Koceja, Gashon Hussein, Jiarui Xu, Yue Zhao, Youjin Song, Shihao Han, Ka Chun Cheung, Jan Kautz, Carlos Guestrin, et al. One-minute video generation with test-time training. *arXiv preprint arXiv:2504.05298*, 2025.
- [25] Tri Dao and Albert Gu. Transformers are ssms: Generalized models and efficient algorithms through structured state space duality. *arXiv preprint arXiv:2405.21060*, 2024.
- [26] Jianru Ding, Ruiqi Cao, Indrajeet Saravanan, Nathaniel Morris, and Christopher Stewart. Characterizing service level objectives for cloud services: Realities and myths. In *2019 IEEE International Conference on Autonomic Computing (ICAC)*, pp. 200–206. IEEE, 2019.
- [27] Jiangfei Duan, Shuo Zhang, Zerui Wang, Lijuan Jiang, Wenwen Qu, Qinghao Hu, Guoteng Wang, Qizhen Weng, Hang Yan, Xingcheng Zhang, et al. Efficient training of large language models on distributed infrastructures: a survey. *arXiv preprint arXiv:2407.20018*, 2024.
- [28] Cooper Elsworth, Keguo Huang, David Patterson, Ian Schneider, Robert Sedivy, Savannah Goodman, Ben Townsend, Parthasarathy Ranganathan, Jeff Dean, Amin Vahdat, et al. Measuring the environmental impact of delivering ai at google scale. *arXiv preprint arXiv:2508.15734*, 2025.
- [29] William Fedus, Barret Zoph, and Noam Shazeer. Switch transformers: Scaling to trillion parameter models with simple and efficient sparsity. *Journal of Machine Learning Research*, 23(120):1–39, 2022.
- [30] Laingjun Feng, Chenyi Pan, Xinjie Guo, Fei Mei, Benzhe Ning, Jianxiang Zhang, Xinyang Liu, Beirong Zhou, Zeng Shu, Chang Liu, et al. Mindspeed rl: Distributed dataflow for scalable and efficient rl training on ascend npu cluster. *arXiv preprint arXiv:2507.19017*, 2025.

[31] Yangyang Feng, Minhui Xie, Zijie Tian, Shuo Wang, Youyou Lu, and Jiwu Shu. Mobiust: Fine tuning large-scale models on commodity gpu servers. In *Proceedings of the 28th ACM International Conference on Architectural Support for Programming Languages and Operating Systems, Volume 2*, pp. 489–501, 2023.

[32] Kazuki Fujii, Kohei Watanabe, and Rio Yokota. Accelerating large language model training with 4d parallelism and memory consumption estimator. *arXiv preprint arXiv:2411.06465*, 2024.

[33] Karim Gamal, Ahmed Gaber, and Hossam Amer. Federated learning based multilingual emoji prediction in clean and attack scenarios. *arXiv preprint arXiv:2304.01005*, 2023.

[34] Hao Ge, Fangcheng Fu, Haoyang Li, Xuanyu Wang, Sheng Lin, Yujie Wang, Xiaonan Nie, Hailin Zhang, Xupeng Miao, and Bin Cui. Enabling parallelism hot switching for efficient training of large language models. In *Proceedings of the ACM SIGOPS 30th Symposium on Operating Systems Principles*, pp. 178–194, 2024.

[35] Sanjay Surendranath Girija, Lakshit Arora, Shashank Kapoor, Dipen Pradhan, Aman Raj, and Ankit Shetgaonkar. Optimizing llms for resource-constrained environments: A survey of model compression techniques. In *2025 IEEE 49th Annual Computers, Software, and Applications Conference (COMPSAC)*, pp. 1657–1664. IEEE, 2025.

[36] Priya Goyal, Piotr Dollár, Ross Girshick, Pieter Noordhuis, Lukasz Wesolowski, Aapo Kyrola, Andrew Tulloch, Yangqing Jia, and Kaiming He. Accurate, large minibatch sgd: Training imagenet in 1 hour. *arXiv preprint arXiv:1706.02677*, 2017.

[37] GPU-Mode Team. Popcorn: Gpu programming with llms. <https://gpu-mode.github.io/popcorn/>, 2025. Accessed: 2025-09-04.

[38] Aaron Grattafiori, Abhimanyu Dubey, Abhinav Jauhri, Abhinav Pandey, Abhishek Kadian, Ahmad Al-Dahle, Aiesha Letman, Akhil Mathur, Alan Schelten, Alex Vaughan, et al. The llama 3 herd of models. *arXiv preprint arXiv:2407.21783*, 2024.

[39] Diandian Gu, Peng Sun, Qinghao Hu, Ting Huang, Xun Chen, Yingtong Xiong, Guoteng Wang, Qiaoling Chen, Shangchun Zhao, Jiarui Fang, et al. Loongtrain: Efficient training of long-sequence llms with head-context parallelism. *arXiv preprint arXiv:2406.18485*, 2024.

[40] Yuxian Gu, Qinghao Hu, Shang Yang, Haocheng Xi, Junyu Chen, Song Han, and Han Cai. Jet-nemotron: Efficient language model with post neural architecture search. *arXiv preprint arXiv:2508.15884*, 2025.

[41] Daya Guo, Dejian Yang, Haowei Zhang, Junxiao Song, Ruoyu Zhang, Runxin Xu, Qihao Zhu, Shirong Ma, Peiyi Wang, Xiao Bi, et al. Deepseek-r1: Incentivizing reasoning capability in llms via reinforcement learning. *arXiv preprint arXiv:2501.12948*, 2025.

[42] Jordan Hoffmann, Sebastian Borgeaud, Arthur Mensch, Elena Buchatskaya, Trevor Cai, Eliza Rutherford, Diego de Las Casas, Lisa Anne Hendricks, Johannes Welbl, Aidan Clark, et al. Training compute-optimal large language models. *arXiv preprint arXiv:2203.15556*, 2022.

[43] Yanping Huang, Youlong Cheng, Ankur Bapna, Orhan Firat, Dehao Chen, Mia Chen, HyoukJoong Lee, Jiquan Ngiam, Quoc V Le, Yonghui Wu, et al. Gpipe: Efficient training of giant neural networks using pipeline parallelism. *Advances in neural information processing systems*, 32, 2019.

[44] Saki Imai, Rina Nakazawa, Marcelo Amaral, Sunyanan Choochotkaew, and Tatsuhiro Chiba. Predicting llm inference latency: A roofline-driven ml method. In *Annual Conference on Neural Information Processing Systems*, 2024.

[45] Sam Ade Jacobs, Masahiro Tanaka, Chengming Zhang, Minjia Zhang, Shuaiwen Leon Song, Samyam Rajbhandari, and Yuxiong He. Deepspeed ulysses: System optimizations for enabling training of extreme long sequence transformer models. *arXiv preprint arXiv:2309.14509*, 2023.

[46] Paras Jain, Ajay Jain, Aniruddha Nrusimha, Amir Gholami, Pieter Abbeel, Joseph Gonzalez, Kurt Keutzer, and Ion Stoica. Checkmate: Breaking the memory wall with optimal tensor rematerialization. *Proceedings of Machine Learning and Systems*, 2:497–511, 2020.

[47] Abhinav Jangda, Jun Huang, Guodong Liu, Amir Hossein Nodehi Sabet, Saeed Maleki, Youshan Miao, Madanlal Musuvathi, Todd Mytkowicz, and Olli Saarikivi. Breaking the computation and communication abstraction barrier in distributed machine learning workloads. In *Proceedings of the 27th ACM International Conference on Architectural Support for Programming Languages and Operating Systems*, pp. 402–416, 2022.

[48] Ganesh Jawahar, Subhabrata Mukherjee, Xiaodong Liu, Young Jin Kim, Muhammad Abdul-Mageed, Laks VS Lakshmanan, Ahmed Hassan Awadallah, Sebastien Bubeck, and Jianfeng Gao. Automoe: Neural architecture search for efficient sparsely activated transformers. *arXiv preprint arXiv:2210.07535*, 2022.

[49] Albert Q Jiang, Alexandre Sablayrolles, Antoine Roux, Arthur Mensch, Blanche Savary, Chris Bamford, Devendra Singh Chaplot, Diego de las Casas, Emma Bou Hanna, Florian Bressand, et al. Mixtral of experts. *arXiv preprint arXiv:2401.04088*, 2024.

[50] Ziheng Jiang, Haibin Lin, Yinmin Zhong, Qi Huang, Yangrui Chen, Zhi Zhang, Yanghua Peng, Xiang Li, Cong Xie, Shibiao Nong, et al. {MegaScale}: Scaling large language model training to more than 10,000 {GPUs}. In *21st USENIX Symposium on Networked Systems Design and Implementation (NSDI 24)*, pp. 745–760, 2024.

[51] Jared Kaplan, Sam McCandlish, Tom Henighan, Tom B Brown, Benjamin Chess, Rewon Child, Scott Gray, Alec Radford, Jeffrey Wu, and Dario Amodei. Scaling laws for neural language models. *arXiv preprint arXiv:2001.08361*, 2020.

[52] Can Karakus, Rahul Huilgol, Fei Wu, Anirudh Subramanian, Cade Daniel, Derya Cavdar, Teng Xu, Haohan Chen, Arash Rahnama, and Luis Quintela. Amazon sagemaker model parallelism: A general and flexible framework for large model training. *arXiv preprint arXiv:2111.05972*, 2021.

[53] Nitish Shirish Keskar, Dheevatsa Mudigere, Jorge Nocedal, Mikhail Smelyanskiy, and Ping Tak Peter Tang. On large-batch training for deep learning: Generalization gap and sharp minima. *arXiv preprint arXiv:1609.04836*, 2016.

[54] Vijay Anand Korthikanti, Jared Casper, Sangkug Lym, Lawrence McAfee, Michael Andersch, Mohammad Shoeybi, and Bryan Catanzaro. Reducing activation recomputation in large transformer models. *Proceedings of Machine Learning and Systems*, 5:341–353, 2023.

[55] Joyjit Kundu, Wenzhe Guo, Ali BanaGozar, Udari De Alwis, Sourav Sengupta, Puneet Gupta, and Arindam Mallik. Performance modeling and workload analysis of distributed large language model training and inference. In *2024 IEEE International Symposium on Workload Characterization (IISWC)*, pp. 57–67. IEEE, 2024.

[56] Zhiquan Lai, Shengwei Li, Xudong Tang, Keshi Ge, Weijie Liu, Yabo Duan, Linbo Qiao, and Dongsheng Li. Merak: An efficient distributed dnn training framework with automated 3d parallelism for giant foundation models. *IEEE Transactions on Parallel and Distributed Systems*, 34(5):1466–1478, 2023.

[57] Dmitry Lepikhin, HyoukJoong Lee, Yuanzhong Xu, Dehao Chen, Orhan Firat, Yanping Huang, Maxim Krikun, Noam Shazeer, and Zhifeng Chen. Gshard: Scaling giant models with conditional computation and automatic sharding. *arXiv preprint arXiv:2006.16668*, 2020.

[58] Dacheng Li, Hongyi Wang, Eric Xing, and Hao Zhang. Amp: Automatically finding model parallel strategies with heterogeneity awareness. *Advances in Neural Information Processing Systems*, 35: 6630–6639, 2022.

[59] Rui Li, Deji Fu, Chunyu Shi, Zhilan Huang, and Gang Lu. Efficient llms training and inference: An introduction. *IEEE Access*, 2024.

[60] Shen Li, Yanli Zhao, Rohan Varma, Omkar Salpekar, Pieter Noordhuis, Teng Li, Adam Paszke, Jeff Smith, Brian Vaughan, Pritam Damania, et al. Pytorch distributed: Experiences on accelerating data parallel training. *arXiv preprint arXiv:2006.15704*, 2020.

[61] Shenggui Li, Fuzhao Xue, Chaitanya Baranwal, Yongbin Li, and Yang You. Sequence parallelism: Long sequence training from system perspective. *arXiv preprint arXiv:2105.13120*, 2021.

[62] Shenggui Li, Hongxin Liu, Zhengda Bian, Jiarui Fang, Haichen Huang, Yuliang Liu, Boxiang Wang, and Yang You. Colossal-AI: A unified deep learning system for large-scale parallel training. In *Proceedings of the 52nd International Conference on Parallel Processing*, pp. 766–775, 2023.

[63] Shengwei Li, Zhiqian Lai, Yanqi Hao, Weijie Liu, Keshi Ge, Xiaoge Deng, Dongsheng Li, and Kai Lu. Automated tensor model parallelism with overlapped communication for efficient foundation model training. *arXiv preprint arXiv:2305.16121*, 2023.

[64] Zhuohan Li, Siyuan Zhuang, Shiyuan Guo, Danyang Zhuo, Hao Zhang, Dawn Song, and Ion Stoica. Terapipe: Token-level pipeline parallelism for training large-scale language models. In *International Conference on Machine Learning*, pp. 6543–6552. PMLR, 2021.

[65] Peng Liang, Yu Tang, Xiaoda Zhang, Youhui Bai, Teng Su, Zhiqian Lai, Linbo Qiao, and Dongsheng Li. A survey on auto-parallelism of large-scale deep learning training. *IEEE Transactions on Parallel & Distributed Systems*, 34(08):2377–2390, 2023.

[66] Heng Liao, Jiajin Tu, Jing Xia, Hu Liu, Xiping Zhou, Honghui Yuan, and Yuxing Hu. Ascend: a scalable and unified architecture for ubiquitous deep neural network computing: Industry track paper. In *2021 IEEE International Symposium on High-Performance Computer Architecture (HPCA)*, pp. 789–801. IEEE, 2021.

[67] Zhiqi Lin, Youshan Miao, Guodong Liu, Xiaoxiang Shi, Quanlu Zhang, Fan Yang, Saeed Maleki, Yi Zhu, Xu Cao, Cheng Li, et al. Superscaler: Supporting flexible dnn parallelization via a unified abstraction. *arXiv preprint arXiv:2301.08984*, 2023.

[68] Zhiqi Lin, Youshan Miao, Quanlu Zhang, Fan Yang, Yi Zhu, Cheng Li, Saeed Maleki, Xu Cao, Ning Shang, Yilei Yang, et al. {nnScaler}:{Constraint-Guided} parallelization plan generation for deep learning training. In *18th USENIX Symposium on Operating Systems Design and Implementation (OSDI 24)*, pp. 347–363, 2024.

[69] Aixin Liu, Bei Feng, Bing Xue, Bingxuan Wang, Bochao Wu, Chengda Lu, Chenggang Zhao, Chengqi Deng, Chenyu Zhang, Chong Ruan, et al. Deepseek-v3 technical report. *arXiv preprint arXiv:2412.19437*, 2024.

[70] Guodong Liu, Youshan Miao, Zhiqi Lin, Xiaoxiang Shi, Saeed Maleki, Fan Yang, Yungang Bao, and Sa Wang. Aceso: Efficient parallel dnn training through iterative bottleneck alleviation. In *Proceedings of the Nineteenth European Conference on Computer Systems*, pp. 163–181, 2024.

[71] Hao Liu, Matei Zaharia, and Pieter Abbeel. Ring attention with blockwise transformers for near-infinite context. *arXiv preprint arXiv:2310.01889*, 2023.

[72] Rui Liu, Young Jin Kim, Alexandre Muzio, and Hany Hassan. Gating dropout: Communication-efficient regularization for sparsely activated transformers. In *International Conference on Machine Learning*, pp. 13782–13792. PMLR, 2022.

[73] Meta. meta-llama/llama-3.2-1b. <https://huggingface.co/meta-llama/Llama-3.2-1B>, 2024. Large language model.

[74] Tianhao Miao, Qinghua Wu, Ting Liu, Penglai Cui, Rui Ren, Zhenyu Li, and Gaogang Xie. MD-Roofline: A training performance analysis model for distributed deep learning. In *2022 IEEE Symposium on Computers and Communications (ISCC)*, pp. 1–8. IEEE, 2022.

[75] Xupeng Miao, Yujie Wang, Youhe Jiang, Chunan Shi, Xiaonan Nie, Hailin Zhang, and Bin Cui. Galvatron: Efficient transformer training over multiple gpus using automatic parallelism. *arXiv preprint arXiv:2211.13878*, 2022.

[76] Deepak Narayanan, Aaron Harlap, Amar Phanishayee, Vivek Seshadri, Nikhil R Devanur, Gregory R Ganger, Phillip B Gibbons, and Matei Zaharia. Pipedream: Generalized pipeline parallelism for dnn training. In *Proceedings of the 27th ACM symposium on operating systems principles*, pp. 1–15, 2019.

[77] Deepak Narayanan, Amar Phanishayee, Kaiyu Shi, Xie Chen, and Matei Zaharia. Memory-efficient pipeline-parallel dnn training. In *International Conference on Machine Learning*, pp. 7937–7947. PMLR, 2021.

[78] Deepak Narayanan, Mohammad Shoeybi, Jared Casper, Patrick LeGresley, Mostafa Patwary, Vijay Korthikanti, Dmitri Vainbrand, Prethvi Kashinkunti, Julie Bernauer, Bryan Catanzaro, et al. Efficient large-scale language model training on gpu clusters using megatron-lm. In *Proceedings of the international conference for high performance computing, networking, storage and analysis*, pp. 1–15, 2021.

[79] Stefan Nastic, Andrea Morichetta, Thomas Puszta, Schahram Dustdar, Xiaoning Ding, Deepak Vij, and Ying Xiong. SLOC: Service level objectives for next generation cloud computing. *IEEE Internet Computing*, 24(3):39–50, 2020.

[80] Nvidia. Nvidia nim llms benchmarking, . URL <https://docs.nvidia.com/nim/benchmarking/llm/latest/metrics.html>.

[81] Nvidia. Nvidia nemo, . URL <https://github.com/NVIDIA-NeMo/NeMo>.

[82] NVIDIA. Nvidia/megatron-lm: Ongoing research training transformer models at scale. <https://github.com/NVIDIA/Megatron-LM>, 2025. Accessed: 2025-09-04.

[83] David Patterson, Joseph Gonzalez, Quoc Le, Chen Liang, Lluis-Miquel Munguia, Daniel Rothchild, David So, Maud Texier, and Jeff Dean. Carbon emissions and large neural network training. *arXiv preprint arXiv:2104.10350*, 2021.

[84] Xuan Peng, Xuanhua Shi, Hulin Dai, Hai Jin, Weiliang Ma, Qian Xiong, Fan Yang, and Xuehai Qian. Capuchin: Tensor-based gpu memory management for deep learning. In *Proceedings of the Twenty-Fifth International Conference on Architectural Support for Programming Languages and Operating Systems*, pp. 891–905, 2020.

[85] Reiner Pope, Sholto Douglas, Aakanksha Chowdhery, Jacob Devlin, James Bradbury, Jonathan Heek, Kefan Xiao, Shivani Agrawal, and Jeff Dean. Efficiently scaling transformer inference. *Proceedings of machine learning and systems*, 5:606–624, 2023.

[86] Bharadwaj Pudipeddi, Maral Mesmakhosroshahi, Jinwen Xi, and Sujeeth Bharadwaj. Training large neural networks with constant memory using a new execution algorithm. *arXiv preprint arXiv:2002.05645*, 2020.

[87] Penghui Qi, Xinyi Wan, Guangxing Huang, and Min Lin. Zero bubble pipeline parallelism. *arXiv preprint arXiv:2401.10241*, 2023.

[88] Samyam Rajbhandari, Jeff Rasley, Olatunji Ruwase, and Yuxiong He. Zero: Memory optimizations toward training trillion parameter models. In *SC20: International Conference for High Performance Computing, Networking, Storage and Analysis*, pp. 1–16. IEEE, 2020.

[89] Jeff Rasley, Samyam Rajbhandari, Olatunji Ruwase, and Yuxiong He. Deepspeed: System optimizations enable training deep learning models with over 100 billion parameters. In *Proceedings of the 26th ACM SIGKDD international conference on knowledge discovery & data mining*, pp. 3505–3506, 2020.

[90] Minsoo Rhu, Natalia Gimelshein, Jason Clemons, Arslan Zulfiqar, and Stephen W Keckler. vdnn: Virtualized deep neural networks for scalable, memory-efficient neural network design. In *2016 49th Annual IEEE/ACM International Symposium on Microarchitecture (MICRO)*, pp. 1–13. IEEE, 2016.

[91] Roy Schwartz, Jesse Dodge, Noah A Smith, and Oren Etzioni. Green ai. *Communications of the ACM*, 63(12):54–63, 2020.

[92] Noam Shazeer. Glu variants improve transformer. *arXiv preprint arXiv:2002.05202*, 2020.

[93] Noam Shazeer, Azalia Mirhoseini, Krzysztof Maziarz, Andy Davis, Quoc Le, Geoffrey Hinton, and Jeff Dean. Outrageously large neural networks: The sparsely-gated mixture-of-experts layer. *arXiv preprint arXiv:1701.06538*, 2017.

[94] Noam Shazeer, Youlong Cheng, Niki Parmar, Dustin Tran, Ashish Vaswani, Penporn Koanantakool, Peter Hawkins, HyoukJoong Lee, Mingsheng Hong, Cliff Young, et al. Mesh-tensorflow: Deep learning for supercomputers. *Advances in neural information processing systems*, 31, 2018.

[95] Mohammad Shoeybi, Mostofa Patwary, Raul Puri, Patrick LeGresley, Jared Casper, and Bryan Catanzaro. Megatron-lm: Training multi-billion parameter language models using model parallelism. *arXiv preprint arXiv:1909.08053*, 2019.

[96] Xian Shuai, Yiding Wang, Yimeng Wu, Xin Jiang, and Xiaozhe Ren. Scaling law for language models training considering batch size. *arXiv preprint arXiv:2412.01505*, 2024.

[97] Siddharth Singh, Olatunji Ruwase, Ammar Ahmad Awan, Samyam Rajbhandari, Yuxiong He, and Abhinav Bhatele. A hybrid tensor-expert-data parallelism approach to optimize mixture-of-experts training. In *Proceedings of the 37th International Conference on Supercomputing*, pp. 203–214, 2023.

[98] Siddharth Singh, Prajwal Singhania, Aditya K Ranjan, Zack Sating, and Abhinav Bhatele. A 4d hybrid algorithm to scale parallel training to thousands of gpus. *arXiv preprint arXiv:2305.13525*, 2023.

[99] Samuel L Smith, Pieter-Jan Kindermans, Chris Ying, and Quoc V Le. Don’t decay the learning rate, increase the batch size. *arXiv preprint arXiv:1711.00489*, 2017.

[100] Emma Strubell, Ananya Ganesh, and Andrew McCallum. Energy and policy considerations for modern deep learning research. In *Proceedings of the AAAI conference on artificial intelligence*, volume 34, pp. 13693–13696, 2020.

[101] Qidong Su, Wei Zhao, Xin Li, Muralidhar Andoorveedu, Chenhao Jiang, Zhanda Zhu, Kevin Song, Christina Giannoula, and Gennady Pekhimenko. Seesaw: High-throughput llm inference via model re-sharding. In *Eighth Conference on Machine Learning and Systems*, 2025.

[102] Stuart H Sul, Simran Arora, Benjamin F Spector, and Christopher Ré. Parallelkittens: Systematic and practical simplification of multi-gpu ai kernels. *arXiv preprint arXiv:2511.13940*, 2025.

[103] Weigao Sun, Zhen Qin, Dong Li, Xuyang Shen, Yu Qiao, and Yiran Zhong. Linear attention sequence parallelism. *arXiv preprint arXiv:2404.02882*, 2024.

[104] Weigao Sun, Disen Lan, Yiran Zhong, Xiaoye Qu, and Yu Cheng. Lasp-2: Rethinking sequence parallelism for linear attention and its hybrid. *arXiv preprint arXiv:2502.07563*, 2025.

[105] Jakub M Tarnawski, Deepak Narayanan, and Amar Phanishayee. Piper: Multidimensional planner for dnn parallelization. *Advances in Neural Information Processing Systems*, 34:24829–24840, 2021.

[106] Youssef Tawfilis, Hossam Amer, Minar El-Aasser, and Tallal Elshabrawy. A distributed generative ai approach for heterogeneous multi-domain environments under data sharing constraints. *arXiv preprint arXiv:2507.12979*, 2025.

[107] Romal Thoppilan, Daniel De Freitas, Jamie Hall, Noam Shazeer, Apoorv Kulshreshtha, Heng-Tze Cheng, Alicia Jin, Taylor Bos, Leslie Baker, Yu Du, et al. Lamda: Language models for dialog applications. *arXiv preprint arXiv:2201.08239*, 2022.

[108] Hugo Touvron, Louis Martin, Kevin Stone, Peter Albert, Amjad Almahairi, Yasmine Babaei, Nikolay Bashlykov, Soumya Batra, Prajjwal Bhargava, Shruti Bhosale, et al. Llama 2: Open foundation and fine-tuned chat models. *arXiv preprint arXiv:2307.09288*, 2023.

[109] Hugo Touvron, Louis Martin, Kevin Stone, Peter Albert, and et al. Llama 2: Open foundation and fine-tuned chat models. *arXiv preprint arXiv:2307.09288*, 2023.

[110] Taegeon Um, Byungsoo Oh, Minyoung Kang, Woo-Yeon Lee, Goeun Kim, Dongseob Kim, Youngtaek Kim, Mohd Muzzammil, and Myeongjae Jeon. Metis: Fast automatic distributed training on heterogeneous {GPUs}. In *2024 USENIX Annual Technical Conference (USENIX ATC 24)*, pp. 563–578, 2024.

[111] Boxiang Wang, Qifan Xu, Zhengda Bian, and Yang You. 2.5-dimensional distributed model training. *CoRR*, 2021.

[112] Boxiang Wang, Qifan Xu, Zhengda Bian, and Yang You. Tesseract: Parallelize the tensor parallelism efficiently. In *Proceedings of the 51st International Conference on Parallel Processing*, pp. 1–11, 2022.

[113] Chengen Wang and Murat Kantacioglu. A review of deepseek models' key innovative techniques. *arXiv preprint arXiv:2503.11486*, 2025.

[114] Linnan Wang, Alexander Renda, Rong Zhao, and Wen mei Hwu. Superneurons: Dynamic gpu memory management for training deep neural networks. In *Proceedings of the 23rd ACM SIGPLAN Symposium on Principles and Practice of Parallel Programming (PPoPP)*, pp. 41–53. ACM, 2018. doi: 10.1145/3178487.3178491.

[115] Shibo Wang, Jinliang Wei, Amit Sabne, Andy Davis, Berkin Ilbeyi, Blake Hechtman, Dehao Chen, Karthik Srinivasa Murthy, Marcello Maggioni, Qiao Zhang, et al. Overlap communication with dependent computation via decomposition in large deep learning models. In *Proceedings of the 28th ACM International Conference on Architectural Support for Programming Languages and Operating Systems, Volume 1*, pp. 93–106, 2022.

[116] Benjamin Warner. Optimī: Fast, modern, and low precision pytorch optimizers. <https://github.com/warner-benjamin/optimi>, 2025. Accessed: 2025-12-02.

[117] Samuel Williams, Andrew Waterman, and David Patterson. Roofline: an insightful visual performance model for multicore architectures. *Communications of the ACM*, 52(4):65–76, 2009.

[118] Guanbin Xu, Zhihao Le, Yinhe Chen, Zhiqi Lin, Zewen Jin, Youshan Miao, and Cheng Li. {AutoCCL}: Automated collective communication tuning for accelerating distributed and parallel {DNN} training. In *22nd USENIX Symposium on Networked Systems Design and Implementation (NSDI 25)*, pp. 667–683, 2025.

[119] Qifan Xu and Yang You. An efficient 2d method for training super-large deep learning models. In *2023 IEEE International Parallel and Distributed Processing Symposium (IPDPS)*, pp. 222–232. IEEE, 2023.

[120] Yuanzhong Xu, HyoukJoong Lee, Dehao Chen, Blake Hechtman, Yanping Huang, Rahul Joshi, Maxim Krikun, Dmitry Lepikhin, Andy Ly, Marcello Maggioni, et al. Gspmd: general and scalable parallelization for ml computation graphs. *arXiv preprint arXiv:2105.04663*, 2021.

[121] Amy Yang, Jingyi Yang, Aya Ibrahim, Xinfeng Xie, Bangsheng Tang, Grigory Sizov, Jeremy Reizenstein, Jongsoo Park, and Jianyu Huang. Context parallelism for scalable million-token inference. *arXiv preprint arXiv:2411.01783*, 2024.

[122] Charlene Yang, Yunsong Wang, Thorsten Kurth, Steven Farrell, and Samuel Williams. Hierarchical roofline performance analysis for deep learning applications. In *Intelligent Computing: Proceedings of the 2021 Computing Conference, Volume 2*, pp. 473–491. Springer, 2021.

[123] Hanmei Yang, Jin Zhou, Yao Fu, Xiaoqun Wang, Ramine Roane, Hui Guan, and Tongping Liu. Protrain: Efficient llm training via memory-aware techniques. *arXiv preprint arXiv:2406.08334*, 2024.

[124] Jiawei Yang, Zhongbo Li, Zeqin Feng, and Yongqiang Xie. A survey on neural network quantization. In *Proceedings of the 2025 6th International Conference on Computer Information and Big Data Applications*, pp. 384–394, 2025.

[125] Menglin Yang, Jialin Chen, Yifei Zhang, Jiahong Liu, Jiasheng Zhang, Qiyao Ma, Harshit Verma, Qianru Zhang, Min Zhou, Irwin King, et al. Low-rank adaptation for foundation models: A comprehensive review. *arXiv preprint arXiv:2501.00365*, 2024.

[126] Jinghan Yao, Sam Ade Jacobs, Masahiro Tanaka, Olatunji Ruwase, Hari Subramoni, and Dharbaleswar K Panda. Training ultra long context language model with fully pipelined distributed transformer. *arXiv preprint arXiv:2408.16978*, 2024.

[127] Yichun Yin, Wenyong Huang, Kaikai Song, Yehui Tang, Xueyu Wu, Wei Guo, Peng Guo, Yaoyuan Wang, Xiaojun Meng, Yasheng Wang, et al. Pangu ultra: Pushing the limits of dense large language models on ascend npus. *arXiv preprint arXiv:2504.07866*, 2025.

[128] Yang You, Igor Gitman, and Boris Ginsburg. Large batch training of convolutional networks. *arXiv preprint arXiv:1708.03888*, 2017.

[129] Yang You, Zhao Zhang, Cho-Jui Hsieh, James Demmel, and Kurt Keutzer. Imagenet training in minutes. In *Proceedings of the 47th international conference on parallel processing*, pp. 1–10, 2018.

[130] Zhihang Yuan, Yuzhang Shang, Yang Zhou, Zhen Dong, Zhe Zhou, Chenhao Xue, Bingzhe Wu, Zhikai Li, Qingyi Gu, Yong Jae Lee, et al. Llm inference unveiled: Survey and roofline model insights. *arXiv preprint arXiv:2402.16363*, 2024.

[131] Fanlong Zeng, Wensheng Gan, Yongheng Wang, and Philip S Yu. Distributed training of large language models. In *2023 IEEE 29th International Conference on Parallel and Distributed Systems (ICPADS)*, pp. 840–847. IEEE, 2023.

[132] Fanlong Zeng, Wensheng Gan, Yongheng Wang, and Philip S Yu. Distributed training of large language models: A survey. *Natural Language Processing Journal*, pp. 100174, 2025.

[133] Peiyuan Zhang, Guangtao Zeng, Tianduo Wang, and Wei Lu. Tinyllama: An open-source small language model. *arXiv preprint arXiv:2401.02385*, 2024.

[134] Zhen Zhang, Shuai Zheng, Yida Wang, Justin Chiu, George Karypis, Trishul Chilimbi, Mu Li, and Xin Jin. Mics: near-linear scaling for training gigantic model on public cloud. *arXiv preprint arXiv:2205.00119*, 2022.

[135] Lianmin Zheng, Zhuohan Li, Hao Zhang, Yonghao Zhuang, Zhifeng Chen, Yanping Huang, Yida Wang, Yuanzhong Xu, Danyang Zhuo, Eric P Xing, et al. Alpa: Automating inter-and {Intra-Operator} parallelism for distributed deep learning. In *16th USENIX Symposium on Operating Systems Design and Implementation (OSDI 22)*, pp. 559–578, 2022.

[136] Size Zheng, Jin Fang, Xuegui Zheng, Qi Hou, Wenlei Bao, Ningxin Zheng, Ziheng Jiang, Dongyang Wang, Jianxi Ye, Haibin Lin, et al. Tilelink: Generating efficient compute-communication overlapping kernels using tile-centric primitives. *arXiv preprint arXiv:2503.20313*, 2025.

[137] Jiahang Zhou, Yanyu Chen, Zicong Hong, Wuhui Chen, Yue Yu, Tao Zhang, Hui Wang, Chuanfu Zhang, and Zibin Zheng. Training and serving system of foundation models: A comprehensive survey. *IEEE Open Journal of the Computer Society*, 5:107–119, 2024.

[138] Xunyu Zhu, Jian Li, Yong Liu, Can Ma, and Weiping Wang. A survey on model compression for large language models. *Transactions of the Association for Computational Linguistics*, 12:1556–1577, 2024.

- [139] Zhanda Zhu, Christina Giannoula, Muralidhar Andoorveedu, Qidong Su, Karttikeya Mangalam, Bojian Zheng, and Gennady Pekhimenko. Mist: Efficient distributed training of large language models via memory-parallelism co-optimization. In *Proceedings of the Twentieth European Conference on Computer Systems*, pp. 1298–1316, 2025.
- [140] Yonghao Zhuang, Lianmin Zheng, Zhuohan Li, Eric Xing, Qirong Ho, Joseph Gonzalez, Ion Stoica, Hao Zhang, and Hexu Zhao. On optimizing the communication of model parallelism. *Proceedings of Machine Learning and Systems*, 5:526–540, 2023.